

ABSTRACT

Title of dissertation: INVESTIGATING COPPER ACQUISITION
AND DELIVERY VIA TRANSPORTERS
AND A PHARMACOLOGICAL CHAPERONE
IN COPPER-DEFICIENT WORMS AND MICE

Sai Yuan
Doctor of Philosophy, 2019

Dissertation directed by: Associate Professor, Dr. Byung-Eun Kim
Department of Animal and Avian Sciences

Copper (Cu) is a key micronutrient required for a variety of essential biochemical pathways. Systemic or tissue-specific Cu-deficiencies, caused by insufficient dietary Cu uptake or mutations in Cu transporting genes, result in impaired growth, neuropathy, ataxia, hypopigmentation, osteoporosis and anemia-like symptoms in mammals. How organisms regulate Cu homeostasis at the systemic levels in response to Cu deficiencies remain elusive. In this study, we use *Caenorhabditis elegans* (*C. elegans*), a genetically tractable, multi-tissue metazoan to explore Cu homeostasis and investigate these unknowns. The high-affinity Cu transporters encoded by *CTR* family genes are required for dietary Cu uptake and maintaining systemic Cu balance from yeast to mammals. However, little is known about Cu acquisition mechanisms in *C. elegans*. We identified ten *CTR* ortholog genes in *C. elegans*; of these, *chca-1* was functionally characterized. Cu availability regulates transcription of *chca-1* in both the intestine and hypodermis, and *chca-1* is essential

for normal growth, and reproduction in the worm. Additionally, altered Cu balance caused by the loss of CHCA-1 results in defects in Cu-responsive avoidance behavior. Identification of this *CTR*-like gene in *C. elegans*, which appears to be essential for normal Cu homeostasis in the worm, illustrates the importance of Cu delivery via CHCA-1 for normal metazoan development and behavioral phenotypes. In addition, we show that a Cu-binding pharmacological chaperone, elesclomol (ES), fully restores the developmental defects and Cu deficiencies in *chca-1*-depleted worms, as well as the lethality in worms lacking *cua-1* expression (Cu exporter *ATP7A* ortholog), suggesting ES is able to efficiently deliver Cu from dietary sources to peripheral tissues through the intestine in *C. elegans*. Our study was further expanded to mammalian models such as cardiac-specific *Ctr1*-depleted (*Ctr1^{hrt/hrt}*) mice. We found that ES administration fully restores the postnatal lethality, developmental defects and cardiac hypertrophy found in *Ctr1^{hrt/hrt}* mice, as well as rescuing the secondary systemic Cu homeostasis responses, including aberrant *ATP7A* protein levels in the liver and intestine. Moreover, ES shows the potential ability to transport Cu across the blood-brain-barrier in *in vitro* studies. These results illustrate the capability of ES to rescue systemic Cu deficiency in worms and mice, independent of the presence of functional Cu transporters, and shed light on the therapeutic usage of ES in Cu-deficient human diseases.

INVESTIGATING THE CU ACQUISITION AND DELIVERY VIA
TRANSPORTERS AND A PHARMACOLOGICAL CHAPERONE
IN CU-DEFICIENT WORMS AND MICE

by

Sai Yuan

Dissertation submitted to the Faculty of the Graduate School of the
University of Maryland, College Park in partial fulfillment
of the requirements for the degree of
Doctor of Philosophy
2019

Advisory Committee:

Dr. Byung-Eun Kim, Chair/Advisor

Dr. Caren Chang, Dean's Representative

Dr. Iqbal Hamza

Dr. John Hanover

Dr. Zhengguo Xiao

© Copyright by
Sai Yuan
2019

Acknowledgments

With my deepest sincerity and gratitude, thank you to everyone I met in the incredible six years I have had at the University of Maryland, College Park.

First of all, I would like to say a special thank you to my advisor, Dr. Byung-Eun Kim for supporting me and guiding me on the fascinating projects over the past six years. When I encountered difficulties or faced interruptions along the path of my research, he was always encouraging and supporting me. Thanks for training me how to think and interpret things in a scientific way, and helping me grow into the researcher I am now. I have learned a great deal of knowledge regarding metal homeostasis, and most importantly, how to conduct research and behave myself.

I would like to deeply thank my committee members, Dr. Caren Chang, Dr. Iqbal Hamza, Dr. John Hanover and Dr. Zhengguo Xiao, for the time and efforts you put into the discussion of my research progress, and offering me valuable suggestions and direction.

I owe thanks to all my colleagues from the Kim lab and the Animal and Avian Science department. Thank you to Haarin for the great advise and discussions on my research. I thank Alex for introducing me to world of *C. elegans*, and Anuj for getting me more familiar with it. Tammy and Tae IL, you showed me the way how senior scientists design and conduct research. I also would like to thank Hamza lab members, Xiaojing, Rini, Ian, Simon, and Jason, I appreciate your kindness help and time to teach me new techniques. And thank you all for being wonderful friends.

I would also like to thank my previous advisor, Dr. Yaofeng Zhao from China

Agricultural University, who offered me the opportunity to work as research associate and helped me gained valuable experiences with molecular biology. Thank to Dr. YingKuan Wang, who offered me an opportunity to get into journal editing and typesetting.

Finally, I would like to thank my friends and family both here and aboard. Thank you my parents, for your love, support and understanding; thank you to Meilings, for being a wonderful companion; and special thank to my husband, Dr. Ruofei Du, I could not have done this without your support.

Dedication

We are cooper.

They can bend us and twist us,

but they can't break us.

– Sonali Dev, *A Change of Heart*

Table of Contents

Acknowledgements	ii
Dedication	iv
List of Tables	viii
List of Figures	ix
List of Abbreviations	xi
1 Introduction	1
1.1 Cellular Cu homeostasis	2
1.1.1 Cu uptake	2
1.1.2 Cu delivery to the secretory pathway and efflux via ATP7A/B	7
1.1.3 Intracellular Cu distribution and storage	9
1.1.4 Cuproenzymes and function	13
1.2 Mammalian Cu homeostasis at the organismal level	16
1.2.1 Dietary Cu uptake and transport into circulation	16
1.2.2 Hepatic Cu storage and excretion	17
1.2.3 Cu metabolism in heart, kidney and brain	18
1.2.4 Cu homeostasis in <i>C. elegans</i>	19
1.3 The anti-cancer drug elesclomol in Cu homeostasis	21
1.3.1 Elesclomol-Cu(II) as cancer therapy	21
1.3.1.1 Elesclomol achieves cytotoxicity through its interaction with copper	22
1.3.1.2 Clinical study of elesclomol in cancer treatment: progress and limitations	25
1.3.2 Elesclomol rescues mitochondrial function in copper-deficient models	26
1.3.2.1 Copper is required for mitochondria energy production	26
1.3.2.2 Elesclomol administration restores mitochondrial function in genetic models of Cu deficiency	27
1.3.3 Copper deficiency-related genetic mouse models	28

1.3.3.1	Tissue-specific Ctr1 depleted mouse models	28
1.3.3.2	Menkes disease	29
2	Materials and Methods	33
2.1	<i>C. elegans</i> experimental procedures	33
2.2	Yeast experiments	40
2.3	Mouse and tissue culture experiments	41
2.4	Statistical analysis	46
3	CHCA-1 is a copper-regulated CTR1 homolog required for normal development, copper accumulation, and copper-sensing behavior in <i>Caenorhabditis elegans</i>	47
3.1	Project summary	47
3.2	Results	48
3.2.1	Cu-responsive transcriptional regulation of CTR1-like genes in <i>C. elegans</i>	48
3.2.2	Importance of <i>CTR1</i> candidate genes for growth, reproduction, and Cu accumulation in worms	54
3.2.3	CHCA-1 is required for normal Cu level and development	63
3.2.4	Intestinal CHCA-1 is critical for Cu-dependent growth and Cu accumulation	75
3.2.5	CHCA-1 localizes to intracellular vesicles in the intestine	86
3.2.6	CHCA-1 is required for behavioral avoidance of potentially toxic levels of Cu	87
3.3	Discussion	95
4	The copper-binding pharmacological agent elesclomol restores systemic copper deficiency in <i>Caenorhabditis elegans</i> and <i>Mus musculus</i>	103
4.1	Summary of the project	103
4.2	Results	104
4.2.1	Elesclomol chemically rescues <i>chca-1</i> phenotypes in <i>C. elegans</i>	104
4.2.2	ES administration rescues lethality, growth defects and cardiac hypertrophy found in cardiac-specific <i>Ctr1</i> knockout mice	105
4.2.3	Cardiac Cu deficiency in <i>Ctr1^{hrt/hrt}</i> mice can be restored by ES-dependent Cu delivery	109
4.2.4	ES supplementation rescues the altered systemic ATP7A protein levels of <i>Ctr1^{hrt/hrt}</i> mice	110
4.2.5	Intestinal CUA-1-associated lethality and embryogenesis defects can be restored by ES treatment	119
4.2.6	ES exhibits potential for Cu-transport through cultured blood-brain-barrier cells	123
4.2.7	Characterizing the effect of ES on tyrosinase activity in <i>ATP7A^{-/-}</i> cells	124
4.3	Discussion	128

5	Conclusions and future directions	137
5.1	Conclusions	137
5.2	Future Directions	140
5.2.1	Characterizing <i>C. elegans</i> <i>CTR</i> ortholog genes	140
5.2.2	Identifying the neuronal components required for Cu sensing in <i>C. elegans</i>	141
5.2.3	Elucidating elesclomol-mediated Cu transport in mouse	143
5.2.4	Evaluation of elesclomol treatment using Menkes disease models	144
	Appendix	146
I	Transcriptional regulation of <i>C. elegans</i> CTR1 candidate genes by Cu	146
II	Cu-dependent neuropeptide maturation is associated with Cu avoid- ance behavior	148
III	Cox1 abundance in P10 Veh/ES administered <i>Ctr1^{hrt/hrt}</i> mice.	149
IV	Primers used for qRT-PCR assays	152
V	List of transgenic animals used in Chapter 3	153
	References	154

List of Tables

1.1	List of cuproenzymes and their functions	14
3.1	<i>C. elegans</i> <i>CTR</i> homolog genes	49
I	Primers used for qRT-PCR assays	152
II	List of transgenic animals used in Chapter 3	153

List of Figures

1.1	Predicted topology of human CTR1 and ATP7A	3
1.2	Cellular Cu metabolism in mammalian cells	11
3.1	Predicted TMD position and N terminal methionine of <i>C. elegans</i> Ctr proteins	52
3.2	Requirement of <i>CTR1</i> candidate genes for Cu-dependent growth . . .	56
3.3	RNAi efficiency of 10 <i>CTR</i> candidate genes	58
3.4	Requirement of <i>CTR1</i> candidate genes for Cu accumulation	60
3.5	<i>F58G6.9</i> RNAi animals exhibited significantly reduced brood size. . .	62
3.6	Expressing <i>F58G6.3</i> , <i>F58G6.7</i> , and <i>F58G6.9b</i> in the MPY17 <i>CTR1</i> Δ <i>CTR3</i> Δ yeast strain.	65
3.7	CUA-1.1::GFP localization in BK015 worms with Ctr candidate RNAi	67
3.8	Depletion of <i>chca-1</i> by RNAi decreases intestinal Cu availability in <i>C. elegans</i>	69
3.9	Schematic of <i>CTR1</i> and <i>chca-1</i> gene loci and protein sequence alignment	71
3.10	<i>chca-1 (tm6506) IV</i> worms exhibit growth defect under Cu-deficient condition.	73
3.11	<i>chca-1 (tm6506) IV</i> worms exhibit low Cu levels under Cu deficiency and defect in Cu acquisition.	77
3.12	Tissue-specific expression of the <i>chca-1</i> gene.	79
3.13	Cu-dependent growth following <i>chca-1</i> gene depletion in specific tissues. 80	
3.14	Intestinal CHCA-1 plays a dominant role in Cu acquisition under Cu-limited conditions.	82
3.15	Effect of tissue-specific <i>chca-1</i> RNAi on intestinal CUA-1.1::GFP distribution.	84
3.16	Expression of CHCA-1::GFP in the intestine	88
3.17	CHCA-1::GFP does not co-localize with the Cu probe CF4	90
3.18	Expression of CHCA-1-2xFLAG protein in the intestine	91
3.19	Intestinal expression of CHCA-1 partially rescued growth of <i>chca-1</i> mutant animals	92
3.20	Design of Cu avoidance assay.	93

3.21	CHCA-1 is required for Cu sensing and Cu-dependent avoidance behavior	96
3.22	The efficacy of RNAi treatments is assessed by qRT-PCR	98
4.1	Elesclomol recovers growth retardation and Cu levels of CHCA-1 depleted <i>C. elegans</i>	106
4.2	ES injection rescues lethality and growth retardation of cardiac-specific Ctr1 knockout mice	111
4.3	Cardiac Ctr1 excision efficiency in <i>Ctr1^{hrt/hrt}</i> mice	113
4.4	Abnormal body mass and organ sizes in <i>Ctr1^{hrt/hrt}</i> mice are rescued by ES supplementation	114
4.5	ES administration rescues cardiac hypertrophy of <i>Ctr1^{hrt/hrt}</i> mice	116
4.6	ES restores bioavailable Cu levels and Cco abundance in <i>Ctr1^{hrt/hrt}</i> mice cardiac tissue	117
4.7	ATP7A protein abundance in the liver and intestinal cells from ES- or vehicle-treated <i>Ctr1^{hrt/hrt}</i> mice	120
4.8	Apical ES treatment of to BBB cells significantly increases Cu levels of cells grown on the basal side	125
4.9	Effect of ES on Cu levels in wild-type and <i>ATP7A^{-/-}</i> MEFs	129
4.10	ATP7A is required for tyrosinase activity.	131
4.11	ES is insufficient to restore tyrosinase activity in <i>ATP7A^{-/-}</i> MEF cells.	132
I	Transcriptional regulation of <i>C. elegans</i> CTR1 candidate genes by Cu	146
II	Cu-dependent neuropeptides maturation is associated with Cu avoidance behavior	148
III	Cox1 abundance of P10 Veh/ES administered <i>Ctr1^{hrt/hrt}</i> mice.	149
IV	ES supplementation rescues reproduction and survival defects in copper-deficient <i>C. elegans</i>	150

List of Abbreviations

ANOVA	Analysis of variance
ATP	Adenosine triphosphate
BCS	Bathocuproinedisulfonic acid
BBB	Blood-brain-barrier
BLAST	Basic Local Alignment Search Tool
BW	Body weight
CCO	Cytochrome c oxidase
CCS	Copper chaperone for superoxide dismutase
Cd	Cadmium
chca-1	<i>CTR1</i> Homolog required for Copper Accumulation
Cp	eruloplasmin
CTR1	High affinity copper uptake protein 1
Cu	Copper
CuCl ₂	Copper(II) chloride
CuRE	Copper response element
DMSO	Dimethyl sulfoxide
ES	elesclomol
ETC	Electron transport chain
Fe	Iron
GFP	Green fluorescent protein
hCMEC/D3	human cerebral microvascular endothelial cell
ICP-MS	Inductively coupled plasma-mass spectrometry
IMS	Intermembrane space
LDH	Lactate dehydrogenase
MBD	Metal binding domain
MEF	Mouse embryonic fibroblast
MRE	Metal responsive elements
MT	Metallothionein
MTF-1	Metal-responsive transcription factor-1

NGM	Nematode growth medium
Ni	Nickle
PAM	Peptidylglycine Î-amidating monooxygenase
PBS	Phosphate-buffered saline
PCR	Polymerase chain reaction
Pt	Platinum
P10	Postnatal day 10
ROS	Reactive oxygen species
RT-PCR	Reverse transcription quantitative PCR
SDS-PAGE	Sodium dodecyl sulfate polyacrylamide gel electrophoresis
SOD1	Cu, Zn superoxide dismutase
TEER	Trans epithelial electrical resistance
TGN	trans-Golgi network
TMD	Transmembrane domain
WGA	Wheat germ agglutinin
WT	Wild-type or wild-type brood/litter mate
Zn	Zinc

Chapter 1: Introduction

Copper (Cu) is a crucial micronutrient required for a wide range of catalytic reactions in living organisms. It serves as a cofactor in Cu-dependent enzymes necessary for mitochondrial ATP synthesis, iron homeostasis, myelination, pigmentation, neurotransmission and various other physiological processes [1, 2, 3, 4]. Most of these Cu-dependent catalytic reactions involve the redox change between Cu(I) and Cu(II). Dietary Cu deficiency or mutations in genes regulating Cu homeostasis can lead to diseased states such as poor growth and development, and cognitive disorders[5, 6]. However, Cu overload can also be toxic to both eukaryotic and prokaryotic cells, as cycling between the two redox states can yield highly toxic free radicals through Fenton reactions. Cu is additionally reactive to thiol groups and may disrupt protein structure upon binding when presence in excess [7, 8, 9]. Therefore, organisms have adopted elaborate Cu homeostatic mechanisms to regulate Cu uptake, detoxification, and distribution at both the cellular and systemic levels.

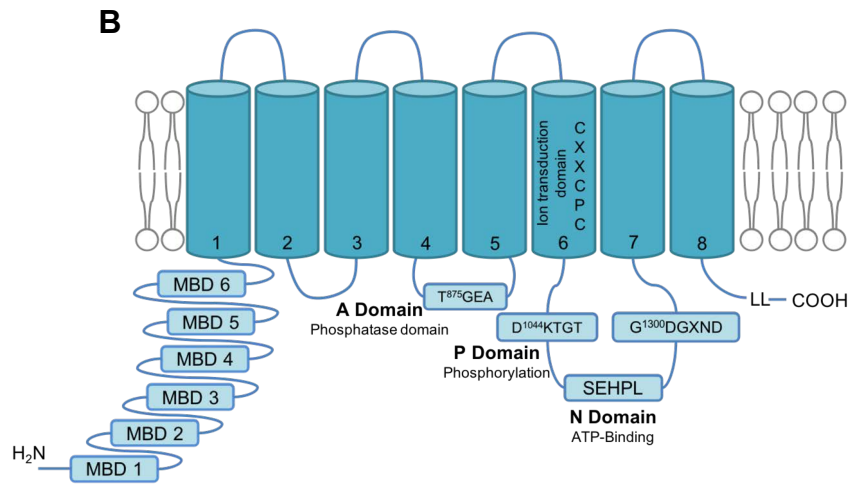
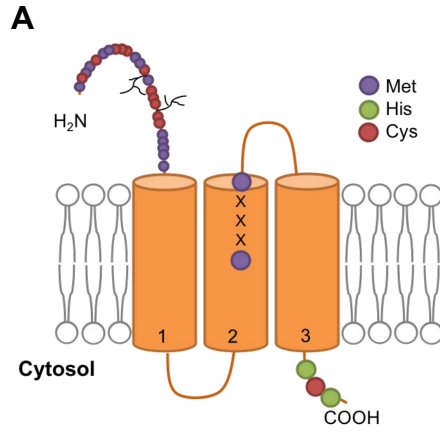
1.1 Cellular Cu homeostasis

1.1.1 Cu uptake

Before entering the cells, Cu is thought to first be reduced from the Cu(II) to the Cu(I) state by a metalloreductase. In *Saccharomyces cerevisiae*, the FRE family of reductases facilitates both iron (Fe) and Cu reduction [10]. In mammalian cells, Steap2, Steap3, Steap4 and DcytB function both as ferric and cupric reductase *in vitro* [11, 12]. The *in vivo* functions of these metalloreductase in Cu uptake are yet to be confirmed.

Cu(I) is imported into eukaryotic cells by the membrane-bound high-affinity copper uptake protein (Ctr). Ctr was first identified in yeast and plant, leading to the discovery of several Ctr family members in humans, mice, fruit flies, and other species by homology searches and functional complementary studies [13]. All characterized Ctr proteins contain a methionine (Met)-rich extracellular amino-terminus and three putative transmembrane domains (TMD) with a Met-X₃-Met domain within or close to the second TMD. Electron crystallography revealed that human Ctr1 (hCtr1) can form trimers at the plasma membrane [14, 15, 16]. The extracellular N-terminal methionine-rich domain, the Met-X₃-Met motif and the cytosolic C-terminal Cys-His-Cys motif are potential Cu binding sites necessary for effective Cu transport [17, 18, 19]. Furthermore, hCtr1 is both N-linked and O-linked glycosylated at the amino terminus at positions Asn15 and Thr27. Glycosylation stabilizes and protects Ctr1 from truncation and internalization [20, 21]. Ctr1 also contains an

Figure 1.1: Predicted topology of human CTR1 and ATP7A. A) Topological model of CTR1 reveals three transmembrane domains with an extracellular Met- and His-enriched N-terminus. The N-terminus also contains two glycosylation sites. The Met-X₃-Met motif is conserved for Cu transport. B) ATP7A contains eight transmembrane domains and an intracellular N-terminus which has six Cu-binding domains. Other highly conserved domains including the phosphatase (A domain), phosphorylation (P-domain) and ATP-binding (N-domain) domains. The dileucine (LL) motif close to the C-terminus is required for internalization.



AP2 μ 2 subunit binding motif, TNSM, in the C-terminus that potentially mediates clathrin-dependent endocytosis [22] (Figure 1.1A).

In human cells, the K_m of Ctr1 for Cu uptake ranges from 1-10 μ M [14, 23], with high metal specificity. The uptake efficiency can be influenced by extracellular pH, as well as Cu and potassium concentrations *in vitro*. In addition to Ctr1, the human zinc importer, hZIP4, has been demonstrated to have Cu(II) transportation activity *in vitro* [24]. While structural models indicate that hCtr1 contains a pore-like structure similar to ion channels, Ctr1 exhibits concentration-dependent Cu uptake and saturates at a rate of ~ 10 ions/s in kinetic assays. This rate is consistent with other transporter proteins, rather than channels that capable of transporting close to the rate of diffusion at $\sim 10^8$ ions/s [14, 15, 16, 25, 26]. Organisms may coordinate multiple Ctr orthologs in order mediate Cu uptake. varying Ctr homologs may be enriched in different cellular localizations, expressed in distinct tissues, expressed during different developmental stages, or as determined by Cu availability. For example, *Drosophila melanogaster* expresses three *Ctr1* genes, *Ctr1A*, *Ctr1B*, and *Ctr1C*. While Ctr1A is ubiquitously and constitutively active through the whole body and all developmental stages, Ctr1B is essential for intestinal Cu uptake in early-mid larvae stages and is transcriptionally upregulated by Cu-deficiency, and Ctr1C functions to transport Cu into the male germline [27, 28, 29]. Yeast Ctr1 and Ctr3 localize to the plasma membrane for Cu intake, and Ctr2 localizes to the vacuolar membrane, suggesting its role is to export Cu from vacuoles [18, 30]. Yeast *CTR1* is transcriptionally upregulated by low Cu through binding of the Mac1 transcription factor to the *CTR1* promoter (CuRE). *D. melanogaster* Ctr1B transcripts

are induced under Cu deprivation via the transcription factor MTF-1 [31, 32].

Mouse and human genomes harbor two Ctr homologs, Ctr1 and Ctr2. Ctr2 shares high sequence and structural similarity to Ctr1, but contains a shorter extracellular N-terminus. While Ctr1 localizes to the plasma membrane and intracellular vesicles required for dietary Cu absorption, Ctr2 is enriched in endosomes, facilitates truncation of the Ctr1 N-terminus ectodomain via Cathepsin B/L proteases, and potentially mediates Cu export from endosomes via truncated Ctr1 [33, 34]. In addition, it has been reported that Ctr1 and Ctr2 physically interact with each other and Ctr2 protein stability depends on the presence of Ctr1 [35]. In mammals, there is no evidence of transcriptional regulation of *Ctr1* by Cu. Instead, mammalian Ctr1 subcellular localization and protein stability are regulated post-translationally. When Cu abundance increases, plasma membrane localized Ctr1 undergoes clathrin-dependent endocytosis and proteasome-mediated posttranslational degradation, in order to prevent excessive Cu accumulation [26, 36]. In mice, depletion of the Cu chaperone Sco1 for mitochondria cytochrome c oxidase assembly induces Ctr1 turnover in the liver as well as Ctr1 mislocalization in the heart, [37, 38].

Cu acquisition via Ctr1 is vital to maintaining cellular and systemic Cu homeostasis. Depleting Ctr1 in mice and zebrafish results in lethality at the embryonic stage [39, 40]. Conditional knockout of this gene in the mouse intestine leads to severe viability defects due to Cu deficiency in peripheral tissues, cardiac hypertrophy, and accumulation of non-bioavailable Cu in the intestine [41].

1.1.2 Cu delivery to the secretory pathway and efflux via ATP7A/B

ATP7A and ATP7B are two mammalian P-type ATPases that are required for delivering Cu(I) to several newly synthesized cuproenzymes in the trans Golgi network (TGN), and exporting excess Cu from cells via the plasma membrane. *ATP7A* and *ATP7B* share around 60% DNA sequence homology and exhibit comparable topology. They are both transmembrane proteins containing eight TMDs, with the N- and C-termini both facing the cytosolic side of the membrane. Cu can associate with the six metal binding domains (MBD) present in the N-terminus, with each domain containing a conserved *Met-X-Cys-X₂-Cys* Cu-binding site [42, 43, 44]. These P-type ATPases harbor another metal binding site, the M domain, and Cu binding to the M domain is necessary to trigger ATPase-dependent Cu transport. Several conserved domains, including the *Cys-Pro-Cys* (CPC) in TMD6, the *Asp-Tyr* (YN) in TMD7 and TMD8 *Met-X₂-Ser* (MxxS) motifs are required to incorporate Cu into the M domain. During one catalytic cycle, ATP first binds to the ATP-binding domain (N) and Cu(I) binds to the MBD and M domains. Next, ATP is phosphorylated in the phosphorylation domain (P) at the *Asp-Lys-Thr-Gly* (DKTG) motif, which is coupled with the release of Cu(I). The cycle is then finished by the dephosphorylation of the intermediates in the actuator domain (A) [45, 46]. In addition, the C-terminus of ATP7A/B contains a dileucine motif required for trafficking to the TGN from the plasma membrane, and ATP7B has an F₃₇AFDNLVGYE₄₅ sequence involved in targeting to the apical membrane in polarized cells [47, 48].

In cultured cells, ATP7A and ATP7B localize to the TGN under basal con-

ditions. When Cu level rises, ATP7A re-distributes to intracellular vesicles and/or basolateral membranes, and protein expression is stabilized. In contrast, depending on the cell type, ATP7B re-localizes to apical membrane or vesicles in the presence of high Cu [49]. ATP7B also undergoes a kinase-mediated phosphorylation induced by Cu [50]. In the mouse intestine, ATP7A localizes to the TGN under basal and dietary Cu-deficiency conditions, and traffics to vesicles near the basolateral membrane after Cu administration. In the liver, ATP7A and ATP7B are mainly expressed in hepatocytes. ATP7B expression can be found in the TGN and intracellular vesicles, as well as the canalicular membrane [51].

In humans, ATP7A is ubiquitously expressed and required for dietary Cu absorption and peripheral tissue Cu transport. Dysfunction of *ATP7A* can lead to Menkes disease in humans with poor Cu distribution in peripheral tissues (See Section 1.3). ATP7B is highly expressed in the liver, and is involved in biliary Cu excretion and Cu delivery to cuproenzymes such as ceruloplasmin [52]. ATP7B expression also can be detected at lower levels in the brain, kidney, intestine and placenta. Mutations in the *ATP7B* gene are associated with Wilson's disease. Wilson's patients exhibit overloaded Cu in the liver and brain that may lead to hepatic disease, central nervous system dysfunction, and death. The administration of zinc acetate to patients has been approved in order to induce the expression of Cu chaperone metallothionein (MT) and limit Cu absorption from the gut [53].

1.1.3 Intracellular Cu distribution and storage

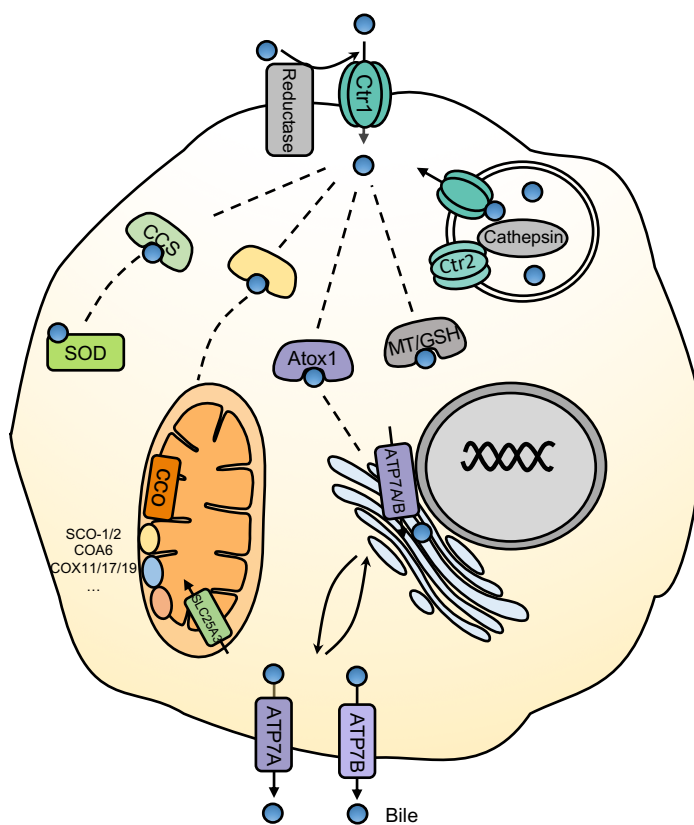
After being imported into cells by Ctr1, Cu(I) is transferred to several chaperone proteins and then delivered to Cu-dependent enzymes in various subcellular compartments, such as the mitochondria and TGN. At the same time, several metal-binding proteins can sense free cytosolic Cu levels and protect cells from toxicity effects (Figure 1.2). The Cu chaperone for superoxide dismutase (CCS) is a Cu binding protein distributed in the cytosol and the mitochondria intermembrane space (IMS) to mediate Cu transfer to Cu, Zn superoxide dismutase (SOD1). The production of reactive oxygen species (ROS) such as hydroxyl radicals and superoxide is intrinsically coupled with mitochondria respiration and these species are harmful to cells. The reaction of Cu(I) with O_2 in the mitochondria generates superoxide and hydrogen peroxide (H_2O_2), and H_2O_2 may further react with Cu(I) to produce highly active hydroxyl radical [54]. SOD1 reduces cellular oxidative stress by converting superoxide to less damaging H_2O_2 and O_2 through the reduction and oxidation of Cu [55]. Deletion of CCS in yeast cells does not affect SOD1 abundance, but interferes with Cu delivery to activate SOD1 functions, and thus CCS-null cells are more susceptible to high levels of ROS [56]. CCS protein abundance is inversely correlated with intracellular Cu levels, as Cu deficiency stabilizes CCS and elevated Cu triggers its degradation through proteasome-mediated pathways. The Cys-X₂-Cys and Cys-X-Cys motifs in CCS domains I and III are responsible for Cu binding to CCS, and domain II is involved in CCS docking to SOD1. In addition, Cu binding to domain III is required for Cu-dependent CCS turnover: Cu binding alters the

conformation of CCS and exposes a *Lys* residue for ubiquitination and degradation [57, 58].

Cu chaperone antioxidant-1 (Atox1) is responsible for delivering cytosolic Cu to ATP7A/B in the TGN and facilitating of Cu excretion. Atox1 localizes to the cytosol and nucleus, and its distribution and abundance are not altered by Cu levels. Atox1 physically interacts with ATP7A/B, and is required for ATP7A exiting from the TGN under elevated Cu conditions. *Atox1* contains a Cu binding motif that shares high similarity with the fourth MBD of ATP7A/B (*Met-X-Cys-X₂-Cys*). Atox1 depletion in cells results in accumulated Cu levels and decreased cuproenzyme activities, and *Atox1*^{-/-} mice exhibit defects in systemic Cu delivery and die within a few weeks after birth [59, 60]. In addition, Atox1 has been proposed to function as a Cu-induced transcriptional factor to regulate cell proliferation [61].

Metallothioneine (MT) is a small, cytosolic, *Cys*-rich protein that is capable of binding several heavy metals, including copper, zinc, selenium and cadmium. There are four MT isoforms in humans. MT1 and MT2 are highly expressed in the intestine, liver and kidney, while MT3 and MT4 are enriched in the brain and skin. Under Cu overload conditions, Cu binding to MT could protect cells from toxicity [62]. Though MT-depleted mice exhibit normal growth and reproduction, they are susceptible to heavy metal-induced oxidative stresses and inflammatory reagents [63]. On the other hand, Cu stored by MT is vital for cells to survive under Cu-limited conditions [64, 65]. In fruit flies and mice, elevated Cu induces the binding of the transcription factor MTF-1 to the metal responsive elements (MREs) in the promoter of the MT gene, and triggers MT gene expression [66]. Besides MT, Cu

Figure 1.2: Cellular Cu metabolism in mammalian cells. Cu is imported as Cu(I) by the Cu transporter Ctr1. Ctr2, the other CTR ortholog, facilitates Ctr1 truncation and Cu export from endosomes. Once entering the cells, Cu(I) binds several chaperone proteins and is delivered to different subcellular destinations: CCS transfers Cu to the Cu, Zn superoxide dismutase (SOD); Atox1 delivers Cu to the Cu exporter ATP7A/B; and COX17 and other chaperones mediate Cu delivery to cytochrome c oxidase in mitochondria. Cu can be stored by metallothionein and glutathione, and excess Cu can be exported by ATP7A into circulation, or secreted into bile by ATP7B.



can also be stored by glutathione (GSH). In GSH-depleted mammalian cells, a Ctrl expression-independent reduction of Cu uptake was observed, suggesting a role for GSH in handling Cu at the entry step [25, 67].

Cu delivery to the mitochondria is crucial for ATP biosynthesis. The Cu-dependent enzyme cytochrome c oxidase (Cco) is the fourth enzyme complex in the electron transport chain (ETC) required for the buildup of the electron gradient in the IMS. The mitochondrial matrix contains a ligand-bound Cu pool that is necessary for Cu incorporation into Cco. Thus, Cu needs to be transported from the cytosol to the mitochondrial matrix and from the matrix to the IMS. The cytosolic and mitochondria IMS-localized Cox17 (COX assembly factor 17) was hypothesized to transport Cu from the cytosol to mitochondria. However, *COX17*-depleted yeast cells have normal mitochondrial Cu pool and normal Cco activity, suggesting alternative machinery for Cco Cu delivery [68, 69, 70]. To date, several Cu chaperones are characterized for their function in this process, including Sco1, Sco2, Coa6, Cox17, Cox11, Cox19 [71, 72, 73, 74, 75, 76]. The delivery of Cu from the mitochondrial inner membrane to the matrix is carried out by the phosphate transporter SLC25A3 (yeast Pic2) [77], yet no transport mechanism is reported to deliver Cu from the matrix to the IMS. In the IMS, Cox17 transfers Cu to Sco1 and Cox11. Sco1 is crucial for incorporating Cu into the Cu_A site in Cco, facilitated by assembly factors Sco2, Coa6 and Cox20. Meantime, Cox11 and several other Cco assembly factors (Cox19, Cox23, Coa5) are responsible for Cu_B site metalation in the IMS [78]. Human patients harboring mutations in *SCO1*, *SCO2* or *COA6* exhibit low Cco activity and syndromes such as cardiac hypertrophy, hepatic failure, and en-

cephalopathy. [79, 80, 81, 82]. Although Cu supplementation could rescue Cco activity in patient-derived cells, it failed to alleviate major symptoms in human patients [83].

1.1.4 Cuproenzymes and function

Here we describe several important Cu-dependent enzymes and their functions in living organisms. Other cuproenzymes and functions are listed in Table 1.1 [84]. Tyrosinase is an oxidase involves in two catalytic steps during melanin synthesis. It requires two Cu atoms in its active site in order to interact with dioxygen and oxidize the substrate. Tyrosinase first oxidizes tyrosine to DOPA and then converts the diphenol in DOPA to quinone. Dopakinone can then be converted to dihydroxyindole and then to melanin in the following reactions. In humans, tyrosinase is highly expressed in the melanosomes of melanocytes in skin and eyes. Tyrosinase dysfunction leads to low pigmentation and vision defects [85, 86].

Dopamine- β -hydroxylase (DBH) is required to convert dopamine to norepinephrine (NE) in the central and peripheral nervous systems. Coupled with this reaction, ascorbic acid and O₂ are converted to dehydroascorbate and water, respectively. NE is an essential neurotransmitter that participates in numerous physiological pathways. It is involved in the regulation of heart rate and blood pressure, glucose and lipid homeostasis, food digestion and renal reabsorption. Cu deficiency in the brain results in low DBH activity and is correlated with several neuronal disorders [87].

Table 1.1: List of cuproenzymes and their functions.

Category	Cuproenzyme	Function
Monooxygenase	Tyrosinase (Monophenol monooxygenase)	Initiate melanin formation from tyrosine
	Peptidylglycine α -amidating monooxygenase (PAM)	Peptides amidation with α -terminal carboxylic acid group of glycine
	Dopamine β -hydroxylase (DBH)	Neurotransmitter norepinephrine generation from dopamine
Oxidase	Cytochrome c oxidase (CCO)	Electron transport in mitochondria
	Galactose oxidase	Catalyzes the oxidation of D-galactose to D-galactohexodialdose in fungi
	Amine oxidase	Deamination of amines and form aldehyde and ammonia
	Protein-lysine-6-oxidase (lysyl oxidase)	Collagen and elastin cross-linking formation (one type of amine oxidase)
	Superoxide dismutase	Superoxide dismutation and antioxidant defense
	Ceruloplasmin (Cp)	Serum ferroxidase
	Hephaestin	Ferroxidase in the intestine
	Ascorbate oxidase	Acting on diphenol of L-ascorbate and convert to dehydroascorbate and H ₂ O
Laccase	Oxidize phenol groups of lignin precursor in order to form cross-linking in plants and fungi	

Neuropeptides serve as signaling molecules for neuronal communication and the regulation of brain activities. Maturation of more than half of neuropeptides to their active form requires amidation by the cuproenzyme peptidylglycine α -amidating monooxygenase (PAM). Loss of PAM is embryonic lethal in mice [88, 89]. PAM contains two functions domains, the peptidylglycine α -hydroxylating monooxygenase (PHM), and the peptidyl- α -hydroxyglycine α -amidating lyase (PAL). In order to be active, PHM must bind two Cu ions. First, PHM hydroxylates the carbon of the peptidylglycine, and then PAL catalyzes the cleavage of nitrogen-carbon bond that generates the amidated peptide [90].

Ceruloplasmin and hephaestin are both Cu-containing ferroxidases. Ceruloplasmin is synthesized in the liver and requires six Cu ions delivered from ATP7B to achieve oxidase function. Ceruloplasmin is primarily a soluble serum oxidase, and ferric ions oxidized by ceruloplasmin can bind transferrin in the blood and then be mobilized to other tissues. Hephaestin is a transmembrane protein expressed in the small intestine required for dietary iron absorption. It functions together with the iron transporter ferroportin in the basolateral membrane of enterocytes to mobilize iron exported from the intestine to circulatory system [91, 92]. Cu deprivation in the intestine would decrease hephaestin activity and lead to systemic iron deficiency.

Lysyl oxidase (LOX) is involved in generating collagen and elastin cross-linking by catalyzing the formation of aldehydes from lysine residues. Cu binding to apo-LOX triggers electron transfer and deamination of lysyl groups in collagen and elastin precursors. Formation of cross-linking is essential to stabilize these fibrils and support tissue structures [93, 94].

1.2 Mammalian Cu homeostasis at the organismal level

1.2.1 Dietary Cu uptake and transport into circulation

The intestinal epithelium is the main site for dietary Cu absorption, and the daily Cu uptake amount ranges 0.6-2.4 mg on average in adult humans [95]. Dietary Cu(II) is reduced, and Cu(I) is imported into enterocytes via Ctr1 localized to the apical membrane. Cu then binds to chaperone proteins and is either targeted to different subcellular destinations, exported, or being stored, as described above. Under Cu adequate conditions, biotin-labeled Ctr1 localized to both the apical surface and intracellular vesicles in the mouse intestine. Ctr1 was localized mainly on the apical membrane when mice were fed with Cu-deficient diet [36]. The expression of Ctr1 is also age-dependent, as infant mice express higher levels of Ctr1 protein compared to adults. This is in accordance with a decrease in systemic Cu levels over time [96]. In mice fed a standard diet, ATP7A localizes primarily to the TGN. After an increase in dietary Cu uptake, ATP7A re-localizes to vesicles close to the basolateral side of enterocytes in order to mediate Cu efflux to the portal circulation [97]. No age-dependent expression regulation has been observed for ATP7A.

Cu in the circulatory system likely binds to ligands in order to be transported to peripheral tissues, as free Cu is oxidative active and harmful. It has been suggested that up to 95 % of Cu in the circulation is bound to ceruloplasmin (Cp) for peripheral delivery. However, Cp-depleted mice exhibit normal tissue Cu distribution [98]. Albumin and macroglobulin may also bind Cu with lower affinity in

the blood stream, but have been demonstrated not essential for systemic Cu transportation, suggesting an alternative but yet unknown mechanism of Cu circulation [99, 100].

1.2.2 Hepatic Cu storage and excretion

Liver is the primary organ for Cu storage and regulation of systemic Cu homeostasis. After export from the intestine, Cu in the circulation is imported into liver by hepatic Ctr1 [96]. When administering high doses of Cu to mice through subcutaneous injection, the increased Cu predominantly accumulates in the liver, with little change of Cu levels in other tissues such as heart, brain or serum. The expression of hepatic Ctr1 is induced simultaneously, indicating Cu uptake through hepatic Ctr1 is responsible for systemic Cu detoxification [101].

Cu stored in the liver can be mobilized to peripheral tissues, transferred into cuproenzymes such as Cp, or excreted into the bile if present in excess. ATP7A is presumably required for exporting Cu from the liver to peripheral tissues, as suggested by elevated hepatic ATP7A expression together with increased serum Cu in the cardiac-specific Ctr1 knockout newborn mice [102]. The function of hepatic ATP7A may be vital during the early postnatal stage, as ATP7A protein abundance decreases from newborn to adulthood. This is in accordance with the total Cu stored in the liver, which remains high around birth and is gradually reduced over the course of life span [103, 104]. Future studies are required to elucidate the functions of liver ATP7A. Excess Cu in the liver is excreted into bile by ATP7B. Elevated

Cu in hepatocytes induces ATP7B trafficking from the TGN to vesicles close to the apical surface for Cu excretion [105, 106, 107]. Notably, COMMD1 (Cu metabolism Murr1 domain 1) is required to stabilize hepatic ATP7B protein and to maintain its proper function [108].

1.2.3 Cu metabolism in heart, kidney and brain

Kidneys balance nutrient homeostasis in the circulation via nutrient filtration from the blood into primary urine and via reabsorption into renal tubules. Little is known regarding Cu trafficking and regulation in the kidney. Urinary Cu levels are highly induced if biliary Cu excretion is blocked or decreased in *ATP7B*^{-/-} mice and by hepatic *Ctr1* deletion. These observations suggest an active role for the kidney in regulating systemic Cu homeostasis [109, 110]. *Ctr1* is expressed in both proximal and distal tubules and may import Cu from primary urine back to renal cells. This is supported by elevated *Ctr1* expression levels in dietary Cu-deficient mice [96]. *ATP7A* and *ATP7B* are both expressed in renal tubules, and *ATP7A* localizes to the basolateral membrane under high Cu conditions, indicating a possible function in exporting Cu from renal cells back into the blood [111].

Relative to other organs, cardiac tissue contains a large amount of mitochondria and is in high demand of Cu to maintain proper mitochondrial function for contraction. Dietary Cu deficient animals exhibit cardiac hypertrophy and abnormal mitochondrial morphology and function, which can be rescued by supplementing Cu back through the diet [112, 113, 114]. In addition, cardiac-specific *Ctr1* deple-

tion in mice resulted in low Cu and cuproenzyme levels in the heart, cardiac Cu hypertrophy, and failure to survive beyond two weeks after birth [102]. Though cardiac hypertrophy can be caused by exercises and pregnancy, prolonged hypertrophy may lead to cardiac dysfunction and heart failure [115, 116].

The brain requires a steady amount of Cu for neurological development and proper functions during peptides maturation and neurotransmitter production through Cu-dependent enzymes as described above. Meanwhile, Cu overload in the brain could result in neurodegeneration and other disorders. In the brain, Ctr1 is localized to the apical membrane of choroid plexus cells and endothelial capillaries. The expression of Ctr1 can be induced by Cu deficiency, indicating a role for Ctr1 in facilitating Cu uptake from cerebrospinal fluid. ATP7/B is expressed in most brain regions, and similar to other tissues, ATP7A/B expression levels in the brain are also age-dependent [117, 118]. How neuronal Cu is being stored and utilized, and how Cu metabolism is regulated in the brain will need to be elucidated in the future.

1.2.4 Cu homeostasis in *C. elegans*

Caenorhabditis elegans (*C. elegans*) is a genetically tractable, multi-tissue organism that has been proven to be amenable to nutrient absorption and distribution studies using zinc, iron and heme [119, 120, 121, 122]. Several orthologs of Cu binding proteins have been identified in worms by sequence homology studies, including CUA-1 (ortholog of ATP7A/B), CUC-1 (Atox1), MTL-1/2 (MT), GCS-1(GSH), SCO-1(Sco1/2), SOD-1(Sod1), COX-17(Cox17), TYR-1-6 (Tyrosinase),

CCO-1(Cco), TBH-1(DBH), as well as putative orthologs for PAM and SLC25A3. Interestingly, no CCS ortholog has yet been identified in worms. The activation of *C. elegans* Cu, Zn-Sod can be achieved in the absence of CCS, but potentially requires GSH for proper activity [123].

Among the components that are required for Cu trafficking, the functions of metallothionein, as well as CUC-1 and CUA-1 have been delineated in *C. elegans* [124, 125]. Expressing the *cua-1* gene could complement the function of yeast Cu exporter by rescuing the growth defect of *ccc2 Δ* cells. In *C. elegans*, *cua-1* is expressed in the intestine, hypodermis, pharynx and neurons. Depletion of *cua-1* causes lethality under Cu deficient conditions that can be rescued by Cu supplementation. Intestinal CUA-1 localizes to the basolateral membrane under basal and Cu-deficient conditions, and traffics to gut granules upon dietary Cu supplementation or Cu injection to the pseudocoelom. This trafficking likely functions to protect peripheral tissues from Cu toxicity. In addition, hypodermal *cua-1* transcription can be induced by Cu deficiency. These findings suggest CUA-1 as a key intestinal Cu exporter responsible for maintaining systemic Cu homeostasis [126, 127, 128]. However, mechanisms by which the *C. elegans* intestine acquires Cu have yet to be characterized.

C. elegans metallothioneins *mtl-1/2* are expressed in the intestine, and the expression of both genes can be induced by the heavy metal cadmium (Cd). Despite the fact that *mtl-1/2*-depleted worms are highly susceptible towards several heavy metals, high concentrations of Cu or Zn are not able to increase *mtl-1/2* expression in *C. elegans*. MTL-1 and MTL-2 have different affinities towards Cd and Zn,

suggesting distinct roles of two MT isoforms in worms. In addition, the promoter of *mtl-2* contains a TATAA box and a MRE sequence and requires the transcription factor ELT-2 to initiate the expression [129, 130, 131, 132]. However, because no MTF-1 or Mac1 homologs have been identified in *C. elegans*, the metal-sensing transcriptional regulators for MTs remains elusive. Worms may adapt unique mechanisms for heavy metal-induced transcriptional regulation [133, 134].

1.3 The anti-cancer drug elesclomol in Cu homeostasis

1.3.1 Elesclomol-Cu(II) as cancer therapy

Elesclomol (STA-4783) is a synthesized chemical compound with the formula of N-malonyl-bis (N'-methyl- N'- thiobenzoylhydrazide). It was originally derived from a screen for molecules with potent proapoptotic activity and has become a first-in-class anti-cancer drug. Elesclomol induces mitochondria oxidative stress by generating reactive oxygen species (ROS) in cancer cells through its interaction with copper [135, 136, 137]. Since 2004, several phase I-III studies have been conducted using elesclomol, with regards to its efficacy in treating several types of cancers, such as metastatic melanoma, prostate cancer, ovarian epithelial cancer, solid tumor, myeloid leukemia, etc. [138, 139, 140].

1.3.1.1 Elesclomol achieves cytotoxicity through its interaction with copper

Cancer progression is often coupled with increased demand for nutrient and energy. With sufficient energy supplementation, cancer cells tend to become hypoxic, invasive, and relatively resistant to treatments like radiation and chemotherapy. During cancer development, the mitochondria plays a vital role: it is not only responsible for energy production, but also participates in ion homeostasis, programmed cell death, and oxidative stress regulation. Cancer cells commonly exhibit altered mitochondrial morphology and redox status, with increased levels of reactive oxygen species [141, 142, 143, 144]. Interestingly, the build-up of ROS could further stimulate oncogenic pathways that favor cell proliferation. However, on the contrary, high ROS levels in cancer cells result in a lower antioxidant capacity. This provides a potential therapeutic strategy by providing high levels of oxidative stress to cancer cells that exceed the threshold for cells to survive. Because normal cells maintain low levels of ROS, they are less susceptible than cancer cells, as long as the oxidative stress inducer is administrated at the correct dose. This is supported by several studies, demonstrating increased cellular ROS levels could effectively erase cancer cells in vitro. Meanwhile, at similar doses, elesclomol showed little to no impact on normal cells [145, 146, 147].

As one of the ROS-inducing drugs, ES administration to a variety of mammalian cancerous cells in culture induces the expression of stress responsive genes including several heat shock proteins, and cell survival proteins and metallothionein.

Meanwhile, within a few hours of administration, cells accumulate high levels of ROS, followed by increased expression of apoptotic genes, reduced mitochondrial membrane potential and leakage of mitochondrial components to into the cytosol [148, 149]. Studies further revealed the interaction with Cu(II) is required for ES cytotoxicity effects [150, 151].

Among metal ions that are able to form complexes with elesclomol, Cu(II) is strongly preferred over zinc, iron, or manganese in competition assays. Cu binds to elesclomol at a 1:1 ratio; the coordination between Cu, sulfur, and nitrogen atoms changes elesclomol to a flat structure and yields a highly hydrophobic molecule, enabling the complex to penetrate cell membranes [152]. The complex is highly stable, as a competition assay at pH 7.4 suggested a 24-fold stronger binding of ES-Cu(II) compared with TRIEN-Cu(II), the latter of which has a stability constant of 10^{-20} M [153, 154, 155]. Although elesclomol could also bind platinum and nickel to form cell membrane-permeable complexes, the elesclomol-Cu(II) complex exhibits much higher cytotoxicity than complexes with Ni(II) or Pt(II), possibly due to the low redox potential of Ni(II) or Pt(II) complex [154]. Under Cu-deprived conditions, elesclomol failed to enter cells or induce apoptosis in cultured cancer cells, suggesting that the drug must enters cells as an ES-Cu(II) complex.

Upon entering cells, the ES-Cu(II) complex preferentially delivers Cu to mitochondria. Cu is then disassociated while ES is shuttled outside of the cell. This is supported by the highly increased radiolabeled Cu levels and less accumulation of ES in the cell shortly after drug administration. Approximately 80% of ES-bound Cu was found in mitochondria, around 14% was distributed in the cytosol and 6% in

the nucleus [156]. The selective accumulation of ES-bound Cu in the mitochondria is unique, and likely accounts for its cytotoxic effect. When compared to another Cu chelator that also induces oxidative stress, disulfiram (DSF), DSF-Cu is mainly retained in the cytosol and exhibits weaker potency in triggering apoptosis than ES-Cu [157, 158, 159]. To date, it is not yet clear how ES-Cu selectively targets the mitochondria.

A comprehensive screen of the yeast deletion collection suggests that ES does not target any specific protein in the cytosol [160, 161]. Nonetheless, yeast with homozygous gene deletions related to electron transport, cytochrome assembly and Cu-related functions revealed high sensitivity to ES administration. Another observation noted that ES-Cu(II) in mitochondria can be quickly reduced to Cu(I), accompanied by the generation of ROS and followed by mitochondria apoptosis in cancer cells [156]. Interestingly, the redox potential of Cu(II) to Cu(I) matches the potential drops in electron transport chain (ETC), suggesting the association between Cu redox and electron transport in mitochondria [23]. Taken together, these findings suggest the possibility that ES-Cu(II): 1) generates ROS through the redox property of Cu after Cu(II) disassociates from ES, perhaps utilizing electrons and redox potential in the ETC; 2) relies on the interaction with ETC components to release Cu(I) from ES, leading to the release of free radicals during the reaction; 3) the possibility that 1) and 2) can take place together to trigger apoptosis. Further studies are required to elucidate this mechanism.

1.3.1.2 Clinical study of elesclomol in cancer treatment: progress and limitations

Elesclomol has been tested with hundreds of cancer or cancer-derived cell lines and revealed to potently kill almost all cancer cell types *in vitro*, with IC₅₀ below 100 nM (results available online from Sanger Institute). Unlike most other Cu-based anti-cancer drugs, little to no toxicity effect was observed in normal cells.

Human clinical studies involving elesclomol were launched in 2004. Several Phase I and II studies demonstrated improvements in progression-free survival and risk reduction for the disease in patients suffered from myeloid leukemia, refractory solid tumors, peritoneal cancer, and stage IV metastatic melanoma, after several weeks of ES administration [138, 139, 140, 162, 163, 164]. ES was often administered together with Paclitaxel, an anti-cancer drug targeting the disruption of microtubules, and the efficacy of which positively correlated with cellular ROS levels [165]. By elevating the oxidative stress, ES may improve the overall efficacy of Paclitaxel when treated in a combination.

Combined results from Phase II and III trials suggested that the therapeutic benefit of ES, however, only applied to a subset of patients. This subset can be distinguished by patients' serum lactate dehydrogenase (LDH) levels. LDH is a cancer prognosis marker, and the levels of LDH in the bloodstream correlate with tumor hypoxia state and metabolism type. Hypoxic cancer cells tend to utilize glycolysis rather than oxidative phosphorylation for metabolism, resulting in high LDH levels in cytosol and circulation. On the contrary, ES mainly targets the

ETC in mitochondria; it may be more active in oxygenated cells with metabolically active mitochondria. This may explain why ES revealed efficacy only in patients with normal serum LDH [166]. In a randomized, double-blinded phase III study of elesclomol for stage IV metastatic melanoma on 651 patients, the combination of ES and Paclitaxel failed to see a significant improvement in progression-free survival when compared to Paclitaxel alone. This study was terminated later in 2014 [167]. Researchers are now looking for novel therapeutic strategies in parallel with ES administration [168, 169, 170, 171].

1.3.2 Elesclomol rescues mitochondrial function in copper-deficient models

1.3.2.1 Copper is required for mitochondria energy production

Cu is required for the assembly and activity of cytochrome *c* oxidase (Cco), the fourth enzyme complex of the ETC. Cco localizes to the mitochondrial inner membrane and is responsible for the reduction of the final electron acceptor oxygen during energy production. Cco consists of 14 subunits, among which Cox1 and Cox2 contain two Cu-binding sites, Cu_B and Cu_A, respectively. The Cu_A site accepts electrons from reduced cytochrome *c*, and Cu_B-heme a₃ is the site for oxygen reduction [172, 173]. Because Cox1 and Cox2 are expressed and assembled inside of mitochondria, Cu must be delivered from cytosol. Cu is thought to be stored in the mitochondrial matrix as a ligand-bound form and utilized as the major Cu source for Cco assembly in the IMS [70, 174]. Cu deficiency in the mitochondria disrupts

Cco assembly and results in respiratory defects.

1.3.2.2 Elesclomol administration restores mitochondrial function in genetic models of Cu deficiency

In a study conducted by S. Soma *et al.*, elesclomol stood out from several other copper-binding small molecules, and rescued Cco activity and mitochondrial Cu levels in *coa6*- and *sco2*-depleted yeast [175]. Unlike in cancer-related studies, the dosage of elesclomol used in this Cu-deficiency rescue study was carefully monitored to avoid over-production of oxidative stress and cytotoxicity. ES could also rescue the respiratory growth defect in yeast harboring mutations in the Cu transporters *ctr1*, *ccc2*, and Cu chaperones *ccs1* and *atx1*. In cultured cells, ES significantly rescued COX1 levels in *Ctr1*-depleted cardiomyocytes as well as in *SCO2* patient cells. Moreover, ES supplementation rescued low Cu-related phenotypes in both *Ctr1*- and *Coa6*- depleted zebrafish.

Given the fact that ES preferentially delivers Cu to mitochondria, it is exciting to observe the rescue phenotype by ES in *ccs1*- and *atx1*- mutant cells, suggesting that ES could potentially deliver sufficient amounts of Cu to cytosolic SOD and to the secretory pathway to rescue Cu-deficiency related disorders. This study shed light on the novel application of ES in treating cellular and mitochondria Cu deficiency disorders, and encouraged further studies in mammals using genetic Cu-deficient models and clinical-related models.

1.3.3 Copper deficiency-related genetic mouse models

While dietary-Cu deficient mice provided insights into systemic responses upon Cu depletion, genetic models are powerful tools for revealing functions of certain genes, discovering mechanisms of systemic Cu homeostasis, and characterizing therapeutic hypotheses. Mouse strains containing mutations in the two major Cu transporters, *Ctr1* and *ATP7A* are available. Whole body knockout of either *Ctr1* or *ATP7A* is embryonic lethal, suggesting normal Cu homeostasis is crucial for embryonic development [40, 176, 177]. This section describes *Ctr1* tissue-specific knockout models and disease-related *ATP7A* mutant mouse models.

1.3.3.1 Tissue-specific Ctr1 depleted mouse models

The role of Ctr1 in intestinal Cu absorption has been characterized using the intestinal *Ctr1* knockout mouse model (*Ctr1^{int/int}*). These mice exhibited poor Cu distribution in peripheral tissues and defects in growth and viability (with a median survival of 15 days). Cco and other Cu-dependent enzymes' activity were significantly reduced in the majority of peripheral tissues. Interestingly, the intestine of *Ctr1^{int/int}* mice accumulated high levels of non-bioavailable Cu. Other pronounced findings include cardiac hypertrophy and accumulated iron in the liver. These defects could be rescued by Cu-histidine administration at the early postnatal stage. The *Ctr1^{int/int}* mice is a useful model to study dietary and peripheral Cu-deficiency [41].

The cardiac-specific *Ctr1* depleted mouse (*Ctr1^{hrt/hrt}*) provides a novel aspect

towards understanding systemic Cu homeostasis regulation. *Ctr1^{hrt/hrt}* mice exhibit low heart Cu levels, reduced Cco activity and cardiac hypertrophy, and the median survival for these mice is 10 days. Cu storage levels in the livers are decreased, coupled with increased serum Cu levels, and hepatic ATP7A protein levels are upregulated. In addition, treatment with *Ctr1^{hrt/hrt}* mice serum induces ATP7A protein expression in cultured cells. These findings strongly suggest a potential systemic signaling communicating between the liver and heart to regulate Cu homeostasis [102]. This model has provided useful insights for several following studies to characterize to understand the function of Sco1 in heart [37, 178].

1.3.3.2 Menkes disease

Introduction to Menkes disease and *mottled* mice

Menkes disease (MNK) is a recessive disorder caused by mutations in the gene encoding the Cu transporter ATP7A, resulting in poor intestinal Cu absorption, poor renal reabsorption, inability of Cu to cross the blood-brain-barrier (BBB), and dysfunction of most cuproenzymes [107, 179, 180], including tyrosinase, lysyl oxidase, dopamine- β -hydroxylase and peptidyl- α -amidating monooxygenase. The incidence of Menkes disease ranges from 1 in 100,000 to 1 in 250,000 newborns. Symptoms of Menkes disease includes kinky hair, growth retardation, hypothermia, weak muscle tone, hypo-pigmentation, low serum ceruloplasmin levels and intellectual disability [181]. The majority of Menkes children die within three years if not given any treatment.

ATP7A protein is highly conserved among animals. It is a membrane protein consisting of eight transmembrane domains, an ATP binding domain, a cytosolic N-terminus containing six Cu-binding motifs, and several other conserved motifs required for proper ATPase function. In cultured cells, ATP7A traffics to the plasma membrane for Cu efflux under Cu sufficient conditions, and is localized to the trans-Golgi network (TGN) in the absence of Cu. TGN-localized ATP7A could deliver Cu to cuproenzymes in the secretory pathway. Thus far, around 370 *ATP7A* mutations have been identified in humans [6, 182]. The major types of mutations found in Menkes patients include missense mutations, splice site mutations, exon deletions, small deletions and nonsense mutations in *ATP7A* [183].

Mice carrying mutations in the *Atp7a* gene are named *mottled* mice, due to the lack of their coating pigmentation. So far, 109 *mottled* alleles have been identified: 24 resulted from spontaneous mutations, while others were generated by gene trapping, chemical induction or targeted mutagenesis [184]; so far 15 *mottled* mouse strains have been characterized. Among these strains, 8 are embryonic lethal, suggesting an important role of ATP7A for prenatal development. Macular, mosaic and brindled mutations are postnatal lethal around two weeks old. These strains share many common phenotypic features with human Menkes disease and serve as powerful tools for early postnatal therapeutic studies [185].

Current therapeutic strategies and challenges

Cu injection is the most common treatment for infant Menkes patients. The daily injections have been shown to partially improve clinical symptoms and prevent lethality only if Cu-histidine is introduced shortly after birth. This therapy results

in poor outcomes, however, if infants harbor loss-of-function *ATP7A* mutations or if they started treatment after two months of age, because the mature blood-brain-barrier prevents Cu from entering neurons [186, 187, 188]. The Cu administered during this treatment also failed to be effectively transported into the TGN to rescue connective tissue abnormalities and other cuproenzyme-related symptoms. *In utero* Cu treatment also revealed similar limitations for babies with severe *ATP7A* mutations [189].

Gene therapy studies have been conducted with *mottled*-brindled mice by introducing ectopic *ATP7A* to the mouse brain. Menkes mice receiving adenoviral-*ATP7A* plus Cu-histidine injections to the lateral cerebral ventricle had an extended lifespan (median survival was 43 days compared to *mottled*-brindled mice median of 16 days), increased brain Cu levels, and enhanced dopamine- β -hydroxylase activity [190]. Recently, the same group of researchers introduced rAAV9-rs*ATP7A* to the cerebrospinal fluid in addition to subcutaneous Cu administration to *mottled*-brindled mice. This strategy improved median lifespan from 16 days to 300 days, with normal growth and development, significantly improved brain neurochemical levels, Cco activity and neurobehavior. Clinical research is expected soon with this method [191].

Chemotherapy that uses oral disulfiram administration together with Cu-histidine injection has been characterized with macular mice and in a limited number of patients. Compared to macular mice or mice with Cu injection only, this method significantly enhanced Cu delivery to the brain, serum and liver, and reduced excess Cu accumulation in kidney. Dopamine- β -hydroxylase had a slight increase of activ-

ity in the brain, indicated by the ratios of noradrenaline and adrenaline to dopamine in cerebral fluid [192, 193, 194]. For Menkes patients, this method was inconsistently effective at improving neurological symptoms and at elevating cerebral Cu levels, and dopamine- β -hydroxylase activity was not altered after the treatment in all cases [195].

Chapter 2: Materials and Methods

2.1 *C. elegans* experimental procedures

Worms Strains and Culture

C. elegans were cultured at 20°C on nematode growth medium (NGM) plates seeded with *E. coli* OP50 for general maintenance or with *E. coli* HT115 dsRNA-expressing bacteria for RNAi experiments [196]. Bristol N2 was used as the wild-type *C. elegans* strain. Mutant and transgenic strains were outcrossed with N2 to obtain wild-type backgrounds, and a wild-type brood mate animal was used following crossing in mutant and transgenic animal growth/avoidance assays. Some strains were provided by the CGC, which is funded by NIH Office of Research Infrastructure Programs (P40 OD010440). The *chca-1 (tm6506) IV* strain was obtained from the National Bioresource Project [197] and outcrossed with N2 six times prior to use to establish heritability; *CB1033 (che-2 (e1033) X)* was obtained from CGC and outcrossed six times before use for the same purpose. A list of transgenic worms used in this study can be found in Appendix Table 2. Transgenic animals in a *chca-1 (tm6506)* mutant background, as well as multiple transgene-presenting strains, were generated with standard mating methods; genotypes were confirmed by PCR and/or DNA sequencing. The *chca-1(tm6506)* genotyping primers were: 5'-

GTATCTAGTCCGATAAGAAG -3' and 5'-TTGAAGCAAAAACAAAGTGC-3'.

RNA Interference (RNAi)

HT115 (DE3) bacterial strains containing plasmids expressing dsRNA against *F27C1.2*, *F31E8.4*, *Y58A7A.1*, *F58G6.7*, *F58G6.9*, *K12C11.6*, and *K12C11.7* genes were obtained from the Ahringer and ORFeome feeding libraries [198, 199]. The empty vector L4440 was used as a control. Portions of *F01G12.1*, *K12C11.3*, and *F58G6.3* DNA constructs were cloned into the L4440 vector and transformed into HT115 bacteria. Each construct was sequenced using the primer 5'- AGC-GAGTCAGTGAGCGAG -3', and evaluated by the E-RNAi online tool (e-rnai.org) to determine the RNAi target. NGM growth media with 12 $\mu\text{g}/\text{mL}$ of tetracycline, 50 $\mu\text{g}/\text{mL}$ carbenicillin, and 2 mM IPTG (isopropyl 1-thio- β -D-galactopyranoside) was used for RNAi experiments.

BLAST and Topology Prediction

The human CTR1 protein sequence was used as a query sequence in a search using PSI-BLAST. Non-redundant protein sequences (nr) were chosen for the database, and results were filtered to include only hits on the *Caenorhabditis elegans* (taxid:6239) genome. Candidates had an E-value cut-off of less than 10^{-3} . TMD of various organisms' CTR homologs were predicted by TMHMM 1.0. Clustal Omega was used to generate sequence alignment.

Axenic Media Growth

The axenic liquid media used in this study ("low Cu" mCeHR) is modified from the mCeHR media described previously [119] by removing extra Cu supplementation in the salt solution. 20 μM hemin was added for every culture condition. N2 worms

grown in “low Cu” mCeHR media were synchronized and hatched overnight in M9 buffer. Approximately 100 L1 stage worms were seeded into a 10 mL liquid media-containing flask with indicated CuCl_2 or BCS concentrations. Flasks were incubated on a rotating platform at 20 °C for 9 days. On day 9, animals were collected, samples were centrifuged (800 xg, 1 min) to collect the worm pellet, and then washed twice with M9 buffer. To count the number of worms, the tube was vortexed to mix, a prescribed amount of sample was drawn up and placed on a slide, and worm counts were calculated. Each condition was tested and counted in triplicate.

qRT-PCR

For assays conducted in axenic media, N2 worms were maintained in 10 μM CuCl_2 “low Cu” mCeHR, and then synchronized and split into flasks containing 10 μM CuCl_2 (optimal), 300 μM CuCl_2 (high Cu), or 100 μM BCS (low Cu) media. Worms were grown in each condition until the population reached the mid-L4 stage. Worms were collected after washing twice with M9 buffer and resuspended in 1 ml Trizol (Invitrogen), then lysed in Lysing Matrix Tubes (MP Biomedicals) using a FastPrep-24 (MP Biomedicals) homogenizer. Total RNA was isolated using the NucleoSpin RNA kit (Macherey-Nagel), and 1 μg RNA was used for cDNA synthesis (SuperScript III First Strand synthesis kit, Invitrogen). Real-time PCR was performed with SYBR Green Taq 2x Mix (BioRad) with three biological replicates and two technical replicates. Fold change values were calculated using the $2(-\Delta\Delta\text{Ct})$ method, with all values normalized to *pmp-3* or *gpd-2* expression. Primers are listed in Appendix Table I.

Quantification of Cu-dependent Worm Growth, Length, Brood Size,

and Cu Levels

Assays were performed as follows, unless specified in figure legends. For worm growth assays and length quantification, stage-synchronized L1 worms (P_0) were grown on RNAi-expressing bacteria until vector-fed control worms reached the L4 stage. P_0 worms were washed off the culture media with M9 buffer and 100 μ L of worms in M9 buffer was transferred into a 96-well culture dish. Animals' body length (TOF), density (extinction), and fluorescence intensity were quantified using a COPAS Biosort system FP-250 (Union Biometrica). To perform these assays on F_1 worms, 20 P_0 worms were transferred to fresh plates at the L4 stage and allowed to lay eggs for 12 h after reaching the gravid adult stage. P_0 worms were removed from the plate, and F_1 progeny were analyzed as above upon reaching the L4 stage.

For brood size analysis, synchronized L1 worms were cultured on dsRNA-expressing bacteria for 50 h until reaching gravid adult stage. Individual worms were then transferred onto fresh plates to allow egg-laying. After 3 consecutive days of egg-laying, the brood size, including both hatched and unhatched embryos was counted.

For Cu-pulse experiments, a mixed stage population was cultured on BCS-supplemented NGM plates for 5 days prior to synchronization. BCS-treated worms were then bleached to generate synchronized L1 animals which were then cultured on BCS plates for 48 h, washed off, and split evenly onto BCS- and Cu-supplemented plates for 12 h prior to worm pelleting. Restored Cu levels for each experimental condition were normalized to BCS-treated samples. See below for ICP-MS measurements.

ICP-MS

Metal contents of worms were measured using ICP-MS as described previously [41]. Values were normalized to wet weight of worms. For sample preparation, synchronized L1 worms were grown on NGM plates seeded with OP50 or HT115 RNAi bacteria and supplemented with the indicated amounts of copper or BCS until worms reached L4 stage. Worm pellets were collected and washed extensively with M9 buffer, transferred to acid-washed tubes, and frozen at -80 °C. At least three independent biological replicates were analyzed.

Generation of Transgenic Worms

Transgene-expressing plasmids were generated using a Multisite Gateway Three-Fragment Vector Construction kit (Invitrogen). Promoter, ORF, and UTR regions were amplified separately and recombined into the plasmid. The *unc-54* 3'UTR region is used in all constructs in this study. Together with the *unc-119* rescue plasmid, the transgene-expressing plasmid was then introduced into *unc-119* (ed3) III worms using a PDS-1000 particle delivery system (Bio-Rad) bombardment system. To generate worm strains expressing multiple transgenes, one worm strain expressing a single transgene was crossed with another transgenic worm using methods previously described [200]. All transgenic worm strains used in this study are listed in Appendix Table II.

Staining with the Cu Probe CF4

Stage-synchronized L4 worms expressing CHCA-1::GFP in the intestine were used for the CF4 assay. Worms were washed three times with M9 buffer, and around 400 worms were suspended in 100 μ L M9 buffer. CF4 Cu probe [126] was

then added to the buffer at a concentration of 25 μM . Worms were stained in the dark at room temperature for 2 h, and then transferred on normal NGM plates outside the bacterial lawn. These plates were kept in the dark for 2 h, and then the worms were collected and washed three times with M9 buffer and imaged via confocal microscopy.

Cu-responsive Behavior Assay

The Cu-avoidance assay in this study utilized rectangular Cu gradient plates. To make Cu gradient media, 4-well rectangular plates were tilted on their lids and 2 mL Cu-containing media (with indicated concentrations of CuCl_2 in 1.7 % agar, 3 mg/mL NaCl, 5 $\mu\text{g}/\text{mL}$ cholesterol, and 2.5 mg/mL bacto-peptone) was added to one third of the plate length. Upon solidification, plates were brought flat and 10 mL NGM agar was added on top. For control experiments with non-Cu containing plates, plates received 12 mL of NGM agar alone. After upper layer solidification, plates were kept at 4°C for 16 h to allow Cu diffusion prior to conducting the assay. Five sections were drawn on the bottom of the plates (indicating low to high Cu) for future quantification of worms per section as delineated by approximate concentration. Synchronized L4 worms were washed three times with M9 solution to remove bacteria, and 40 μL of worm-M9 solution was pipetted in the middle section of the plate (section three). Following a 2.5 h drying period, images of the plates were captured by camera and animals in each section were counted using Image J software. Each assay included at least 150 animals, and at least three independent experiments were performed for each condition. Avoidance behavior of the high Cu regions (sections four and five) were denoted by an *Avoidance Index*

(*AI*) derived from the following formula:

$$\textit{Avoidance Index}(\textit{AI}) = \frac{\text{Percentage of worms in section } [(4+5)-(1+2)]}{\text{Percentage of worms in section } [(4+5) + (1+2)]}$$

Worms in section three were not calculated, as not all worms translocated to different sections in the given time frame.

Immunofluorescence and Western Blot

The antibodies applied in the worm immunofluorescence assays are rabbit anti-FLAG (Rockland) at 1:300, and Alexa594 goat anti-rabbit IgG (ThermoFisher) at 1:300. For each condition, 75 μg of protein was loaded into gels. Transgenic animals expressing CHCA-1-2xFLAG::SL2::GFP in the intestine were stage-synchronized and L4 worms were fixed and stained with antibody as previously described [201]. Worms stained with secondary antibody only served as negative controls.

***C. elegans* treatment with elesclomol**

WT worms (Bristol N2), BK015 (*P_{vha-6} ::CUA-1.1::GFP::unc-54 3'UTR; cua-1(ok904)*) worms, *chca-1(tm6506 IV)* and the wild-type brood mate (WT) worms were maintained at 20 °C on nematode growth medium (NGM) plates seeded with *E. coli* OP50 or HT115 (DE3). For brood size counting, N2 worms were exposed to *cua-1* or control (L4440 vector) RNAi from synchronized L1 stage with or without 100 μM BCS treatment, supplemented with vehicle (DMSO) or 5 μM ES. After 4 days, worms under each condition were picked to individual plates in triplicate, allowed to lay eggs, and transferred to fresh plates every 24 h for 3 days. Eggs were

incubated overnight to allow hatching and progeny number was determined as the total hatched larvae. For the survival assay, BK015 transgenic worms were cultured on RNAi plates supplemented with either vehicle (DMSO) or 5 μ M ES from the L1 stage for 4 days, and then score for survival. Animals were considered dead when no signs of viability (movement, pharyngeal pumping, or response to prodding) were detected. WT and *tm6506* worms were cultured using basal media or media containing 100 μ M BCS conditions plus 10 μ M CuCl₂ or various concentrations of ES. Worms were collected at young adult stage for ICP-MS analysis or for size quantification.

2.2 Yeast experiments

Yeast Strain and Spotting Assay

The MPY17 *Saccharomyces cerevisiae* strains used in this study contained a *scCTR1* and *scCTR3* double deletion [18]. Genes were tagged at the carboxyl terminals with a 2x FLAG sequence and inserted into a pYES3 vector [202]. Plasmids containing either FLAG gene insertions or FLAG tag only were transformed into *CTR1* Δ *CTR3* Δ yeast. Yeast strains were maintained in a synthetic complete medium (SC) lacking uracil for plasmid selection. Spotting assays were conducted on YPD (1.5 % agar, 2 % bacto-peptone, 2 % glucose, 1 % yeast extract) and YPEG (1.5 % agar, 2 % bacto-peptone, 3 % glycerol, 2 % ethanol, 1 % yeast extract) media. Cells with an OD₆₀₀ of 0.2 (7 μ L) were spotted onto growth media in a series of 10-fold dilutions. Expression was induced by adding 0.4 % galactose into the me-

dia. Pictures were taken following incubation at 30°C for 5 days following spotting. For the yeast Western blots, rabbit anti-FLAG (Rockland) at 1:2000, and mouse anti-PGK1 (Molecular Probes) at 1:1000 were applied as primary antibodies.

2.3 Mouse and tissue culture experiments

Mouse strains

The cardiac-specific *Ctr1* deletion mouse ($Ctr1^{hrt/hrt}$) was generated by crossing *Ctr1^{flox/flox}* mice (Dr. Dennis J. Thiele lab at Duke University) with mice expressing Cre recombinase driven by the promoter of cardiac-expressed alpha-Myosin Heavy Chain (MHC) (Jackson Lab). Age-matched *Ctr1^{flox/+}* or *Ctr1^{flox/flox}* siblings not expressing Cre were served as control group (WT) in this study. All mice genotype were confirmed by heart *Ctr1* excision genotyping PCR, as previously described in [41], and selected mice heart Ctr1 protein levels were determined by immunoblot. All mice were maintained on the C57BL/6 genetic background. All animal procedures were performed in accordance with National Institutes of Health Guide and approved by the Institutional Animal Care and Use Committee at the University of Maryland, College Park (protocol # R-APR-18-14).

Antibodies

The anti-ATP7A antibody (generous gift from Dr. Betty A Eipper, University of Connecticut), anti-Ctr1 antibody (generous gift from Dr. Dennis J. Thiele, Duke University), and anti- β -tubulin antibody (Sigma #T9026), were used at 1:2,000 dilution. The anti-tyrosinase antibody (T311)(Santa Cruz Biotechnology #20035)

was used at 1:300 dilution. The anti-CCS antibody (Santa Cruz Biotechnology) and anti-GAPDH antibody (Sigma) were used at 1:1,000 dilution and 1:5,000 dilution, respectively. The anti-ZO-1 antibody (Invitrogen 33-910-0) and anti-Claudin 5 antibody (Abcam AB15106) were applied at 1:1000 dilution. The anti-MTCO1 antibody (Abcam Ab14705) and the anti-COXIV antibody (Thermo Fisher A21348) were used at 1:1,000 dilution. The HRP-conjugated anti-mouse or anti-rabbit IgG (Sigma) were used as secondary antibody at 1:5,000 dilution.

Elesclomol (ES) administration to $\text{Ctr1}^{hrt/hrt}$ mice

Starting from postnatal day 5 (P5), 10 mg /kg body weight of ES (Selleckchem) or vehicle was subcutaneously injected to $\text{Ctr1}^{hrt/hrt}$ or WT pups every three days until P26. During administration, depending on individual mice weight, an appropriate amount of ES was dissolved in DMSO, and then mixed with 5 % methyl cellulose solution (Sigma Cat. #64605) to reach a 2 % final concentration of ES-DMSO. The vehicle control solution only contains 0.5 % methyl cellulose solution with 2 % DMSO. Mice body weight was recorded every day from P5 to P26. After P26, the ES-treated WT and $\text{Ctr1}^{hrt/hrt}$ mice were re-grouped, with half of the population continued with 10 mg /kg ES administration once per week (ES-ES), and the other half switched to vehicle treatment (ES-vehicle). Mice body weight was recorded every week until P54.

Tissue preparation and immunoblotting

Several tissues were collected from P10-P12 pups after three times of ES administration, or from P54 mice following several ES-ES or ES-vehicle treatments. Tissues were frozen in liquid nitrogen and stored under -80°C before use. In order

to isolate the intestinal enterocytes, the whole small intestine was cut open, washed with cold-PBS and incubated in cold PBS containing 1.5 mM EDTA and protease inhibitor cocktail (Roche) with gentle rotation. After 30 minutes, enterocytes were release and the rest of intestine containing lamina propria was discarded. The enterocytes were then washed twice with cold PBS and collected by centrifugation at 2000 x g for 3 minutes, stored under -80 °C for subsequent analysis [203]. For immunoblotting, frozen tissues were homogenized first in cold lysis buffer (PBS pH 7.4, 1 % Triton X-100, 0.1 % SDS, 1 mM EDTA and protease inhibitor cocktail) with a pellet mixer (VWR) on ice, incubated for 45 minutes with several times of vortex, and then centrifuged at 15,000 x g, 15 minutes at 4 °C. The supernatant was transferred to a fresh tube, followed by protein concentration measurement with a BCA Assay Kit (Thermo Scientific). Equal amounts of protein were loaded and separated in a 4-20 % gradient gel (Bio-Rad), and then transferred to a nitrocellulose membrane. After developing antibodies, immunoblots were detected with Pico or Femto Chemiluminescent Substrate Reagents (Thermo Fisher) with Bio-Rad Chemidocumentation Imaging System.

Cardiac tissue histology and immunofluorescence

Freshly collected heart tissues were fixed in 4 % paraformaldehyde/ PBS solution at 4 °C for overnight with gentle agitation, and then washed twice with 100 % ethanol and dehydrated in 70 % ethanol. Paraffin embedding, tissue sectioning and hematoxylin/ eosin staining were then performed by HistoServ, Inc. Cardiac myocytes size and morphology were observed with a Leica DMI6000 microscope. For immunofluorescence, the Alexa Fluoro 488 conjugated anti-WGA (Wheat germ

agglutinin, Invitrogen W11261) was applied to sectioned cardiac tissues at 1:500 dilution. Cells were imaged by a confocal microscope, and 45 cells under each condition were quantified for surface area using Image J.

Mouse embryonic fibroblasts (MEF) culture and tyrosinase and lysyl oxidase activity assay

Wild-type (*ATP7A^{+/+}*) and *ATP7A^{-/-}* MEFs were cultured in Dulbecco's Modified Eagle Medium (DMEM; Lonza) supplemented with 10 % (v/v) heat-inactivated fetal bovine serum (VWR). Cells were cultured at 37 °C with 5 % CO₂. When cells grown to 70 % confluence, single or double plasmids (8 μg DNA /each) were transfected with the PolyJet transfection reagent (SignaGen). 24 hours after the transfection, indicated concentrations of ES were administrated into culture media and incubated for another 24 hours. Cells were then collected for protein extraction. For tyrosinase activity assay, proteins were extracted with lysis buffer containing PBS pH 7.4, 1 % Triton X-100, 1 mM EDTA and Halt protease inhibitor cocktail (Thermo Fisher). 100 μg protein/sample was fractioned on a 10 % non-reducing SDS-free polyacrylamide gel. The gel was first stabilized in 50 mM PBS (pH 6.8) for 30 minutes at room temperature and then stained at 37 °C in solution containing 10 mM PBS (pH 6.8), 1.5 mM L-3,4-dihydroxyphenylalanine and 4 mM 3-methyl-2-benzothiazolinone hydrazone (Sigma). The relative activity of tyrosinase is colormetrically determined by the formation from L-DOPA to DOPA-chrome [204], and the intensity was quantified by Image J.

Human cerebral microvascular endothelial cells (hCMEC/D3) culture, permeability assay and transwell co-culture with *Ctr1^{-/-}* MEFs

The hCMEC/D3 cells were purchased from CELLutions BIOSYSTEMS and used between passage 28-32. The final culture media for hCMEC/D3 contains 5 % (v/v) heat-inactivated fetal bovine serum (VWR), 100 U/mL Penicillin/Streptomycin, 1.4 μ M Hydrocortisone (Sigma H0135), 5 μ g/ml Acid Ascorbic (Sigma A4544), 1x Chemically Defined Lipid Concentrate (Thermo), 10 mM HEPES and 1ng/ml bFGF (Sigma F0291) in EBM-2 media (Lonza). The transendothelial electrical resistance (TEER) of hCMEC/D3 in transwell inserts was measured with a EVOM2 epithelial voltohmmeter (WPI) daily after plating. hCMEC/D3 used in all transwell experiments had TEER higher than 60 ohm.cm². For the permeability assay, approximately 4x10⁶ hCMEC/D3 cells were plated on the type I rat collagen-coated transwell insert (for 6-well plates, culture area was 4.67 cm²) for 1, 5 or 10 days; and then DMSO or 30 nM elesclomol was added to the apical side culture media. After 24 hours, 4 kDa FITC-dextran (Sigma) was added to the apical side media at 4.15 mg/ml. 50 μ L of basal side culture media was collected every 45 minutes for fluorescence measurements at 490/530 nm. The permeability coefficient (Pe) was calculated according to previous studies [205, 206]. For the co-culture assay with *Ctr1* knockout MEF cells (*Ctr1*^{-/-} MEFs), approximately 4x10⁶ hCMEC/D3 cells were plated on collagen-coated transwell inserts and cultured for 10 days, followed by ES administration to the apical side culture media. Simultaneously, *Ctr1*^{-/-} MEFs were cultured in the bottom chamber. 24 hours after the ES treatment, both hCMEC/D3 and *Ctr1*^{-/-} MEF cells were collected. Wild-type (*Ctr1*^{+/+}) and *Ctr1*^{-/-} MEFs were cultured in DMEM supplemented with 10 % (v/v) heat-inactivated fetal bovine serum, 1x MEM nonessential amino acids (Lonza), 50 μ g/mL uridine, 100

U/mL penicillin/streptomycin (Lonza), and 55 μ M 2-mercaptoethanol.

2.4 Statistical analysis

Immunoblot and tyrosinase activity were quantified using the a Bio-Rad Chemi- documentation Imaging System or ImageJ. Statistical analysis was performed with one-way ANOVA followed by Sidak post hoc test, or two-way ANOVA followed by Tukey's post hoc test, using GraphPad Prism 6 (GraphPad). ANCOVA was performed using SPSS Statistics version 23 (IBM). Statistical significant differences are considered at $p < 0.05$.

Chapter 3: CHCA-1 is a copper-regulated CTR1 homolog required for normal development, copper accumulation, and copper-sensing behavior in *Caenorhabditis elegans*

3.1 Project summary

Copper (Cu) plays key roles in catalytic and regulatory biochemical reactions essential for normal growth, development, and health. Dietary Cu deficiencies or mutations in Cu homeostasis genes can lead to abnormal musculoskeletal development, cognitive disorders, and poor growth. In yeast and mammals, Cu is acquired through the activities of the CTR1 family of high-affinity Cu transporters. However, the mechanisms of systemic responses to dietary or tissue-specific Cu deficiency remain unclear. Here, taking advantage of the animal model *Caenorhabditis elegans* for studying whole-body Cu homeostasis, we investigated the role of a *C. elegans* CTR1 homolog, CHCA-1, in Cu acquisition and in worm growth, development, and behavior. Using sequence homology searches, we identified ten potential orthologs to mammalian CTR1. Among these genes, we found that *chca-1*, which is transcriptionally upregulated in the intestine and hypodermis of *C. elegans* during Cu deficiency, is required for normal growth, reproduction, and maintenance of

systemic Cu balance under Cu deprivation. The intestinal Cu transporter CUA-1 normally traffics to endosomes to sequester excess Cu, and we found here that loss of *chca-1* caused CUA-1 to mislocalize to the basolateral membrane under Cu overload conditions. Moreover, animals lacking *chca-1* exhibited significantly reduced Cu avoidance behavior in response to toxic Cu conditions compared with wild-type worms. These results establish that CHCA-1-mediated Cu acquisition in *C. elegans* is crucial for normal growth, development, and Cu-sensing behavior.

3.2 Results

3.2.1 Cu-responsive transcriptional regulation of CTR1-like genes in *C. elegans*

To identify potential genes for Cu acquisition in *C. elegans*, a Basic Local Alignment Search Tool (BLAST) search was performed using the human CTR1 protein sequence as a probe. Unlike many characterized organisms that contain two or three CTR homologs [18, 32, 39, 207], fifteen protein orthologs encoded by ten gene loci are predicted to be potential *C. elegans* CTR genes. The BLAST result scores for the fifteen candidate proteins demonstrate that, in general, worm CTR candidates share 30-40 % amino acid sequence identity with hCTR1 (Table 3.1).

Worm CTR1 candidate proteins were further analyzed based on the conserved features of CTR proteins, such as number of the transmembrane domains and Cu-transporting motifs at the amino (N) and carboxyl (C) terminus, and the second predicted TMD. In general, *C. elegans* CTR candidates have a shorter N terminus as

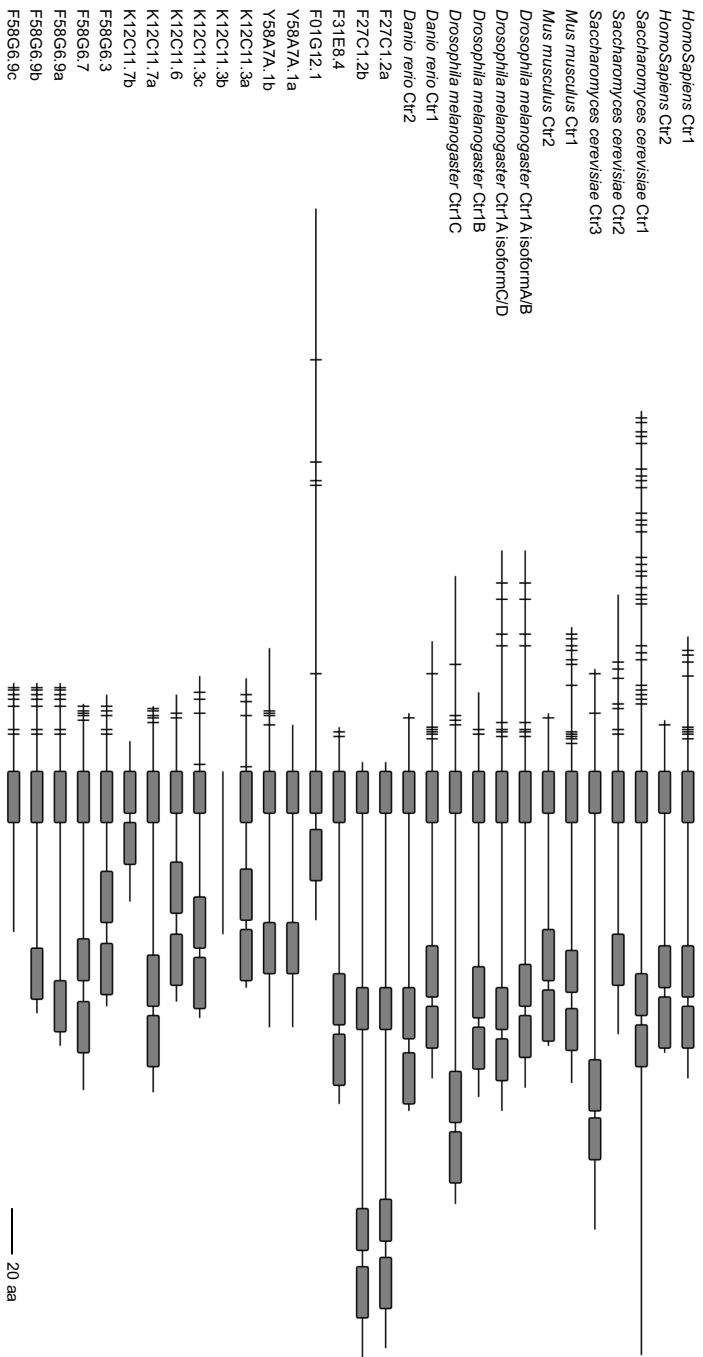
Table 3.1: *C. elegans* Ctr homolog genes. PSI-BLAST was conducted to search *C. elegans* Ctr candidates using the human CTR1 (hCTR1) amino acid sequence. 10 gene loci that express 17 potential proteins are listed, within which 15 proteins had E values beneath the threshold of 10⁻³. F58G6.9c and K12C11.3b (labeled with #) proteins were among candidate gene loci, but had E values greater than 10⁻³. Protein identities, similarities, and scores are listed. Based on known features of hCtr1, *C. elegans* Ctr1 candidate proteins were annotated by their conserved Cu transporter features. Transmembrane domains (TMD) were predicted by TMHMM 1.0, and N-terminal methionine (Met) and histidine (His) enrichment levels were characterized by calculating the percentage of Met or His before the first predicted TMD (0–5 % *, 5 %–10 % **, ≥ 10 % ***). All candidate proteins contain *Met-X₃-Met* domains in or close to one of the predicted TMD (✓); non-candidate proteins do not (-). Proteins labeled with (✓) in the last column contain one or more cysteines (Cys) and/or His at the C-terminus.

Gene	Protein	Blast Result			Predicted Features					
		E Value	Identity	Similarity	Score	TMD Number	MxxxM	N' Met Rich	N' His Rich	C' Cys/His
<i>hCTR1</i>	<i>hCTR1</i>					3	✓	***	***	✓
<i>F27C1.2</i>	<i>F27C1.2a</i>	2e-13	31%	47%	150	4	✓	-	-	✓
	<i>F27C1.2b</i>	7e-13	31%	45%	145	4	✓	-	-	✓
<i>F31E8.4</i>	<i>F31E8.4</i>	6e-12	28%	46%	135	3	✓	***	**	✓
<i>F01G12.1</i>	<i>F01G12.1</i>	8e-11	53%	75%	131	2	✓	*	**	✓
<i>Y58A7A.1</i>	<i>Y58A7A.1a</i>	1e-10	32%	45%	125	2	✓	-	**	✓
	<i>Y58A7A.1b</i>	3e-12	32%	44%	137	2	✓	**	***	✓
<i>K12C11.3</i>	<i>K12C11.3a</i>	1e-07	39%	68%	103	3	✓	***	*	-
	<i>K12C11.3b#</i>	>10				0	-	-	-	-
	<i>K12C11.3c</i>	1e-07	30%	48%	104	3	✓	***	*	-
<i>K12C11.6</i>	<i>K12C11.6</i>	1e-08	46%	68%	110	3	✓	**	**	-
<i>K12C11.7</i>	<i>K12C11.7a</i>	4e-04	25%	40%	79	3	✓	***	*	✓
	<i>K12C11.7b</i>	2e-04	36%	54%	76	2	✓	-	***	✓
<i>F58G6.3</i>	<i>F58G6.3</i>	1e-10	32%	50%	124	3	✓	***	**	-
<i>F58G6.7</i>	<i>F58G6.7</i>	2e-06	31%	47%	95	3	✓	***	**	✓
<i>F58G6.9</i>	<i>F58G6.9a</i>	5e-09	23%	48%	114	2	✓	***	**	-
	<i>F58G6.9b</i>	8e-07	21%	46%	98	2	✓	***	**	-
	<i>F58G6.9c#</i>	>10				1	-	***	**	-

compared to human and mouse CTR1 (Figure 3.1). Candidate proteins expressed at *F31E8.4*, *Y58A7A.1*, *F58G6.3*, *F58G6.7*, and *F58G6.9* gene loci are enriched with both methionine and histidine at the N-terminus. All fifteen candidates contain a *Met-X₃-Met* domain within or close to one of the predicted TMD.

CTR1 abundance is regulated by Cu availability. In yeast and mammalian cells, high Cu induces CTR1 protein degradation, while Cu deprivation stabilizes the protein [36, 208, 209]. In yeast, such regulation occurs at the transcriptional level. *Ctr1* expression is induced under Cu-depleted conditions by the transcriptional factor Mac1 [4]. To test whether worm *CTR* mRNA abundance can be regulated by altered Cu status, qRT-PCR was performed for the ten candidate genes under optimal, high, and low Cu conditions in liquid axenic growth media. To determine the desired range of Cu concentration for worm growth, the *C. elegans* Habituation and Reproduction (mCeHR) axenic liquid culture [119] was further modified to contain minimal levels of Cu ("low Cu" mCeHR). Around 100 synchronized L1 stage worms were grown in axenic culture supplemented with various concentrations of copper chloride (CuCl₂) or bathocuproinedisulfonic acid (BCS, a Cu(I) chelator) for 9 days; total worm number was counted for each condition on day 9. Supplementation with 10 μ M Cu was most favorable for worm growth, while worms exhibited the defects in development or embryogenesis under both Cu-replete and Cu-deficient conditions, resulting in significantly decreased total populations (Appendix Figure I A). Either 10 μ M Cu, 300 μ M Cu, or 100 μ M BCS was applied to generate normal, strong Cu overload and strong Cu deficiency conditions, respectively, to measure changes in gene expression. Synchronized L1 worms were cultured to the L4 stage, and levels

Figure 3.1: TMD (grey box) and N-terminal Met (short line) alignment for human, yeast, mouse, and zebrafish Ctr amino acid sequences and worm Ctr candidate proteins encoded by the 10 candidate gene loci. TMHMM (1.0) was used to identify TMDs. Proteins are aligned at the position of the first TMD for visualizing the relative length and Met enrichment at the N-terminus. K12C11.3b has no predicted TMD. Scale bar indicates a length of 20 amino acids (aa).



of mRNA of each candidate gene under high and low Cu conditions were calculated by normalizing to expression levels under 10 μ M Cu condition. Under Cu deprived conditions, expression of only *F58G6.3*, *F58G6.7*, and *F58G6.9* was significantly elevated (Appendix Figure I B). These three genes, together with other candidate genes such as *F01G12.1*, *Y58A7A.1*, and *K12C11.6*, had expression suppressed by 300 μ M Cu (Appendix Figure I C).

3.2.2 Importance of *CTR1* candidate genes for growth, reproduction, and Cu accumulation in worms

Our recent studies have shown that limited availability of dietary Cu causes developmental defects in worms, and that depletion of the Cu exporter CUA-1 in the intestine inhibits Cu distribution to peripheral tissues, resulting in reduced growth and brood size [126]. To test whether our potential *CTR* genes were required for worm growth in a Cu-dependent manner, L1 stage worms were grown on NGM media plates seeded with OP50 bacteria. Plates were supplemented with either 150 μ M CuCl₂, 50 μ M BCS, or nothing. Milder Cu conditions were used (as compared to the experiments with axenic culture) to more closely mimic physiologically-relevant conditions of Cu abundance and deprivation and to enable observation of intermediate growth phenotypes. Following 3 days of growth, *F58G6.9*- and *F27C1.2*-depleted P₀ animals cultured with 50 μ M BCS were found to be stage-delayed, as indicated by time of flight (TOF, worm length quantification), in comparison to vector-treated animals (Figure 3.2 A-D). There were no apparent growth defects observed in worms

treated with RNAi against other Ctr-like genes under different Cu conditions (Figure 3.2 A-C) suggesting an important role of the proteins encoded by *F27C1.2* and *F58G6.9* in response to Cu deficiency in worms.

To determine the efficiency of knockdown, qRT-PCR was performed to test candidate gene expression levels after RNAi treatment. All candidate genes' mRNA levels were significantly decreased after worms were fed RNAi bacteria. While *F01G12.1*, *F31E8.4*, and *K12C11.3* transcripts exhibited a mild reduction (~80–60 % of wild type expression), silencing of all other CTR candidates was highly effective (less than 30 % of wild type expression) (Figure 3.3).

To further test whether CTR candidates are important for normal Cu levels in worms, each gene was individually silenced, and whole-body metal levels were examined by ICP-MS. When providing synchronized L1 (P₀) with sufficient Cu (10 μ M) for two generations, F1 worms lacking a number of the candidate genes displayed decreased Cu accumulation (73-80 % of that of vector) (Figure 3.4 A). To identify the gene most strongly associated with Cu accumulation in *C. elegans*, a Cu-pulse assay was conducted on each RNAi-treated candidate by pre-culturing worms in Cu-limited conditions followed by a 12-hour (h) 50 μ M CuCl₂ pulse (Figure 3.4 B). Following BCS treatment, all worms had extremely low whole-animal Cu concentrations, in a range of 0.03-0.06 μ g/g (data not shown). When calculating the level of Cu acquired during the Cu pulse, *F58G6.3*-, *F58G6.7*-, and *F58G6.9*-depleted worms displayed significant defects in restoration of Cu levels. Of these, the most defective were the *F58G6.9* RNAi animals, which only accumulated 40 % of the Cu measured in vector-treated worms (Figure 3.4 C). Depleting a number of other

Figure 3.2: Requirement of *CTR1* candidate genes for Cu-dependent growth. A-C) Cu-dependent growth assay under basal (A), high Cu (B) and limited Cu (C) conditions. Synchronized L1 stage N2 worms were cultured on RNAi plates until the vector-treated worms reached L4 stage. Worm length (TOF) was quantified using a COPAS BioSort system, and worm length under each RNAi condition was normalized to vector TOF. ~ 400 individual animals were analyzed under every condition. Values with asterisk are significantly different from vector (one-way ANOVA, Dunnett post hoc test, $*p < 0.05$, $**p < 0.01$, $***p < 0.001$). D) Representative images of P_0 worms treated with indicated dsRNA-expressing bacteria.

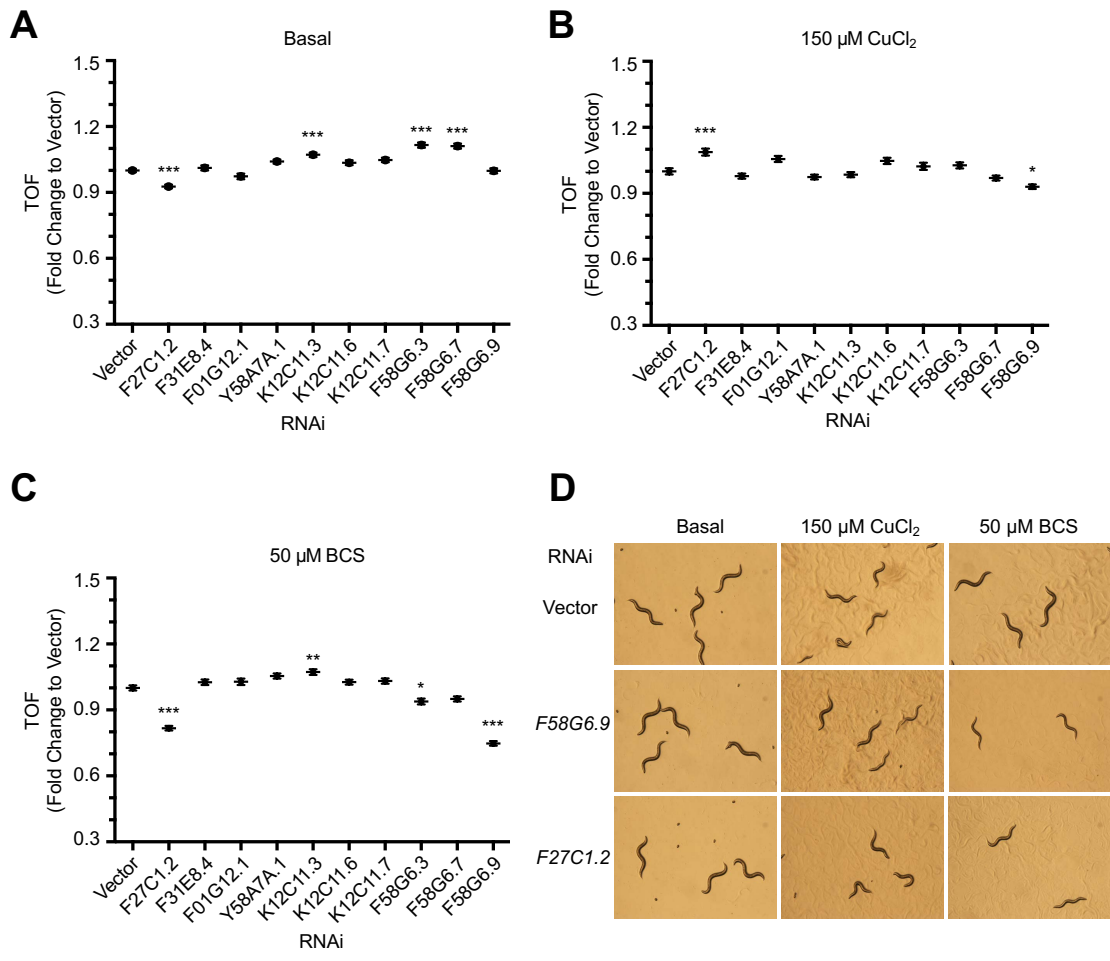
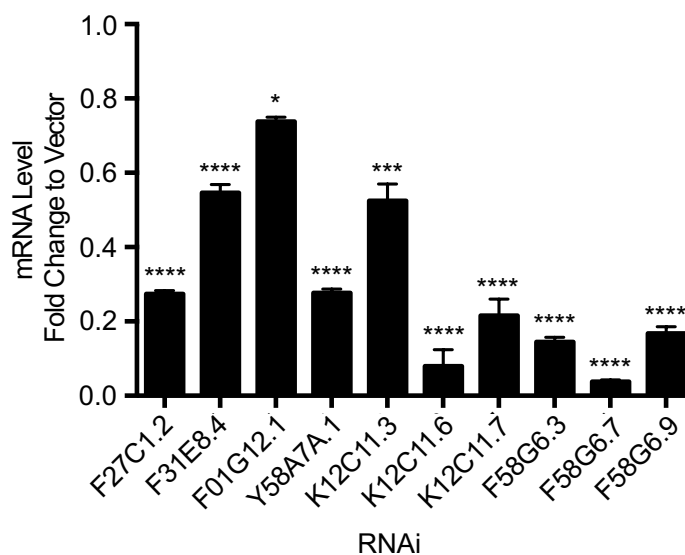


Figure 3.3: **RNAi efficiency of 10 *CTR* candidate genes.** N2 worms were cultured on 50 μ M BCS plates from synchronized L1 worms to the L4 stage. Transcript levels measured in animals treated with indicated RNAi were normalized to levels measured in vector-treated animals. Three independent experiments were conducted under each condition. Asterisks indicate significant difference from indicated gene expression levels under optimal conditions. (t-test, * $p < 0.05$, *** $p < 0.001$, **** $p < 0.0001$). Error bars, mean \pm SEM.



candidate genes decreased body Cu accumulation under prolonged Cu treatment (Figure 3.4 A). However, these conditions did not significantly impact Cu restoration from a Cu-deficient state within the time frame assayed, suggesting that these genes, when functioning independently, are not required for effective Cu uptake.

Our results narrowed down the *CTR*-like gene list, leading to *F58G6.9* as the strongest candidate Cu importer in worms. To further explore the role of *F58G6.9* in worm regeneration, we measured brood size in *F58G6.9*-silenced worms under Cu-limited conditions. P₀ worms after one generation of *F58G6.9* RNAi under 50 μ M BCS supplementation showed substantially smaller brood sizes compared with control animals. Similarly, worms treated with *F58G6.9* RNAi exhibited severe defects in generating embryos when treated with 100 μ M BCS (Figure 3.5). Given that the *F58G6.9* gene showed significantly elevated transcript levels under low Cu conditions, and that it is required for normal growth, reproduction, and Cu accumulation in a low-Cu environment, we focused on the *F58G6.9* gene as a potential CTR candidate and named it CTR1 Homolog required for Copper Accumulation-1 (*chca-1*).

Figure 3.4: **Requirement of *CTR1* candidate genes for Cu accumulation.** A) Cu levels in *C. elegans* were measured by ICP-MS after exposure to 10 μM Cu for two generations. Values with asterisk are significantly different from vector with three independent trials (One-way ANOVA, Dunnett post hoc test, $*p < 0.05$). B) A schematic presentation of Cu-pulse assays. *C. elegans* worms were cultured in axenic media supplemented with 25 μM BCS for 5 days prior to synchronization. Synchronized L1 animals were cultured on 50 μM BCS NGM agar plates expressing indicated dsRNA for 72 h. Animals were then washed, aliquoted, and re-plated on fresh 50 μM BCS or 50 μM CuCl_2 plates for 12 h. Restored Cu levels are indicated by normalizing Cu-treated worms to BCS-cultured animals. C) Restored Cu levels under indicated RNAi treatments. Values with asterisk are significantly different from vector (One-way ANOVA, Dunnett post hoc test, $***p < 0.001$, $****p < 0.0001$).

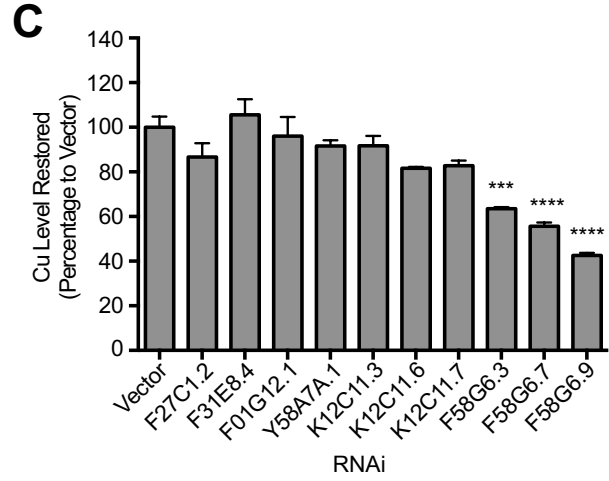
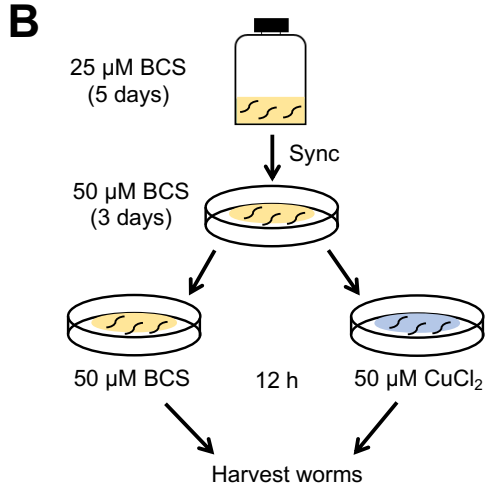
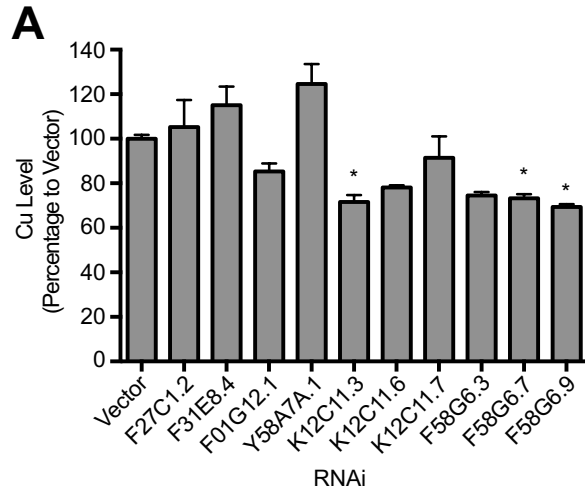
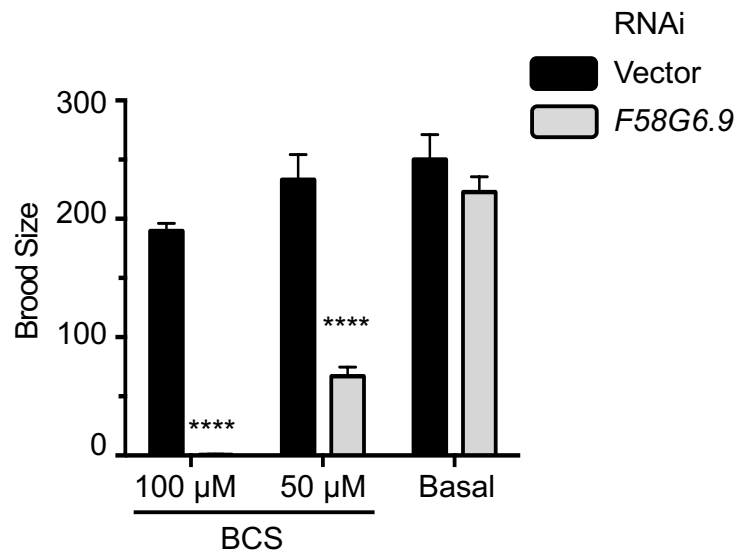


Figure 3.5: ***F58G6.9* RNAi animals exhibited significantly reduced brood size.** Brood size analysis of *F58G6.9* RNAi animals. Error bars indicate mean \pm SEM of five independent experiments. Values with asterisk are significantly different from vector under same culture condition (Two-way ANOVA, Sidak post hoc test, **** $p < 0.0001$). Error bars in this figure represent mean \pm SEM.



3.2.3 CHCA-1 is required for normal Cu level and development

We tested functional complementation by worm CHCA-1 in yeast cells defective in the high affinity Cu transporters, Ctr1 and Ctr3, on non-fermentable carbon sources [207]. Expression of CHCA-1 protein with a carboxyl-terminal FLAG epitope tag (CHCA-1-2xFLAG) in the heterologous system failed to restore yeast growth (Figure 3.6). To test functional consequence of loss of the endogenous CHCA-1 *in vivo* system, we exploited an established Cu-responsive CUA-1-trafficking reporter animal model. Our recent studies have demonstrated that the intestinal CUA-1.1 Cu exporter maintains systemic Cu homeostasis by altering its subcellular localization [126]. It localizes to the basolateral membrane during Cu deficiency, and upon Cu overabundance, re-distributes to lysosome-like organelles, called gut-granules, to protect peripheral tissues from Cu toxicity. As ICP-MS assays only measure whole body Cu levels, we silenced *chca-1* in transgenic worms expressing CUA-1.1::GFP from the constitutive, intestine-specific *vha-6* promoter [210] (BK015 strain) to evaluate whether the depletion of *chca-1* yields any change in intestinal Cu status. Importantly, when given sufficient dietary Cu, worms lacking *chca-1* showed CUA-1.1::GFP localized to the intestinal basolateral membrane with significantly decreased distribution to the gut granules when compared with vector-treated animals (Figure 3.7 A and Figure 3.8 A). Individual silencing of all other *CTR* candidate genes did not change CUA-1.1 localization in the intestine (Figure 3.7), suggesting the CHCA-1 is a major player in intestinal Cu homeostasis. Our studies have also shown that endogenous CUA-1.1 expression is induced in the

hypodermis under dietary Cu restriction [126]. Upon depleting *chca-1* in transgenic worms expressing CUA-1.1::GFP driven by its own promoter (BK017 strain), CUA-1.1 expression was significantly enhanced in the hypodermis under basal culture conditions at a comparable level to that of the transgenic strain grown in 25 μ M BCS (Figure 3.8 B). Together, Cu dependent CUA-1.1 distribution and expression in worms lacking *chca-1* was similar to dietary Cu deficient worms, suggesting a role for CHCA-1 in Cu acquisition in *C. elegans*.

To further characterize CHCA-1 and to verify the RNAi-based findings, a *chca-1* mutant animal (*chca-1 tm6506 IV*) was obtained from the National Bioresource Project [197]. The *tm6506* allele found in this mutant contains a 464-bp deletion which begins in the 5' UTR and spans the second intron of the *F58G6.9* gene; this deletion is predicted to affect the entire N terminus and first TMD (Figure 3.9 A and B). Worms homozygous for the *tm6506* allele exhibited defects in growth under basal and Cu-replete conditions (10 μ M CuCl₂) and showed a severe growth phenotype under BCS treatment within one generation (P₀). However, the growth defects were fully rescued by Cu supplementation at 25 μ M (Figure 3.10 A and B).

To test the metal specificity of CHCA-1-dependent growth, 50 μ M BCS and several metal sources (CuCl₂, ZnCl₂, FeCl₂, and MnCl₂) were mixed together in the growth media, and the growth of the *tm6506* mutant strain and its wild-type outcrossing brood mate (WT) were compared after 3 days of culture. Only Cu supplementation rescued the growth defect observed in *chca-1* mutant worms, suggesting a function for this gene in Cu-specific regulation (Figure 3.10 C). Compared to WT animals, *chca-1 tm6506 IV* worms contained significantly lower Cu levels

Figure 3.6: **Expressing *F58G6.3*, *F58G6.7*, and *F58G6.9b* in the MPY17 *CTR1* Δ *CTR3* Δ yeast strain.** Worm Ctr candidate genes and yeast *CTR1* (*scCTR1*) were tagged at the C terminus with 2xFLAG tags. Expression was induced by adding 0.4 % galactose into growth media. A) Growth assay of *CTR1* Δ *CTR3* Δ strain expressing *scCtr1*, *F58G6.3*, *F58G6.7*, and *F58G6.9b*. Media containing a fermentable carbon source (YPD media with glucose) or non-fermentable source (YPEG media with ethanol and glycerol) was used in the assay. B) Expression of the indicated genes assayed by immunoblot using an anti-FLAG antibody. Expression of phosphoglycerate kinase1 (PGK1) served as a loading control.

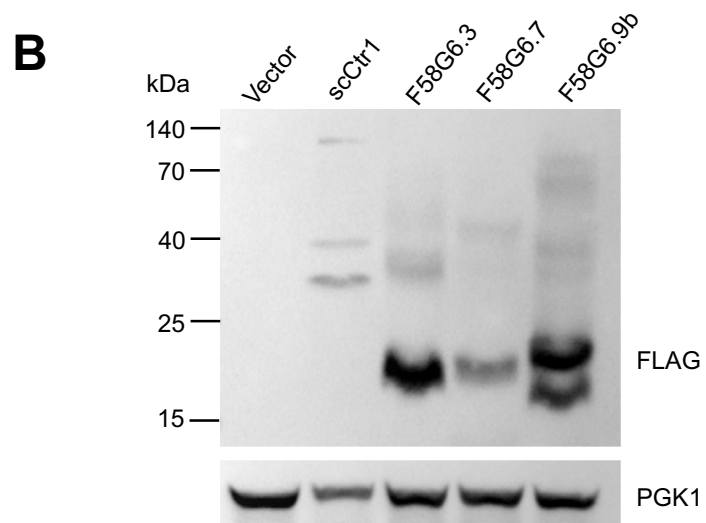
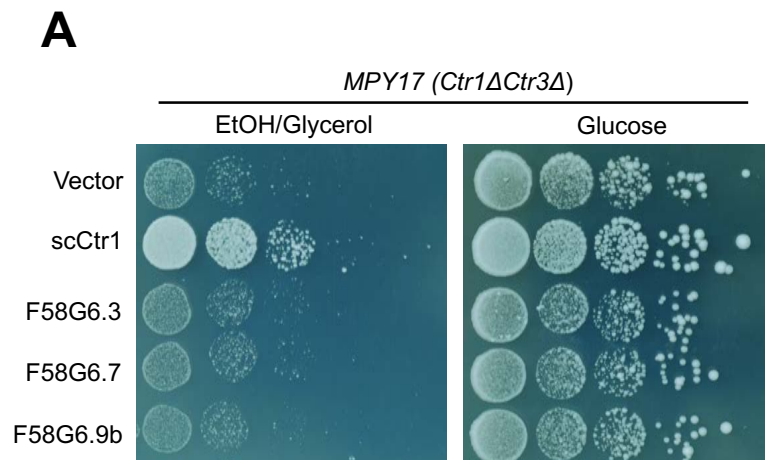


Figure 3.7: **CUA-1.1::GFP localization in BK015 worms with Ctr candidate RNAi.** CTR candidate genes were silenced from the the L1 stage in BK015 worms and cultured on 50 μ M BCS or 50 μ M Cu plates until the L4 stage. Images of CUA-1.1::GFP localization were taken with a confocal microscope. Scale bar, 15 μ M.

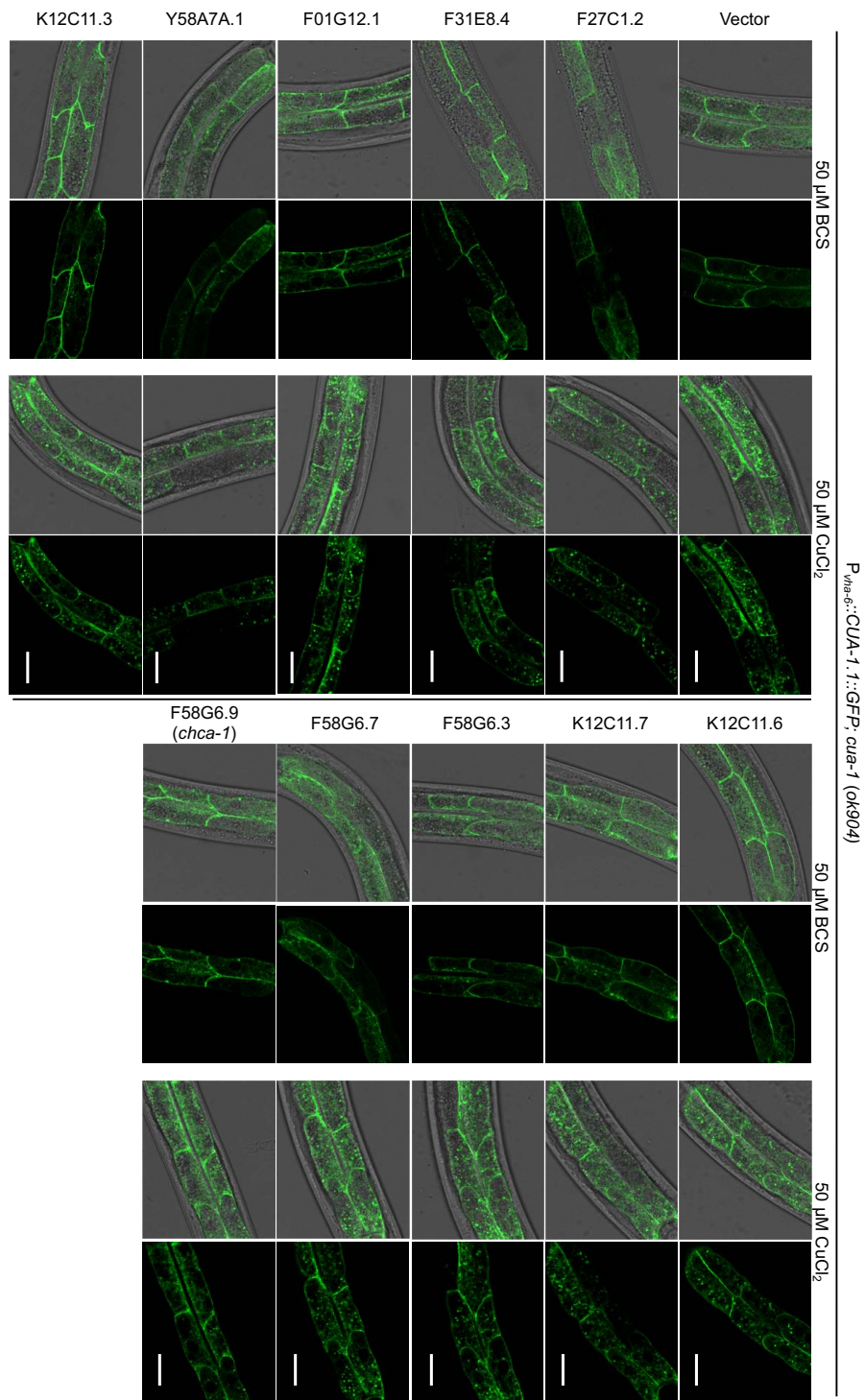


Figure 3.8: **Depletion of *chca-1* by RNAi decreases intestinal Cu availability in *C. elegans*.** A) Synchronized L1 stage BK015 transgenic worms [$P_{vha-6}::CUA-1.1::GFP::unc-54$ 3'UTR; *cua-1 (ok904)*] were cultured on NGM agar plates seeded with *E. coli* expressing dsRNA against *CHCA-1* or vector. CUA-1.1::GFP localization in L4 worms was examined using confocal microscopy. Scale bar, 15 μ M. B) *chca-1*-depleted worms display increased endogenous CUA-1.1::GFP expression in the hypodermis. BK017 [$P_{cua-1}::CUA-1.1::GFP::unc-54$ 3'UTR; *cua-1 (ok904)*] transgenic animals were maintained on 10 μ M CuCl₂ plates prior to synchronization. L1 animals were then re-plated for *chca-1* RNAi. After 60 h culture, CUA-1.1::GFP expression levels in L4 animals were examined using confocal microscopy. Scale bar, 50 μ M.

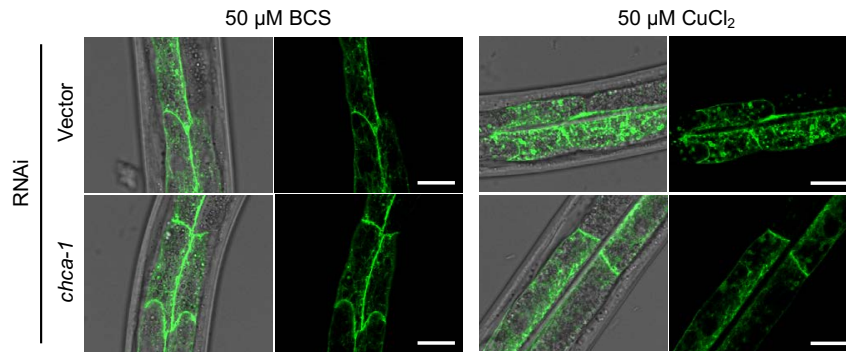
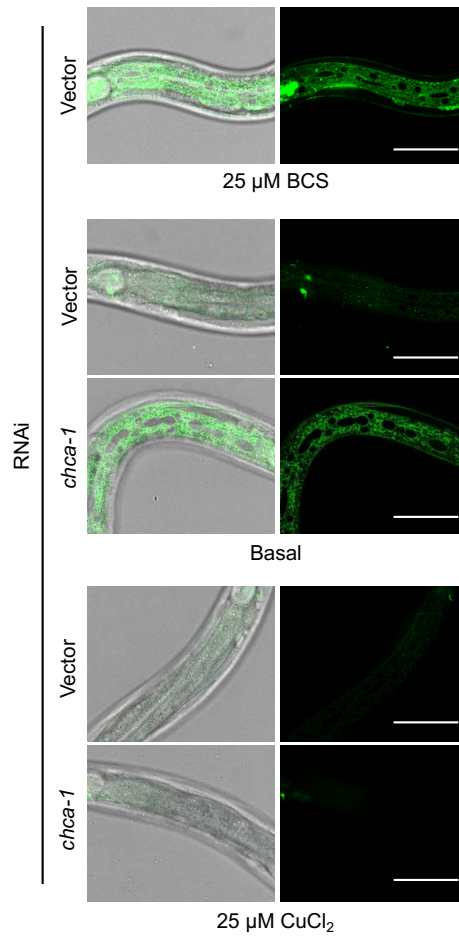
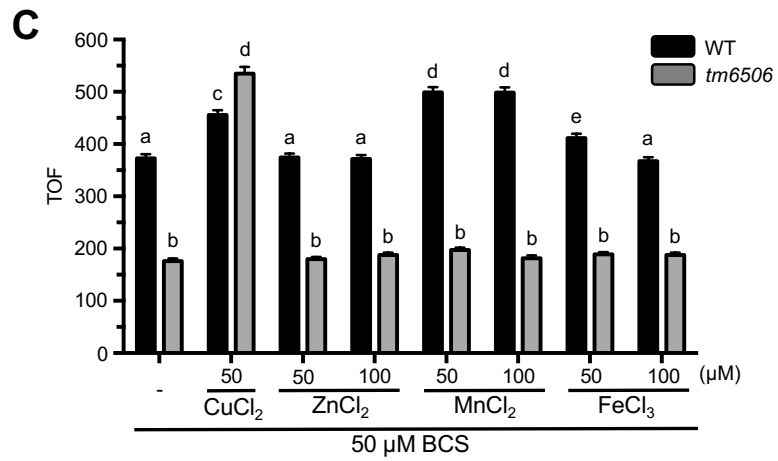
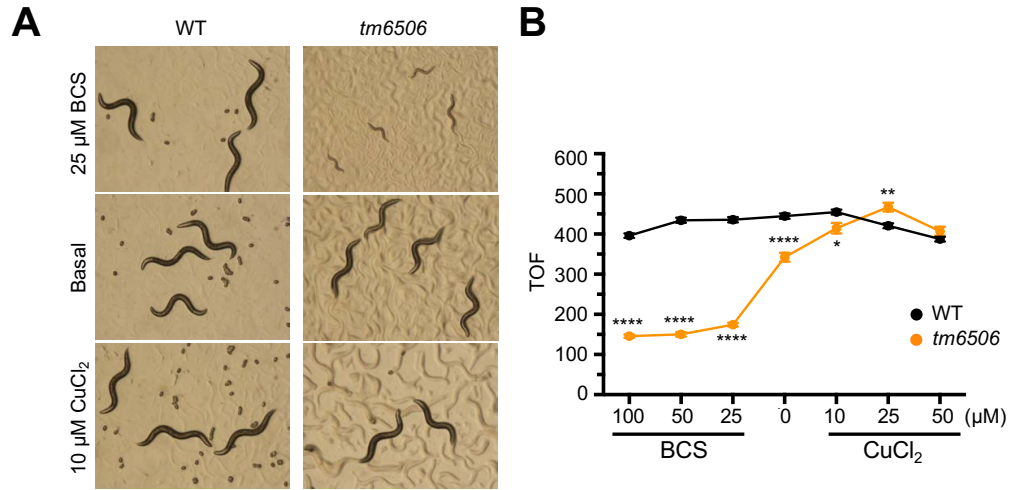
A $P_{vha-6}::CUA-1.1::GFP; cua-1(ok904)$ **B** $P_{cua-1}::CUA-1.1::GFP; cua-1(ok904)$ 

Figure 3.9: **Schematic of *CTR1* and *chca-1* gene loci and protein sequence alignment.** A) Schematic of human *CTR1* and *C. elegans chca-1* gene loci, with blue-colored ORFs and grey-colored UTR regions. Note that CHCA-1b1 and CHCA-1b2 isoforms differ at the 5'UTR region but express identical proteins. The deleted region in the *tm6506* allele is indicated by the red bar. Scale bar indicates 100-base pairs (bp). B) Sequence alignment of hCTR1, CHCA-1a, and CHCA-1b proteins. Transmembrane domains (TMD) of hCTR1 and deleted regions of CHCA-1a and CHCA-1b in the *tm6506* allele are indicated. Clustal Omega was used to perform the alignment.

Figure 3.10: ***chca-1 (tm6506) IV* worms exhibit growth defect under Cu-deficient condition.** A) and B) Growth of *tm6506* animals under various CuCl_2 or BCS-supplemented conditions. Worms homozygous for the *tm6506* allele and their outcrossing wild type brood mates (WT) were cultured from synchronized L1s for 72 h. A) Representative images of animals growing under indicated conditions. B) Worm growth quantification using a COPAS BioSort system. Error bars indicate mean \pm SEM of around 75 worms. Values with asterisk are significantly different from WT animals under the same Cu or BCS concentrations (Two-way ANOVA, Dunnett post hoc test, * $p < 0.05$, ** $p < 0.01$, **** $p < 0.0001$). C) WT and *tm6506* mutant worms grown on 50 μM BCS plates or 50 μM BCS plus indicated concentrations of metals. Error bars indicate mean \pm SEM of around 100 individual animals. Means with different letters are significantly different at $p = 0.05$ (Two-way ANOVA, Tukey's post hoc test).



under Cu deficiency (ranging from 15 μ M BCS up to 10 μ M supplemented Cu conditions), while Fe levels were not affected in mutant worms (Figure 3.11 B); this defect could only be rescued by supplementing the media with 25 μ M CuCl₂ (Figure 3.11 A). Consistent with our RNAi-based results (Figure 3.4 C), the mutant worms also demonstrated defects in dietary Cu acquisition upon Cu-pulse (Figure 3.11 C).

3.2.4 Intestinal CHCA-1 is critical for Cu-dependent growth and Cu accumulation

To further understand the role of CHCA-1 in Cu homeostasis, transgenic worms expressing GFP driven by the endogenous *chca-1* promoter were used to examine tissue-specific expression of this gene. While the GFP reporter in this strain was barely detectable under Cu-replete conditions, it was induced in the intestine and hypodermis upon severe dietary Cu deprivation (Figure 3.12). Tissue-specific *chca-1* knockdowns were performed to determine the contribution of CHCA-1 in these two tissues to its systemic role in Cu accumulation. This was performed using *rde-1* mutant animals which are RNAi-resistant. In a whole-animal *rde-1* knockout background, knockdown is only effective in a tissue expressing *rde-1* cDNA [211]. In this study, the intestine- and hypodermis-specific RNAi-sensitive strains (VP303 and NR222, respectively) were used to deplete *chca-1*, and their growth was compared to whole-body *chca-1* silencing in the N2 strain. Whole animal RNAi-resistant (WM27) and muscle-specific RNAi-sensitive (WM118) strains served as negative controls. After normalizing the growth of *chca-1* RNAi worms to vector in both P₀

and F1 generations following RNAi, worms depleted for intestinal CHCA-1 in 100 μ M BCS exhibited comparable growth and reproduction defects as to those exposed to whole-body *chca-1* RNAi depletion. On the other hand, worms lacking CHCA-1 only in the hypodermis did not reveal growth defects until the F1 generation under the same Cu-deficient conditions (Figure 3.13A and B). The loss of intestinal *chca-1* was also able to phenocopy the decreased Cu levels observed in a whole animal *chca-1* knockdown (Figure 3.14 A and B). These results suggest a dominant function of intestinal CHCA-1 for Cu-dependent growth under a Cu-limited condition. Meanwhile, CHCA-1 depletion in both the intestine and hypodermis resulted in similar effects on Cu accumulation when worms were exposed to 25 μ M CuCl₂, a Cu-abundance condition (Figure 3.14 C).

To determine which tissue, when lacking CHCA-1, most significantly contributes to aberrant CUA-1.1 localization in the intestine (Figure 3.8 A), BK014 transgenic worms (*Pvha-6::CUA-1.1::GFP*) were crossed with each of the WM27, VP303, and NR222 strains. Compared to a whole-body knockdown effect (Figure 3.15 d and e), loss of CHCA-1 solely in the intestine or hypodermis was not sufficient to increase CUA-1.1::GFP basolateral membrane distribution, nor to reduce its gut granule expression in the presence of 10 μ M Cu (Figure 3.15 n, o, s, t). These results suggest that both intestinal and hypodermal CHCA-1 play important roles in regulating Cu level in *C. elegans*, and raise a possibility that CHCA-1 in the hypodermis could function to compensate Cu deficiency in the intestine and/or at the organismal level.

Figure 3.11: ***chca-1 (tm6506) IV* worms exhibit low Cu levels under Cu deficiency and defect in Cu acquisition.** A) Cu levels of *tm6506* and WT animals. Synchronized L1 animals were cultured on indicated concentrations of Cu or BCS-supplemented media for 60 h and then pelleted for ICP-MS. For each condition, 3 or 4 samples were analyzed. Values with asterisk are significantly different from those of WT animals (t-test for each treatment, * $p < 0.05$, *** $p < 0.001$, **** $p < 0.0001$). B) Fe levels in *tm6506* and WT animals in panel A). Values with asterisk indicate significant differences between *tm6506* and WT animals under indicated conditions (t-test for each treatment, ** $p < 0.01$). C) Cu-acquisition capacity of *tm6506* worms. WT or *tm6506* worms pre-treated with 15 μM BCS were washed, and separately cultured on fresh 15 μM BCS or 50 μM CuCl_2 NGM plates for 12 h, followed by ICP-MS analysis. Three independent samples were assayed for each condition. Asterisks indicate that Cu levels in *tm6506* worms post-pulse are significantly different from those in the WT strain (ANCOVA, Bonferroni post hoc test, $p = 0.016$).

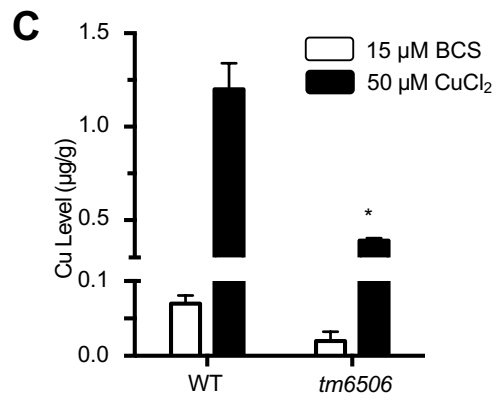
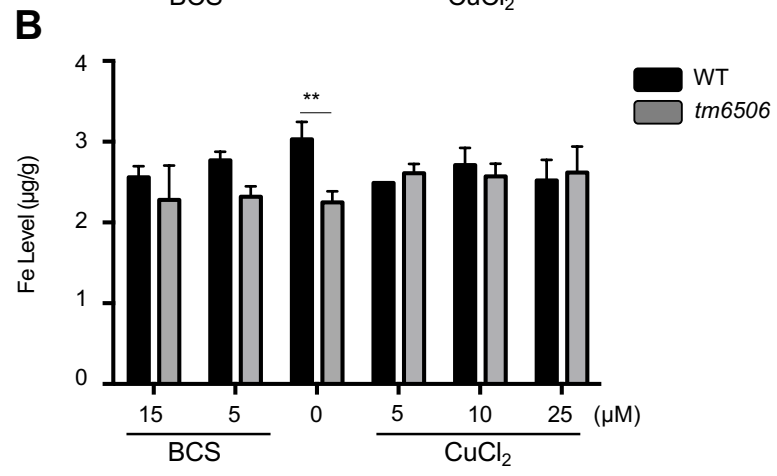
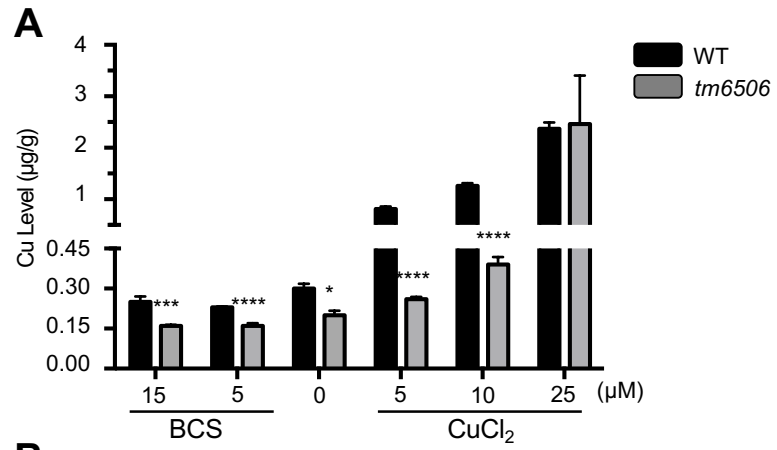


Figure 3.12: **Tissue-specific expression of the *chca-1* gene.** Transgenic animals expressing GFP driven by the 2.8 kb *chca-1* promoter region were cultured on NGM plates containing 10 μ M CuCl₂ (a, b) or 200 μ M BCS (c-f, same animal, different focus layers). Arrowhead indicates intestine, and arrow indicates hypodermis cells. a, c, e: bright field; b, d, f: fluorescence. Scale bar, 50 μ M.

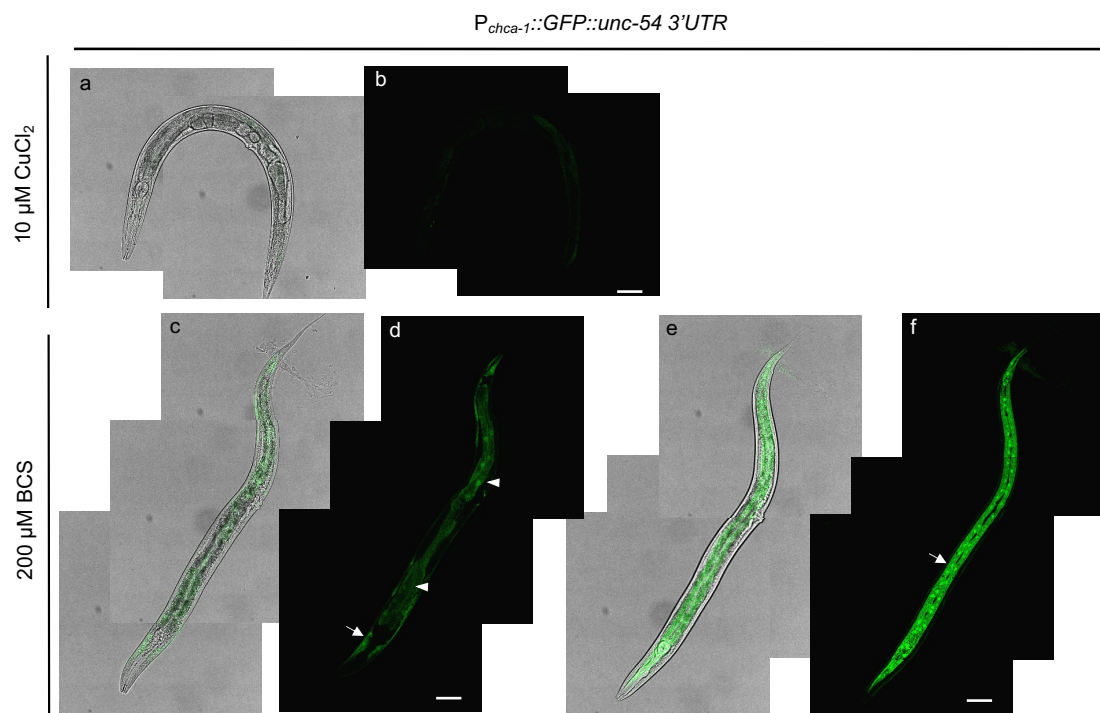


Figure 3.13: Cu-dependent growth following *chca-1* gene depletion in specific tissues. N2, RNAi-resistant strains (*rde-1*, WM27) and tissue-specific *rde-1* expressing strains (VP303, NR222, and WM118) were used to knock down the *chca-1* gene in the indicated tissues (Int: intestine, Hyp: hypodermis, Mus: muscle). Synchronized L1s were cultured to the L4 stage (panel A, P₀), or re-synchronized and cultured for another generation (panel B, F1) on indicated Cu-deficient NGM plates prior to quantification. Under each condition, ~200 P₀ or F1 worms' TOF was quantified by a COPAS BioSort. Growth of *chca-1*-depleted worms was normalized to vector for each condition. *chca-1* RNAi in N2 and VP303 strains on 100 μ M BCS plates exhibited severe defects in P₀ reproduction (U.D., under detection limit). Error bars indicate mean \pm SEM of ~200 individual animals. Values with asterisks are significantly different from the same strain under basal conditions (Two-way ANOVA, Dunnett post hoc test, * $p < 0.05$, ** $p < 0.01$, *** $p < 0.001$, ns = not significant).

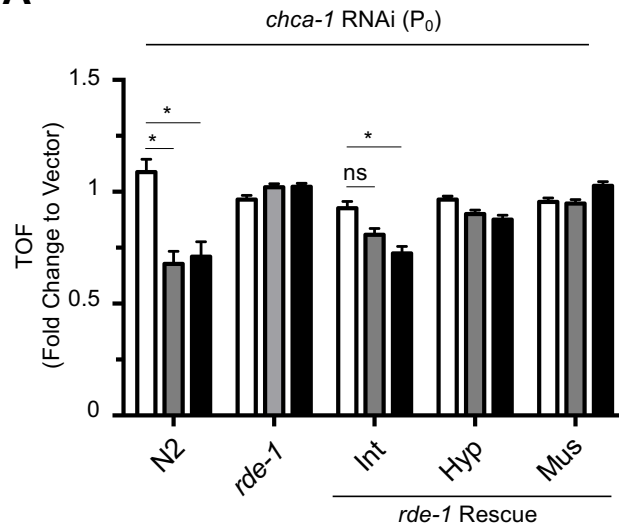
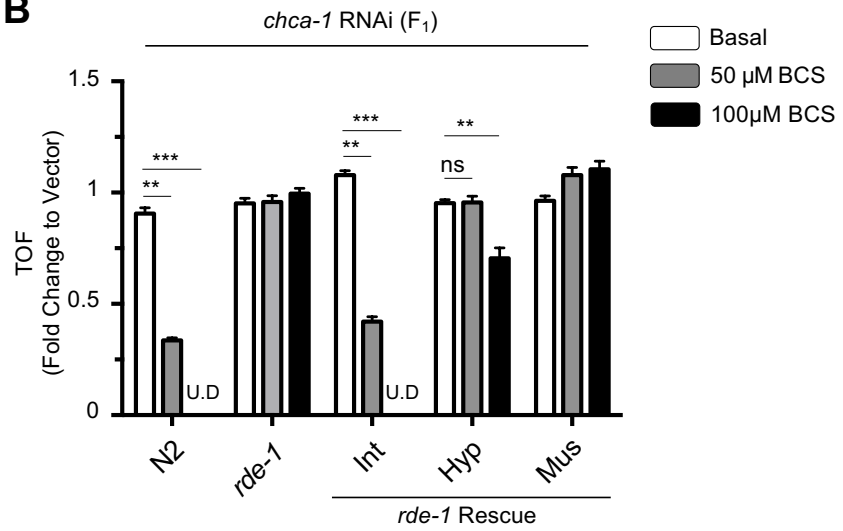
A**B**

Figure 3.14: **Intestinal CHCA-1 plays a dominant role in Cu acquisition under Cu-limited conditions.** A and B) Cu accumulation in N2 and tissue-specific *chca-1*-depleted animals. Different strains of worms were pre-cultured on 50 μ M BCS NGM plates and then half of the population was separated and treated with Cu. A) Restored Cu levels after normalizing to BCS-cultured samples. Error bars represent mean \pm SEM of four independent experiments. Values with asterisk are significantly different from vector (Two-way ANOVA, Sidak post hoc test, *** $p < 0.001$, **** $p < 0.0001$). Cu levels following BCS pre-culture were not significantly different among strains by Two-way ANOVA (data not shown). B) Percentage of Cu levels restored by *chca-1* RNAi after normalizing to vector animals under the same conditions. Error bars, mean \pm SEM of four independent experiments. Values with asterisk are significantly different from one another (One-way ANOVA, Dunnett post hoc test, * $p < 0.05$, ** $p < 0.01$, ns = not significant). C) Synchronized L1 stage N2, tissue-specific RNAi strains and RNAi-resistant worms treated with with indicated RNAi were cultured on 25 μ M CuCl₂ NGM plates for 60 h, followed by washing and pelleting for ICP-MS analysis. Data from four individual experiments were analyzed (Two-way ANOVA, Tukey's post hoc test, *** $p < 0.001$).

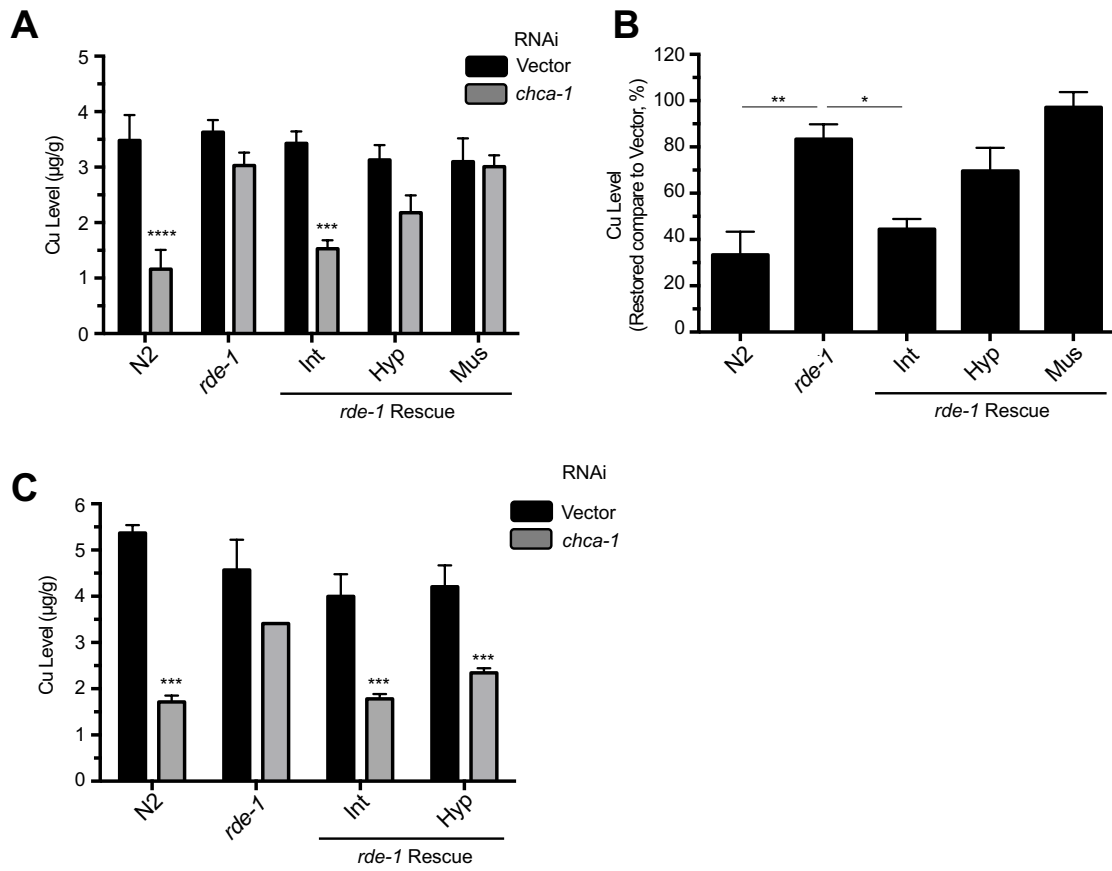


Figure 3.15: Effect of tissue-specific *chca-1* RNAi on intestinal CUA-1.1::GFP distribution. BK014 transgenic animals expressing intestinal CUA-1.1::GFP were crossed with RNAi resistant or tissue-specific RNAi sensitive strains (WM27, VP303 and NR222). CUA-1.1::GFP distribution was observed at L4 stage by confocal microscopy. Scale bar, 25 μ M.

3.2.5 CHCA-1 localizes to intracellular vesicles in the intestine

Given the importance of enterocytes in regulating dietary Cu uptake, we generated transgenic worms expressing a CHCA-1::GFP fusion protein driven by the intestine-specific *vha-6* promoter. This fusion protein localizes to vesicles throughout the intestine under basal, Cu-deficient, and Cu-replete conditions (Figure 3.16 A and B). In addition, CHCA-1::GFP expression levels were not altered by Cu availability (Figure 3.16 C). While CUA-1.1 co-localized with a fluorescent Cu probe (CF4) in gut granules [126] CHCA-1::GFP did not co-localize with CF4 or gut granules, the latter of which are auto-fluorescent (Figure 3.16 B and Figure 3.17). To test whether GFP-tagging could lead to CHCA-1 protein mislocalization, a 2xFLAG tag, followed by a stop codon and an SL2 splicing leader sequence, were inserted between CHCA-1 and GFP (*Pvha-6::CHCA-1-2xflag::SL2::GFP*). Both GFP and FLAG tags in this study were placed at the C-terminus of CHCA-1 to avoid N-terminal truncation observed in mammalian Ctr1 [21]. Immunofluorescence analysis showed similar vesicle localization of FLAG-tagged CHCA-1 protein (Figure 3.18). The function of intestinal CHCA-1 was then tested by crossing the transgenic worms expressing WT CHCA-1 (*Pvha-6::CHCA-1::SL2::GFP*) driven by an intestine-specific promoter onto a *tm6506* mutant background. Transgenic worms expressing WT CHCA-1 in the intestine in the *tm6506* mutant background exhibited significantly rescued *tm6506* growth during Cu deficiency (Figure 3.19). These results suggest a role for vesicular CHCA-1 in mediating Cu acquisition in the worm intestine, and that CHCA-1 protein abundance, in contrast with mammalian CTR1, is not regulated

by Cu status.

3.2.6 CHCA-1 is required for behavioral avoidance of potentially toxic levels of Cu

Animals navigate complex natural environments containing both dangerous and valuable items, such as predators and food. *C. elegans* must approach and obtain nutrients while avoiding various threats, which include toxic levels of Cu. Worms detect threats via primary sensory neurons that then propagate such information through an interneuron network to ultimately reach pre-motor command interneurons that direct controlled locomotion. Thus far, several ciliated sensory neurons (ASH, ASE, ADL, ASI, and ADF) are known to correlate with Cu sensing and/or avoidance behavior [212, 213]. We studied whether altered Cu status in a worm affects its Cu avoidance behaviour. To quantify levels of avoidance, assays were performed on rectangular plates containing a gradient of CuCl_2 , from no Cu supplementation on one end, to toxic Cu levels on the other end. After production, assay plates were kept in a cold chamber for a defined period of time to allow for Cu diffusion and concentration gradient formation, and marked in sections (Figure 3.20 A). With Cu supplementation, plates generated with the method described above contain a sharp Cu gradient ranging from section 3 to section 5, as measured by ICP-MS performed on agar samples from the gradient plates (Figure 3.20 B).

Stage-synchronized L4 young adult worms were seeded in the middle of the bacteria-free Cu gradient plates, and worm distribution after 2.5 h was visualized.

Figure 3.16: Expression of CHCA-1::GFP in the intestine. A) Intestinal expression of CHCA-1::GFP under basal conditions ($P_{vha-6}::CHCA-1::GFP$, *unc-54* 3'UTR). Scale bar, 50 μ M. B) CHCA-1::GFP expression in the intestine under basal, Cu-deficient, and high Cu conditions. A DAPI channel was used to observe intestinal auto-fluorescence from gut granules. Scale bar, 15 μ M. C) CHCA-1::GFP signal intensity was quantified under high, low, or replete Cu conditions using a COPAS BioSort system. At least 100 synchronized L4 CHCA-1::GFP-expressing worms were used following 2.5 days of growth in Cu or BCS-supplemented cultures per condition (One-way ANOVA, Dunnett post hoc test, ns = not significant).

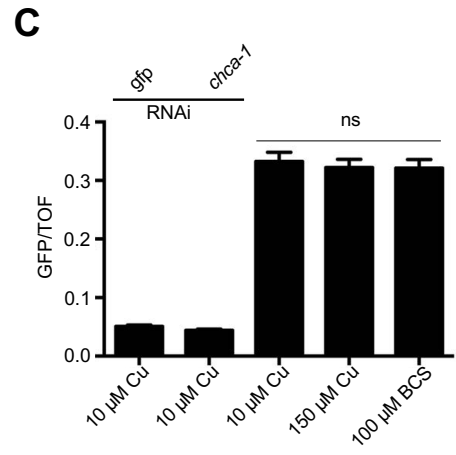
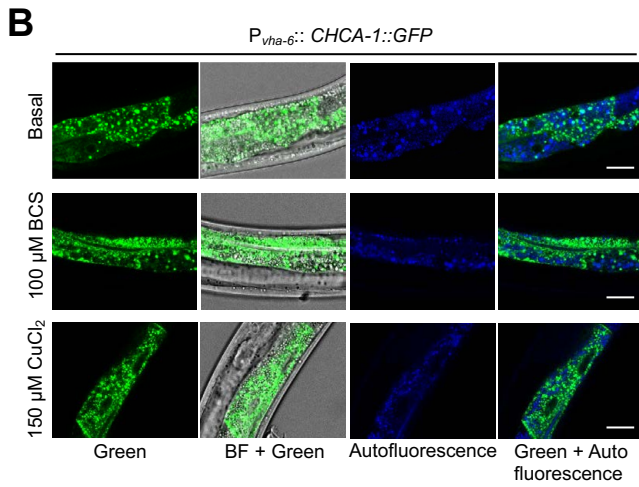
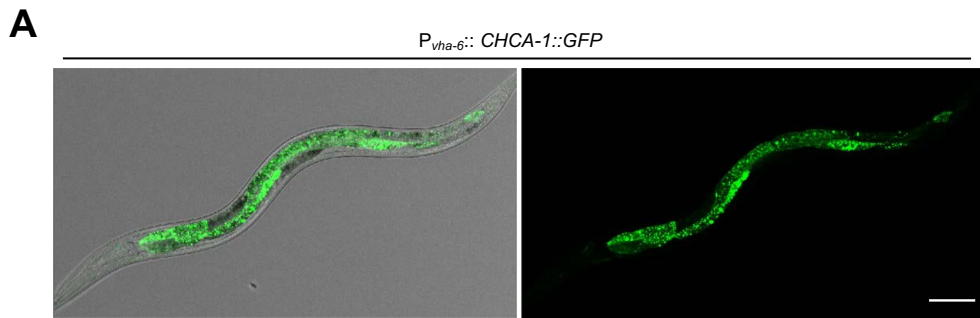


Figure 3.17: **CHCA-1::GFP does not co-localize with the Cu probe CF4.** CF4 Cu probe staining. Transgenic worms expressing CHCA-1::GFP in the intestine were cultured for 60 h from the L1 stage on 25 μM CuCl_2 or 50 μM BCS-supplemented plates. Images were taken via confocal microscopy. Scale bar, 15 μM .

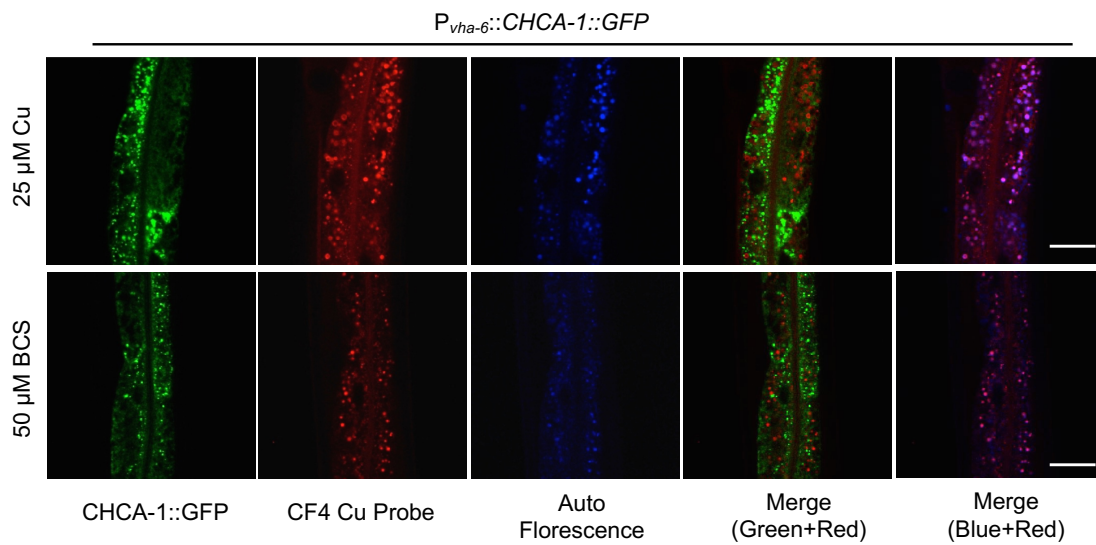


Figure 3.18: **Expression of CHCA-1-2xFLAG protein in the intestine.** Synchronized L1 worms expressing CHCA-1-2x FLAG::SL2::GFP in the intestine were incubated on basal, 50 μ M BCS, or 75 μ M CuCl₂ media for 55 h before being washed from plates and fixed on slides. Animals stained with secondary antibody only (Alexa594) served as negative controls. Images were taken with confocal microscopy. Scale bar, 15 μ M.

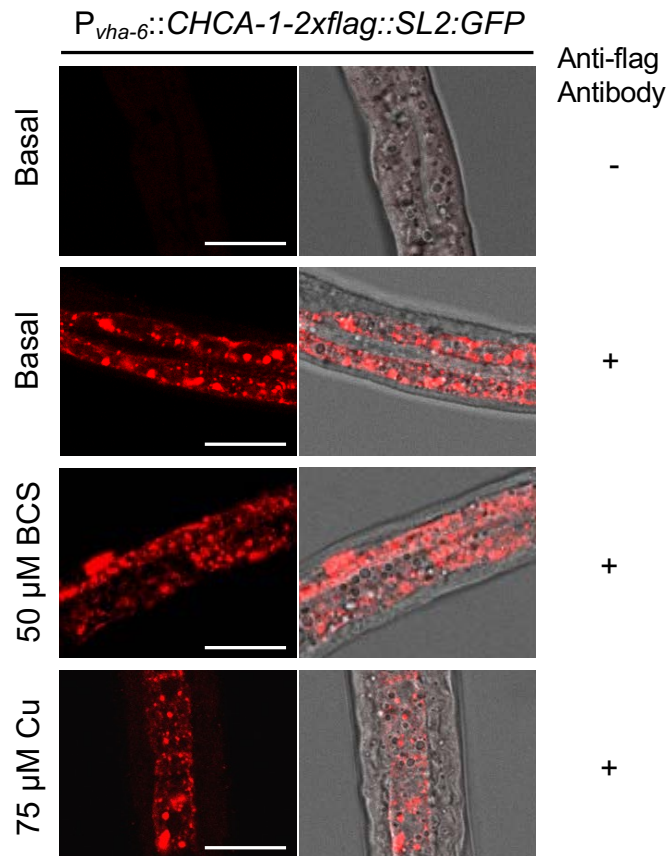


Figure 3.19: **Intestinal expression of CHCA-1 partially rescued growth of *chca-1* mutant animals.** Transgenic animals expressing CHCA-1::SL2::GFP protein were crossed with *tm6506* animals to generate an intestinal CHCA-1 expression animal in a whole body *chca-1* mutant background. These transgenic animals, together with their wild-type brood mates (WT), as well as *tm6506* animals, were quantified by TOF after 60 h culture from synchronized L1s in indicated conditions. Error bars indicate mean TOF \pm SEM of \sim 150 individuals. Values with asterisk are significantly different from *tm6506* worms cultured under indicated conditions (Two-way ANOVA, Tukey's post hoc test, * $p < 0.05$, ** $p < 0.01$, *** $p < 0.001$, **** $p < 0.0001$).

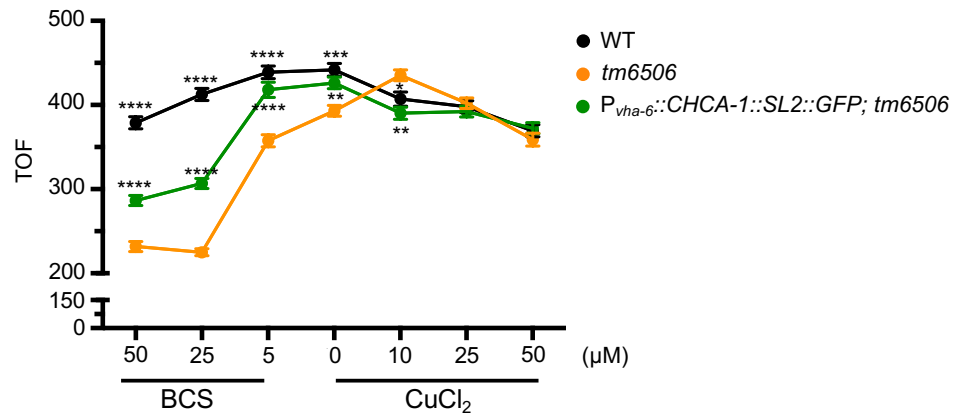
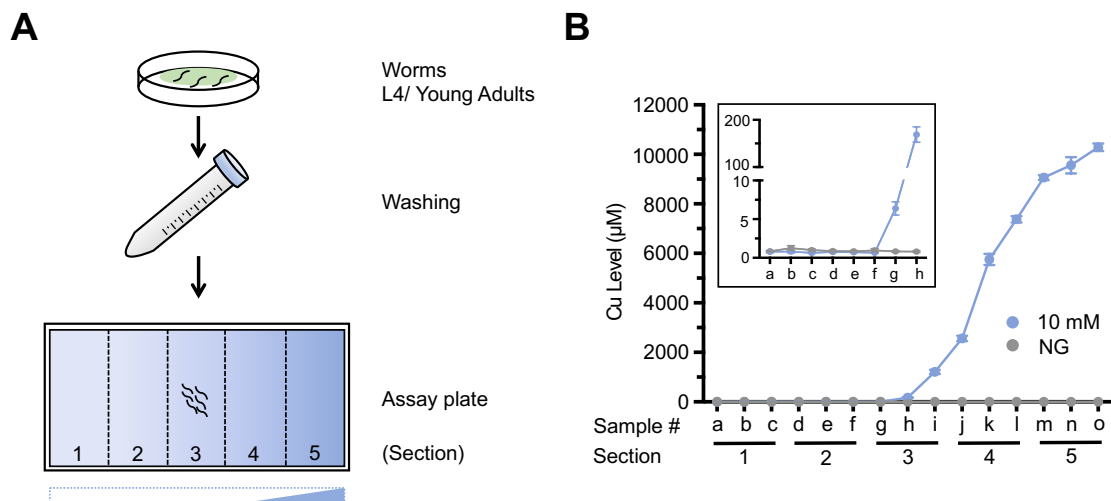


Figure 3.20: **Design of Cu avoidance assay.** A) Schematic of Cu avoidance assay: Cu gradient plates were made by adding a given concentration of CuCl_2 to one side of a rectangular plate. Non-Cu containing plates were used as controls. At least 150 animals were used on each plate with total three independent experiments. B) Cu levels of 10 mM Cu-gradient plates. 15 agar samples (a-o) were evenly taken from the five sections (1-5) in Cu gradient or non-Cu supplemented plates (3 samples per subsection) for ICP-MS analysis. Inset shows detailed measurements for samples a-h. Error bars represent SEM from four independent samples.



During quantification, each plate was evenly divided into five sections (with section 5 representing the highest Cu level area), and a formula was used to calculate the avoidance index (AI) as described in the Methods.

We observed that wild type N2 worms on the Cu gradient plates (10 mM Cu) had a strong tendency to avoid high Cu-containing areas (Figure 3.21 A) as compared to normal distribution of worms on non-Cu plates. Changing the maximum concentrations found in the Cu gradient from 1 mM to 10 mM led to N2 worms exhibiting enhanced avoidance (Figure 3.21 B) For further assays, 8 mM or 10 mM Cu gradients were chosen in order to achieve clear resolution under tested conditions. On 8 mM Cu gradient plates, *che-2* mutant animals (CB1033), of which sensory cilia formation are defective [214], lacked Cu avoidance behavior compared with N2 worms, supporting the importance of the chemosensory axis in Cu sensing. Meanwhile, *chca-1*(RNAi) worms demonstrated decreased levels of avoidance (Figure 3.21 C), suggesting that CHCA-1 is required for a role in sensing and avoiding toxic Cu concentrations. To test whether altered systemic Cu levels in *chca-1*(RNAi) worms result in changes to avoidance behaviors, both Cu-deprived and Cu-overloaded worms were generated by pre-culturing N2 worms in 100 μ M BCS or 100 μ M Cu conditions, and along with N2 worms cultured in basal media, placed on Cu gradient and non-Cu plates. The Cu-deficient worms exhibited less avoidance compared with non-pre-cultured worms, which recapitulated the behavior of *chca-1*(RNAi) worms. However, interestingly, Cu-overloaded worms also revealed less avoidance of toxic Cu (Figure 3.21 D). These results suggest that *C. elegans* Cu sensing behavior is correlated with abnormal Cu levels, although the precise

mechanisms that determine this behavior remain elusive.

Cu is known to be crucial for the neuropeptide maturation process through the Cu-dependent peptidyl-glycine alpha-amidating monooxygenase (PAM) [90]. To test whether neuropeptides are important for Cu-sensing behavior in worms, using RNAi hypersensitive strains that allow mRNA silencing in neurons [215], the pro-protein convertase *egl-3* and the carboxy peptidase *egl-21* were silenced individually [216, 217] and a significantly decreased avoidance behavior was observed (Appendix Figure II A). Furthermore, depletion of all predicted *PAM* orthologs in *C. elegans* (*pgal-1*, *pghm-1* and *pamn-1*) caused reduced Cu avoidance (Appendix Figure II B). Gene silencing efficiency was tested by qRT-PCR performed in parallel to the RNAi experiments. After RNAi treatment, mRNA levels of *che-2*, *egl-3*, *egl-21* and *PAMs* were decreased (Figure 3.22). Taken together, our results suggest that Cu-sensing and/or corresponding behavior of *C. elegans* is associated with the Cu-dependent neuropeptides maturation in neurons that requires CHCA-1 activity and balanced body Cu levels.

3.3 Discussion

Cu acquisition via Cu transporter (CTR) family proteins is critical for survival during fluctuations in environmental Cu levels. Our studies reveal that, similar to yeast, fish, and mammals, worms lacking CHCA-1 have lower systemic Cu levels and exhibit profound growth and reproductive defects under low Cu availability. Our results with worm CTR candidates also suggest that the pathway for Cu traffick-

Figure 3.21: **CHCA-1 is required for Cu sensing and Cu-dependent avoidance behavior.** A) Representative results of N2 worm distribution on a non-Cu plate (left) or 10 mM Cu-gradient plate (right). Error bars, mean \pm SEM of two independent experiments. Asterisk indicate the percentage of animals in the low Cu area (sections 1 and 2) is significantly different from the percentage in the high Cu area (sections 4 and 5) (Two-way ANOVA, Sidak post hoc test, $**p < 0.01$, ns = not significant). B) N2 worm avoidance index on Cu gradient plates with varied concentrations of Cu. Error bars indicate mean \pm SEM of three independent experiments. Asterisk values are significantly different from the avoidance index on non-Cu plates (One-way ANOVA, Dunnett post hoc test, $***p < 0.001$, $****p < 0.0001$). C) Avoidance index of CB1033 (*che-2 (e1033) X*) and N2 vector worms or *chca-1* RNAi worms on 8 mM Cu gradient plates. Three independent experiments for CB1033 and six independent experiments for N2 were analyzed (One-way ANOVA, Dunnett post hoc test, $*p < 0.05$, $***p < 0.001$). D) Worms were pre-cultured with 100 μ M CuCl₂ or 100 μ M BCS for one generation and assayed on 8 mM Cu gradient plates. (One-way ANOVA, Dunnett post hoc test, $***p < 0.001$, $****p < 0.0001$).

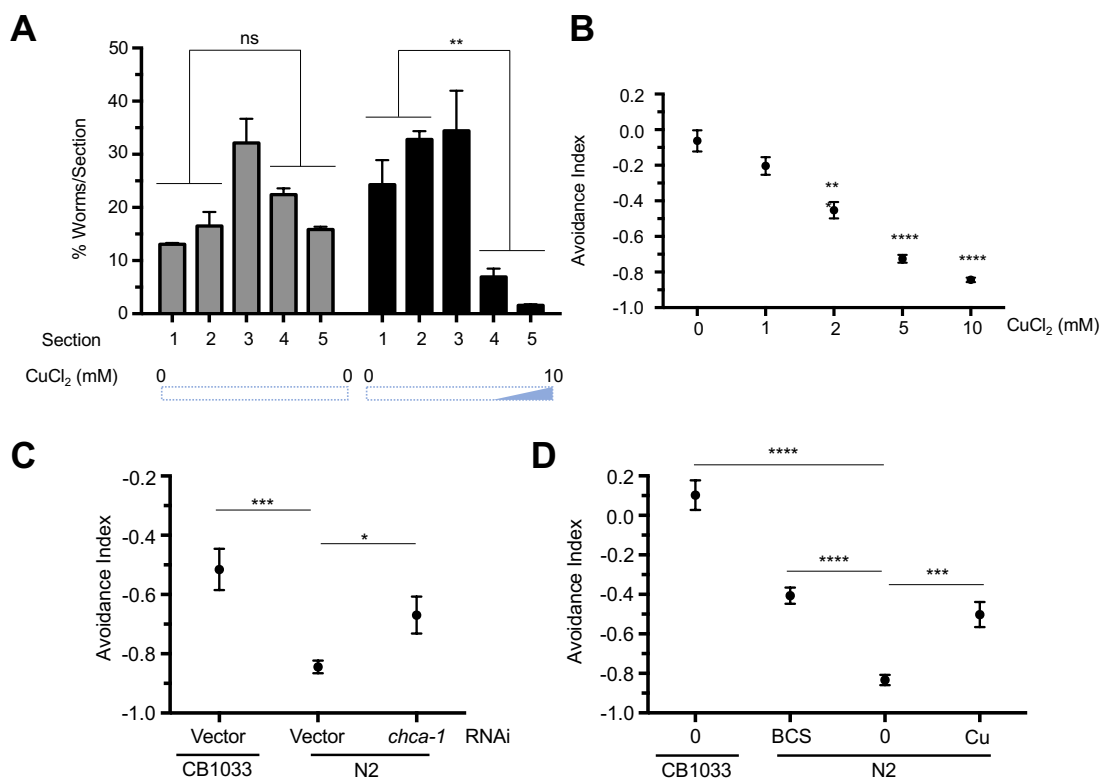
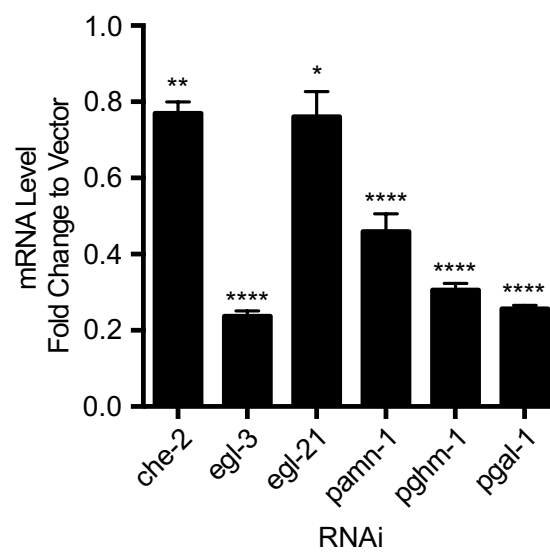


Figure 3.22: **The efficacy of RNAi treatments is assessed by qRT-PCR.** TU3335 worms treated with vector or indicated RNAi were cultured under basal condition till L4 stage followed by qRT-PCR analysis. Results from three or four independent experiments were analyzed by t-test ($*p < 0.05$, $**p < 0.01$, $****p < 0.0001$).



ing to the secretory pathway via the CTR1-ATOX1-ATP7A/B axis in mammals is conserved in worms. *C. elegans* can thus be exploited as a facile whole live animal system to isolate novel components regulating Cu homeostasis, as well as providing additional insight into known components.

For example, the fact that *C. elegans* CHCA-1 is predicted to lack a third TMD, as well as lacking a C-terminal cysteine or histidine residue, calls into question the minimal structural requirements for a high affinity Cu transporter. Additionally, while yeast Cu metabolism components are regulated transcriptionally, and mammalian Cu metabolism components are generally regulated at the post-translational level, worms exhibit characteristics of both. *CTR* homolog genes, such as *F58G6.3* and *F58G6.7*, are transcriptionally regulated by Cu. The worm ATP7A/B homolog, CUA-1, is regulated both transcriptionally and post-translationally [126]. *C. elegans* may thus shed light on the evolutionary history of Cu metabolism regulation. Importantly, we show differing contributions of CHCA-1 to systemic Cu metabolism depending on whether it is expressed in the intestine or in the hypodermis. Thus, *C. elegans* also provides insight into coordination of Cu homeostasis in multi-tissue organisms.

Uncovering ten *CTR* candidate genes in *C. elegans* was unexpected, as other model organisms contain fewer *CTR* homologs. Individually silencing these candidate genes did not severely affect worm growth or Cu accumulation under basal or Cu replete conditions (Figure 3.2 A and Figure 3.4 A). While non-CTR ortholog metal importers could contribute to dietary Cu uptake in *C. elegans*, it is also likely that several *CTR* genes function redundantly, or that CTR proteins form higher-

order heteromultimers which serve as fully active Cu transporters [218]. Considering that CHCA-1 is dominantly enriched only in the intestine and hypodermis, it is possible that other CTR proteins in *C. elegans* are expressed in different tissues, and/or are required under different Cu conditions or during specific developmental stages.

While studies demonstrate that mammalian CTR1 constitutively cycles from endosomal compartments to the plasma membrane in many cultured cell lines [208], and endogenous mouse CTR1 is localized to both the apical membrane and intracellular compartments of intestinal epithelial cells in mouse models [41], our data demonstrate that CHCA-1 localizes mainly to intracellular vesicles with minimal localization to the apical membrane. Reports in *C. elegans* have identified lysosome-like compartments known as gut granules in the intestine that could serve as a buffering subcellular organelle by transporting metals in the compartment under Cu or Zn overload conditions [126, 219]. It is plausible that Cu stored in gut granules could be recycled by CHCA-1 upon Cu-starvation. However, CHCA-1::GFP was not found to co-localize with gut granules. These results suggest that CHCA-1 may function to transport Cu across from the lumen of an as-yet-unidentified intracellular compartment, while other Cu importers drive Cu transport across the plasma membrane. Further studies will be necessary to ascertain whether CHCA-1 is important for the mobilization of Cu from endosomes.

In addition to the intestine, a significant induction of *chca-1* expression in the hypodermis is also observed under Cu deprivation. Similarly, *cua-1* abundance also increases in the hypodermis during Cu deficiency, for which regulation may also occur at the transcriptional level [126]. The hypodermis is known to play a role in

Fe [220] and heme homeostasis in worms [221]; as such, these findings strengthen its potential role in Cu homeostasis. It is plausible that hypodermal CHCA-1 acquires Cu to incorporate into the secretory pathway through CUA-1 activity. Alternatively, CHCA-1 in the endosomes together with CUA-1 in the plasma membrane may function to recycle stored Cu in the hypodermis to peripheral tissues in response to systemic Cu deficiency, as the worm hypodermis is known to store other nutrients [222].

Dwelling in the soil, *C. elegans* encounters a complicated and mercurial environment requiring flexible responses to pathogen exposure, gas composition, and temperature transitions, as well as undesirable nutrient concentrations. Behavioral studies in worms under varying environmental stimuli have led to important discoveries, establishing the sensing and signaling axis towards CO₂/O₂ and temperature [223, 224, 225, 226, 227]. High concentrations of Cu are used as a chemical repellent and several Cu chemosensory neurons have been identified [212, 213]. In this study, CHCA-1 was shown to be required for sensing and avoiding Cu, possibly via downstream effects of systemic Cu scarcity, as worms lacking CHCA-1 or with limited dietary Cu sources both revealed significantly decreased avoidance to toxic levels of Cu. Further experiments suggest that a neuropeptide maturation process, which is Cu-dependent in many organisms, is involved in worm Cu sensing and avoiding (Appendix Figure II). Cu deficient worms may have an increased capacity to uptake Cu and to be resistant to toxic Cu levels, resulting in decreased avoidance in the time frame of our assays. Alternatively, this altered behavior may be due to defects in biogenesis of neuropeptides required for Cu sensing, or altered signal transmission

to downstream interneurons or motor neurons.

An unanticipated observation from our studies was that dietary Cu-overload worms also showed reduced avoidance of toxic Cu. It is reported that acute Cu exposure induces ASH neuron activity, but repeated Cu stimulation leads to the reduction in the avoidance response and in ASH neuronal activity. This may result in changes to receptor activity and any downstream signaling pathways [228]. Another explanation could be the failure of sensing caused by Cu toxicity during pre-culture in high Cu conditions [229]. Is there a Cu-specific receptor on the neuronal cell surface that elicits subsequent behavioral responses? Could there be a Cu-sensing olfactory receptor? While the vertebrate olfactory system has a single receptor gene expressed in each sensory neuron [230], worms have limited numbers of chemosensory neurons, with multiple receptors expressed in one sensory neuron. There are ~1300 receptor genes found based on phylogenetic analysis. While electrical and hormonal signals are commonly used for neuronal signaling, neuropeptides, many of which are thought to be Cu-dependent, function as crucial signaling regulators as well [231, 232]. Identification of the essential components in the signaling events will provide leads for future studies seeking to understand Cu-responsive decision-making and behavior in *C. elegans*.

Chapter 4: The copper-binding pharmacological agent elesclomol restores systemic copper deficiency in *Caenorhabditis elegans* and *Mus musculus*

4.1 Summary of the project

Copper (Cu) is a crucial micronutrient that serves as a cofactor for several enzymes such as cytochrome c oxidase for energy production. Failure to supply sufficient Cu to Cu-dependent enzymes is correlated with developmental and neurological disorders. In humans, Cu deficiency is associated with Menkes disease (MNK), a severe disease caused by mutations in the Cu transporter ATP7A. A recent study revealed the potential of the anti-cancer drug elesclomol (ES) to restore intracellular Cu homeostasis and mitochondrial function in cells lacking the expression of several Cu transporters and chaperones. In our study, we further investigated this drug using several genetic models of Cu-deficiency. In *chca-1*-depleted *C. elegans* (ortholog of the Cu importer *Ctr1*), ES administration fully rescued the growth defect and Cu levels under Cu-deprived culture conditions. In addition, ES also restored the lethality in worms lacking *cua-1* (*ATP7A* ortholog) expression, suggesting ES-mediated restoration of dietary Cu uptake into intestine and to peripheral tissues

in *C. elegans*. In cardiac-specific *Ctr1* knockout mice (*Ctr1^{hrt/hrt}*), subcutaneous injection of ES significantly rescued lethality, developmental retardation, and cardiac mitochondrial function. Aberrant elevation of ATP7A protein in the liver and intestine in *Ctr1^{hrt/hrt}* in response to cardiac Cu deficiency also returned to normal levels after ES treatment. In cultured cells, ES mediated Cu transport through tight junctions of blood-brain-barrier (BBB) cells. Meanwhile, ES was found ineffective in delivering Cu to the cuproenzyme tyrosinase in the absence of *ATP7A in vitro*. Our study reveals the capability of ES to rescue Cu deficiency in mouse and *C. elegans* independent of Cu transporters, and sheds light on the clinical application of ES in Cu-deficiency diseases.

4.2 Results

4.2.1 Elesclomol chemically rescues *chca-1* phenotypes in *C. elegans*

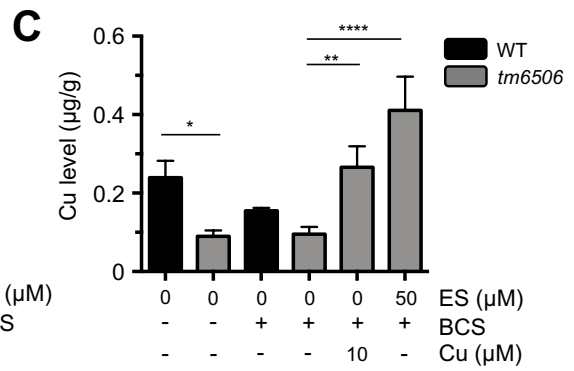
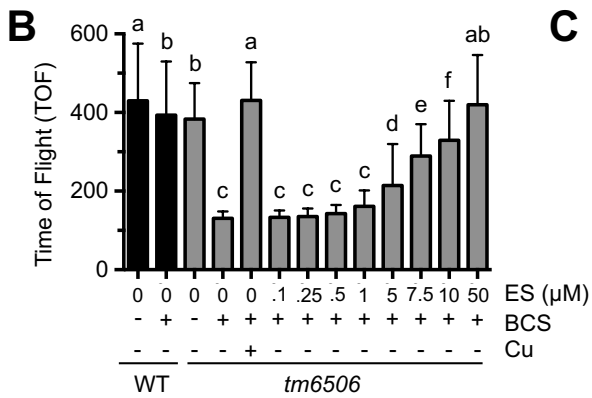
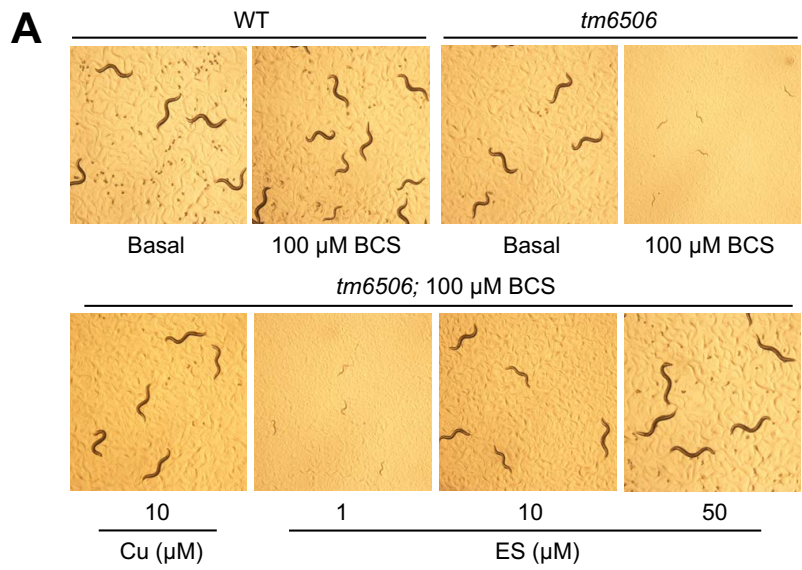
ES was first characterized using *Ctr1*-associated Cu-deficiency models. Cu import through *Ctr1* is crucial for organisms to maintain Cu homeostasis, and impaired Cu uptake results in defects in growth, development, and causes neurological disorders. In *C. elegans*, loss of function of CHCA-1, a *Ctr1* ortholog expressed in the intestine and hypodermis resulted in reduced Cu accumulation in the whole worm, as well as growth retardation and embryogenesis defects under low Cu conditions [233]. Mutant *chca-1* worms (*chca-1 (tm6506) IV*) and wild-type brood mates (WT) were synchronized by bleaching and L1 larva were plated on NGM

growth media containing 0 or 100 μM bathocuproinedisulfonic acid (BCS), a Cu(I) chelator. Additionally, 10 μM copper chloride (CuCl_2) or various concentrations of ES (from 0.1 to 50 μM) were added to BCS-containing plates. After three days, *tm6506* worms exhibited a slight developmental delay under basal conditions and a severe growth defect when grown on low Cu. This defect could be fully rescued by adding Cu to the media (Figure 4.1 A). ES supplementation was able to rescue growth of *tm6506* worms in a dose-dependent manner. Quantification of worm body length suggested that rescue of *tm6506* worm growth occurred with 5 μM or higher concentrations of ES added to 100 μM BCS-containing media, until full growth rescue was achieved with 50 μM ES supplementation (Figure 4.1 B). Additionally, the reduced overall Cu levels found in *tm6506* animals were fully restored by ES supplementation (Figure 4.1 C).

4.2.2 ES administration rescues lethality, growth defects and cardiac hypertrophy found in cardiac-specific *Ctr1* knockout mice

Cardiac-specific *Ctr1* depleted mice (*Ctr1^{hrt/hrt}*) were chosen in order to further characterize ES using a Cu-deficient mammalian model. *Ctr1^{hrt/hrt}* mice exhibit cardiac hypertrophy, low bioavailable Cu in the heart, and increased Cu levels in the serum. Compared to wild-type mice, *Ctr1^{hrt/hrt}* mice showed reduced weight gain around P6 or P7, and the median survival of mutant mice is P10 [102]. In this study, 10 mg/kg of ES or vehicle were given to *Ctr1^{hrt/hrt}* mice (KO) and their wild-type littermates (WT) via subcutaneous injection once every three days

Figure 4.1: Elesclomol rescues growth retardation and Cu levels in *chca-1* depleted *C. elegans*. A) Representative images of *chca-1* depleted worms (*tm6506*) treated with ES under Cu-deficient conditions. Wild-type (WT) brood mates and *tm6506* worms were synchronized and L1 stage worms were then seeded on basal NGM media or media containing 100 μM BCS. 10 μM Cu or various concentrations of ES (from 0.1 to 50 μM) were simultaneously added to the media. An equal volume of DMSO was added to every culture plate as a vehicle control. Images were taken 72 hours after seeding worms. B) Worm body length quantification (TOF, time of flight) by the COPAS BioSort system. Groups with different letters are significantly different from each other at $p = 0.05$ (one-way ANOVA, Sidak post hoc test). C) Total worm body Cu levels measured by ICP-MS with three biological replicates. Significance among treatments are labeled with asterisk (**** $p < 0.0001$, ** $p < 0.01$, * $p < 0.05$, one-way ANOVA, Bonferonni's post hoc test). Error bars represent mean \pm SD.



starting from P5. As reported previously, administering 25-100 mg/kg ES to a tumor-bearing nude mouse model did not show any toxic effects on either cancerous or normal cells [149]. Therefore, the dose of 10 mg/kg of ES used in this experiment is likely to be a safe dose for wild-type mice.

While all vehicle-treated *Ctr1^{hrt/hrt}* pups began to lose weight from P7 and died by P12, ES-treated KO pups showed normal development and weight gain compared to WT (Figure 4.2 A). To test whether ES supplementation up to four weeks of age is sufficient to rescue the developmental defect of *Ctr1^{hrt/hrt}* mice, ES-injected WT and KO mice were regrouped on P26, where half of the mice continued to receive ES while the other half were switched to vehicle. Note that the injection interval was extended from three days to one week. After being switched from ES to vehicle, *Ctr1^{hrt/hrt}* mice continued to gain weight and showed no significant difference in body mass compared to other groups (Figure 4.2 B). The genotypes of all mice used in this study were confirmed by PCR using heart genomic DNA, as described previously [110] (Figure 4.3 A). Cardiac Ctr1 protein levels were tested by immunoblot using tissue lysates from P12 mice, and *Ctr1^{hrt/hrt}* mice showed decreased expression of both glycosylated and truncated forms of Ctr1 (17 kDa and 35 kDa, respectively) (Figure 4.3 B). These results indicate that Ctr1 was partially deleted in *Ctr1^{hrt/hrt}* mice, and the deletion was sufficient to cause growth and survival defects. Importantly, ES injection did not alter Ctr1 depletion efficiency or protein expression levels.

P10 *Ctr1^{hrt/hrt}* mice were examined to determine the effect of ES on growth defects and cardiac hypertrophy. *Ctr1^{hrt/hrt}* mice on P10 (after only two ES injec-

tions) appeared normal in size, and the body mass was fully rescued compared to WT (Figure 4.4 A and B). While vehicle-treated *Ctr1^{hrt/hrt}* mice exhibited enlarged hearts (with a higher heart/body mass ratio), ES administration significantly rescued heart size back to WT levels (Figure 4.4 C). Furthermore, *Ctr1^{hrt/hrt}* mice exhibited absent or tiny thymus sizes and smaller spleens compared to wild-type. Cu has been suggested to play a crucial role during lymphatic organ development, as dietary Cu-deficient mice had underdeveloped thymus glands with reduced Cu accumulation and low cytochrome c oxidase activity [234, 235, 236]. However, the mechanism for this is not understood. In *Ctr1^{hrt/hrt}* mice, ES administration significantly restored the thymus and spleen sizes to normal mass ratios (Figure 4.4 D and E). Meanwhile, WT mice after ES treatment revealed no difference in body mass/tissue mass ratio compared to vehicle-injected WT (Figure 4.4 B-E).

4.2.3 Cardiac Cu deficiency in *Ctr1^{hrt/hrt}* mice can be restored by

ES-dependent Cu delivery

Ctr1^{hrt/hrt} mice exhibit enlarged cardiomyocytes, reduced Cu levels and decreased Cco component abundance in their heart compared to WT mice. Cardiomyocyte morphology was observed by hematoxylin and eosin staining. P10 *Ctr1^{hrt/hrt}* mice exhibited enlarged cardiomyocytes with large nuclei. Upon ES treatment, cell sizes were decreased in these knockout mice (Figure 4.5 A). Immunostaining of WGA (wheat germ agglutinin) in these tissues revealed a significantly reduced cell surface area, though not reduced to the size of cardiomyocytes in WT mice (Figure 4.5 B and

C). Next, cardiac Cu levels were determined using inductively coupled plasma mass spectrometry (ICP-MS). After two ES injections, P10 *Ctr1^{hrt/hrt}* mice exhibited increased cardiac Cu levels, through again, not rescued to the levels in WT mice. ES-injected WT mice accumulated more Cu in their hearts than vehicle-injected WT mice (Figure 4.6 A). Bioavailable Cu levels were estimated using CCS (Cu chaperone for Cu, Zn superoxide dismutase) protein abundance, the expression of which is stabilized by Cu-deficiency in *Ctr1^{hrt/hrt}* mice. After ES injections, the cardiac CCS abundance of *Ctr1^{hrt/hrt}* mice was similar to WT levels (Figure 4.6 B and C), suggesting that ES could mediate Cu delivery into cardiac tissues. Furthermore, the abundance of cytochrome c oxidase component Cox1 in hearts of P10 *Ctr1^{hrt/hrt}* mice was significantly increased by ES administration, though not restored to WT levels after two injections (Appendix Figure III). After extending the ES treatment until P26 or P54, the Cco components abundance in *Ctr1^{hrt/hrt}* mice were similar to levels found in WT mice (Figure 4.6 D,E and F). Taken together, these findings suggest that Cu delivery through ES to *Ctr1*-depleted cardiac cells could restore the abnormal cardiomyocyte morphology and mitochondrial function.

4.2.4 ES supplementation rescues the altered systemic ATP7A protein levels of *Ctr1^{hrt/hrt}* mice

Ctr1^{hrt/hrt} mice show elevated serum Cu levels, as well as elevated ATP7A Cu exporter protein abundance in the liver and the intestine epithelial cells. It is hypothesized that ATP7A may be able to mobilize Cu from Cu absorption and

Figure 4.2: ES injection rescues lethality and growth retardation of cardiac-specific Ctr1 knockout mice. A) Control littermates ($Ctrl1^{flox/flox}$ or $Ctrl1^{flox/+}$, referred to as WT), or cardiac-specific Ctr1 depleted mice ($Ctrl1^{hrt/hrt}$, referred to as KO) were injected subcutaneously with 10 mg/kg body weight of ES or vehicle (0.5 % methyl cellulose solution containing 2 % DMSO). Injections were performed once every three days from postnatal day 5 (P5) until P26, and body weight was recorded every day. The number of mice treated under each condition are indicated (N). The three vehicle treated KO mice were found dead on P8, P12 and P12. No death was found in ES-injected KO mice. Asterisk marks indicate significant difference compared to the WT vehicle group (two-way ANOVA, Tukey's post hoc test, $*p < 0.05$, $***p < 0.001$). B) ES supplemented WT or KO mice were split on P26, half of the mice continued with ES injection once per week, and the other half were switched to vehicle treatment. Body weight was recorded once a week until P54. No significant difference was found among groups by two-way ANOVA. For the entire figure, error bars represent mean \pm SD.

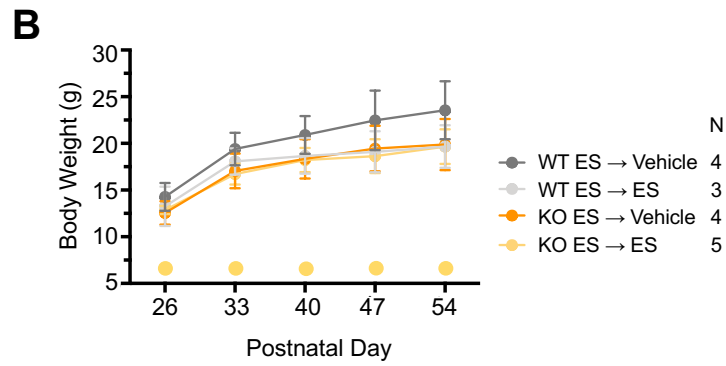
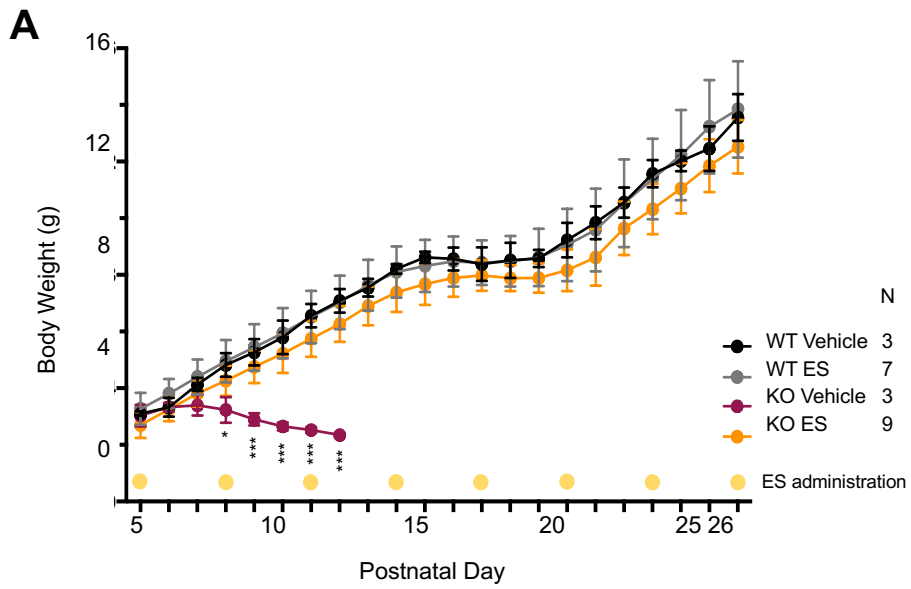


Figure 4.3: Cardiac *Ctrl1* excision efficiency in *Ctrl1^{hrt/hrt}* mice. A) Representative genotyping result from *Ctrl1^{flox/flox}* and *Ctrl1^{hrt/hrt}* heart genomic DNA at P10. The lower 241 bp band and the upper 281 bp band reflect the floxed *Ctrl1* allele and the deleted *Ctrl1*, respectively. B) Cardiac *Ctrl1* and CCS protein abundance from WT and KO mice at P12. Tubulin serves as loading control.

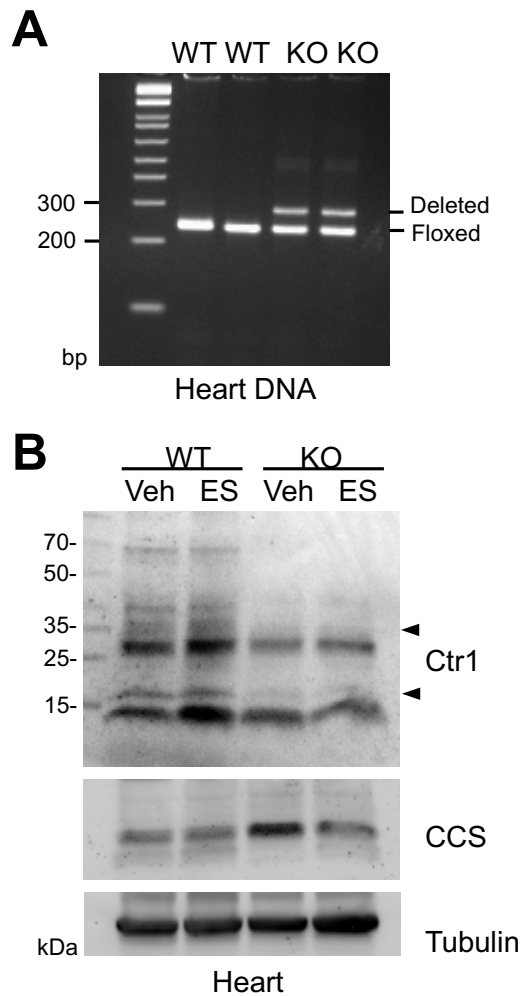


Figure 4.4: Abnormal body mass and organ sizes in $Ctr1^{hrt/hrt}$ mice are rescued by ES supplementation. A) Cardiac $Ctr1$ KO mice and WT littermates at P10 after ES or vehicle treatment. Scale bar, 1 cm. B) Quantification of mouse body weight under each treatment condition. Mouse numbers are indicated (N). C-E) Relative organ sizes, presented as organ weight /body weight, for heart (C), spleen (D), and thymus (E). Representative organ images are provided below each panel. Scale bars, 1 cm. For panel B-E, differences among groups are analyzed by one-way ANOVA (Sidak post hoc test), groups with different letters are significantly different from each other at $p = 0.05$. For the entire figure, error bars represent mean \pm SD.

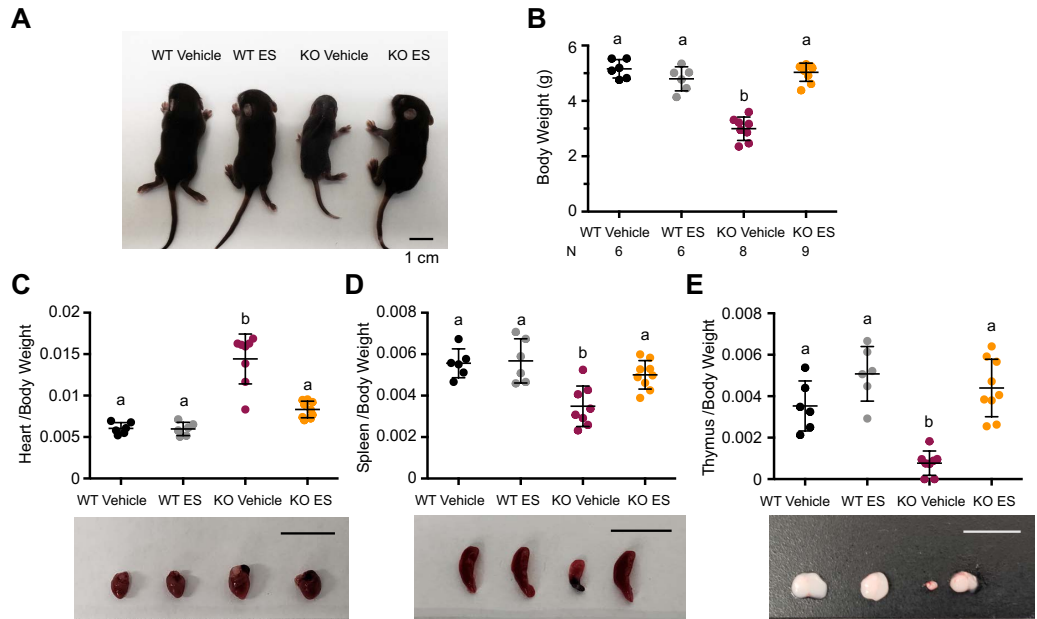


Figure 4.5: **ES administration rescues cardiac hypertrophy of *Ctr1^{hrt/hrt}* mice.** A) H&E staining of heart sections from P10 *Ctr1^{hrt/hrt}* and WT littermates supplemented with vehicle or 10 mg/kg ES on P5 and P8. Scale bars, 25 μm . B) and C) Quantification of cardiomyocyte surface area. P10 heart sections were immunostained with wheat germ agglutinin, and cell surface area was quantified by Image J (45 cells for each condition). Groups with different letters are significantly different from each other at $p = 0.05$ (one-way ANOVA, Sidak post hoc test). Error bars, mean \pm SD. Scale bars, 25 μm .

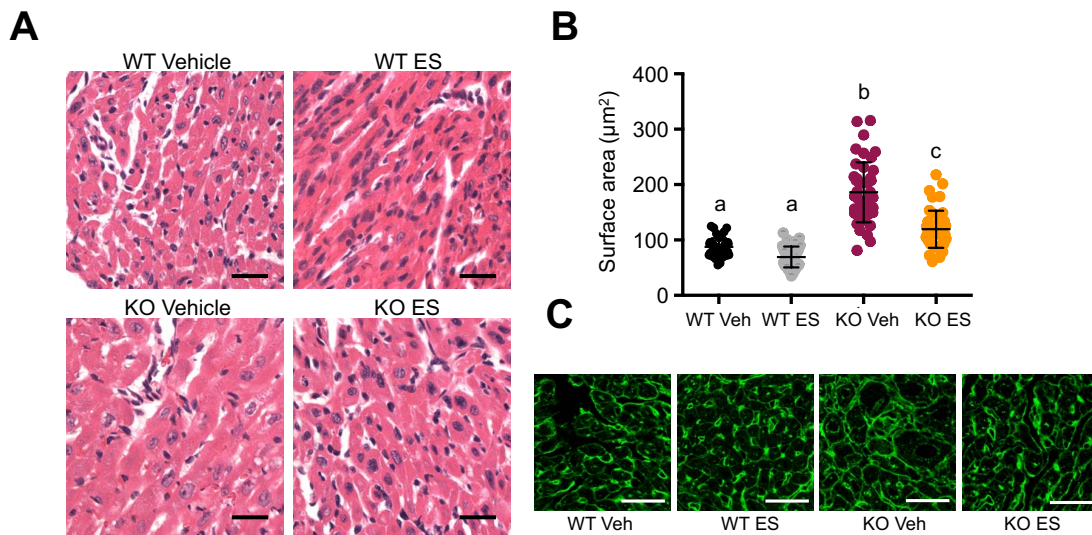
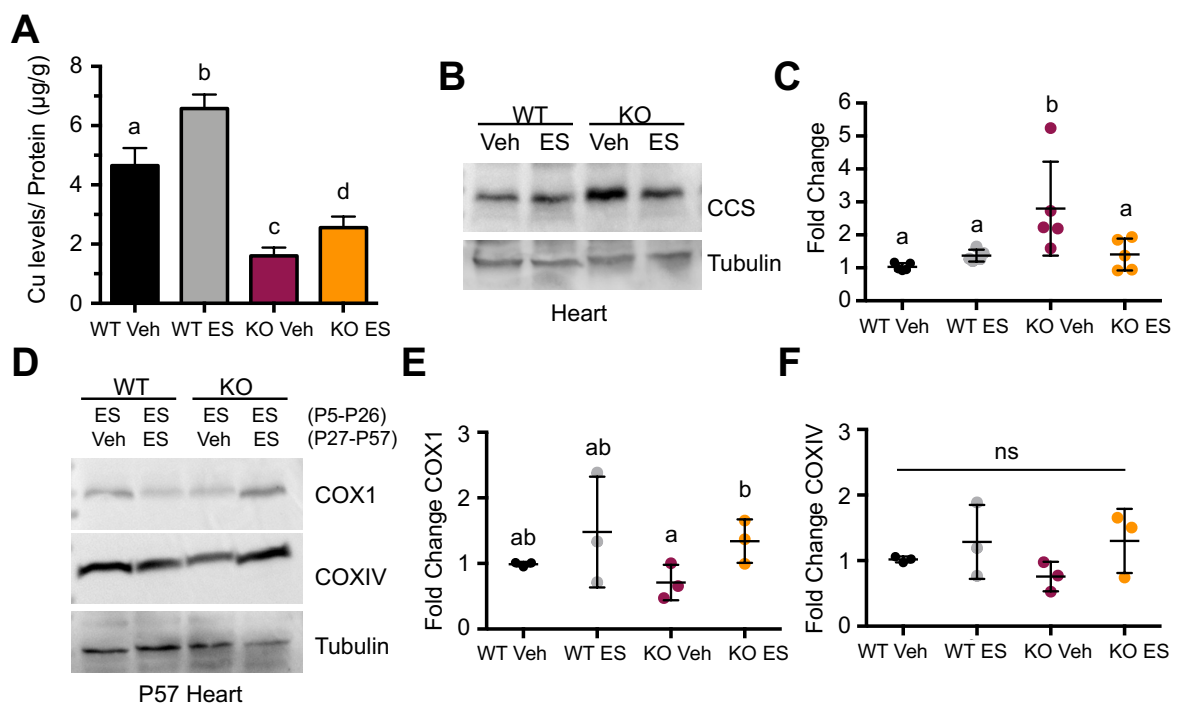


Figure 4.6: **ES restores bioavailable Cu levels and Cco abundance in *Ctr1^{hrt/hrt}* mice cardiac tissue.** A) Cu levels in cardiac tissues from P10 WT or in *Ctr1^{hrt/hrt}* mice supplemented with vehicle or 10 mg/kg ES on P5 and P8. N=3 or 4 for each condition. Error bars, mean \pm SD. Differences among groups are analyzed by one-way ANOVA at $p = 0.05$ (Sidak post hoc test) and indicated by differing letters. B) Representative Western blot results and C) quantification of cardiac CCS abundance in P10 mice with vehicle or ES treatment. N=4 for each treatment. Tubulin abundance serves as loading control. Groups with different letters are significantly different from each other at $p = 0.05$ (one-way ANOVA, Sidak post hoc test). Error bars, mean \pm SD. D) Representative Western blot of P54 mice cardiac tissue ETC complex IV and its subunit protein abundance. E) and F) Quantification of COX1 and COXIV abundance from D). N=3 for each condition. Tubulin abundance serves as loading control. Groups with different letters are significantly different from each other at $p = 0.05$; ns, not significant (one-way ANOVA, Sidak post hoc test). Error bars, mean \pm SD.

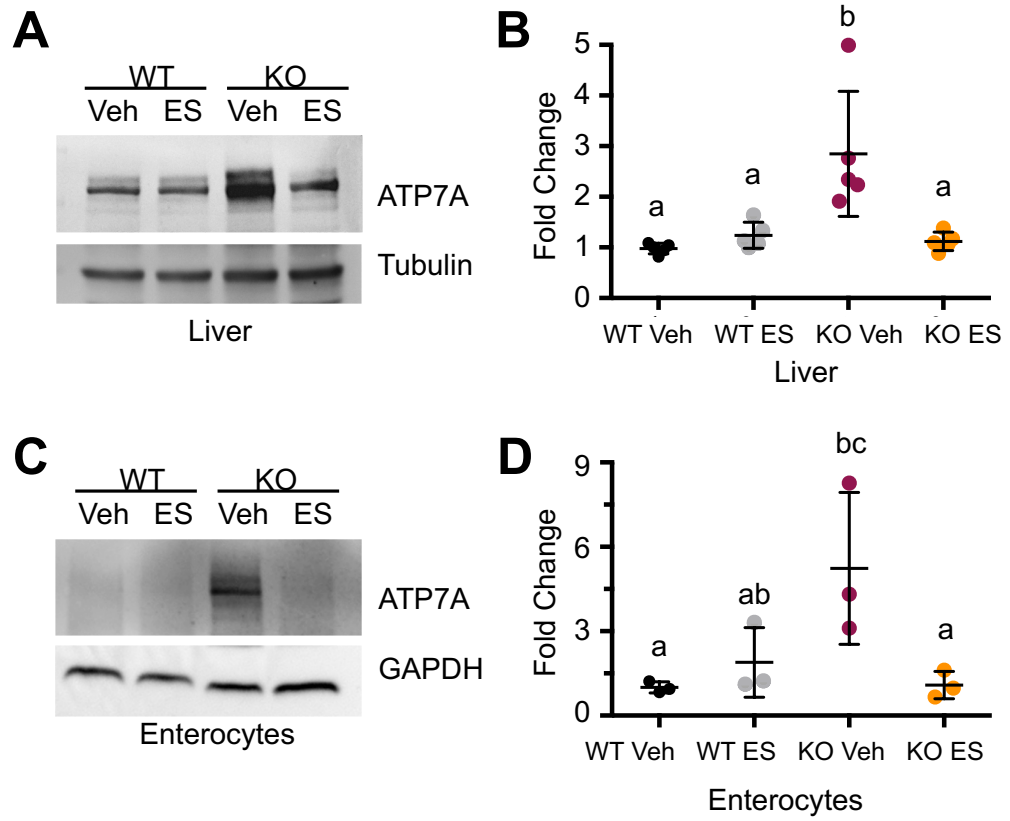


storage sites to the Cu-deficient cardiac tissue, and that the heart may communicate with both of these tissues by secreting signaling molecules into the serum in order to induce hepatic and intestinal ATP7A expression [102]. In this study, ES treatment suppressed ATP7A protein abundance in P10 or P12 *Ctr1^{hrt/hrt}* mouse liver and enterocytes back to WT levels (Figure 4.7). Because liver and intestine ATP7A protein expression were not affected by ES treatment in WT mice liver and intestine, this is a possible consequence of adequate Cu supply to heart tissues via ES, which in turn downregulates the cardiac deficiency-triggered systemic Cu homeostasis responses.

4.2.5 Intestinal CUA-1-associated lethality and embryogenesis defects can be restored by ES treatment

ATP7A is crucial for dietary Cu transport from the intestine to peripheral tissues, is required for Cu delivery to cuproenzymes in the secretory pathway. Mutations in ATP7A can lead to the Cu-deficient Menkes disorder in humans. In *C. elegans*, the ATP7A ortholog CUA-1 is expressed in the intestine, neurons, hypodermis and pharynx, and is required for normal growth and embryogenesis under dietary Cu-deficient conditions [126]. While RNAi depletion of *cua-1* in wild-type N2 worms resulted in lethality under low Cu conditions, it could be fully rescued by ES supplementation into the culture media (Appendix Figure IV A). In addition, the ES-treated *cua-1* RNAi worms were able to generate similar brood sizes compared to vector-treated worms (Appendix Figure IV B). Under all conditions, ES-treated

Figure 4.7: **ATP7A protein abundance in the liver and intestinal cells from ES- or vehicle-treated *Ctr1^{hrt/hrt}* mice.** A) and C) ATP7A abundance in P10-12 *Ctr1^{hrt/hrt}* mice and WT littermates liver (A) and enterocytes (C) after ES or vehicle (veh) injection. B) Quantification of liver ATP7A abundance from 5 individual experiments. D) Quantification of enterocyte ATP7A abundance from 3 individual experiments. ATP7A abundance was normalized to WT vehicle group and present as fold change in panel C and D. Error bars represent mean \pm SD. Groups with different letters are significantly different from each other at $p = 0.05$ (one-way ANOVA, Sidak post hoc test).



worms yielded slightly more hatched progeny, indicating ES alone or ES-mediated Cu delivery favors embryogenesis for worms grown under basal or Cu-deficient conditions.

BK015 transgenic worms (*Pvha-6::CUA-1.1::GFP; cua-1(ok904)*) constitutively express intestinal CUA-1 in a whole-body *cua-1* knockout background. RNAi depletion of *cua-1* in BK015 results in lethality, which can be rescued by Cu supplementation [126]. To further investigate the ability of ES to facilitate intestinal Cu absorption in *C. elegans*, *cua-1* RNAi was performed in BK015 strains. Synchronized L1 larvae were plated on NGM media containing vehicle control or up to 500 nM of ES, or 1 μ M CuCl₂. After three days, live and dead worms were counted and the survival percentage for each condition was calculated. Vector-treated worms showed 25% survival under basal condition, while *cua-1* RNAi worms were all found dead (Appendix Figure IV C). The lethality could be rescued by addition of 1 μ M of Cu. ES treatment (> 250 nM) significantly rescued worm survival up to 85%, and survival was fully restored to wild-type level by 500 nM of ES. Moreover, ES significantly rescued the survival of vector-treated worms, suggesting the effect of ES on Cu homeostasis in peripheral CUA-1-expressing tissues (Appendix Figure IV D). These results strongly suggest ES could facilitate dietary Cu absorption into the intestine and mediate Cu transport to peripheral organs, independent of CUA-1 expression.

4.2.6 ES exhibits potential for Cu-transport through cultured blood-brain-barrier cells

In Menkes patients and *mottled* mice, Cu cannot be effectively transported from blood to neuronal tissues through the blood-brain-barrier (BBB) due to mutations in ATP7A. Low Cu levels in the brain result in the dysfunction of several cuproenzymes that are directly related to the neurological disorders and early fatalities observed in Menkes patients [190, 237]. In order to test whether ES is capable of delivering Cu through the tight junctions of BBB cells, we used a well-established BBB cell line co-culture system *in vitro*, the immortalized human cerebral microvascular endothelial cell (hCMEC/D3) [238, 239, 240]. Consistent with previous reports, hCMEC/D3 cells exhibited trans-epithelial electrical resistance (TEER) above 60 ohm.cm² after several days of culture in the transwell insert, and expressed several BBB tight junction proteins (Figure 4.8 A and B). The permeability coefficient (Pe) of hCMEC/D3 to 4 kDa FITC-dextran in our culture system was approximately 5-6 10⁻⁶ cm/s after 10 days of culture (Figure 4.8 C), which is comparable to other reports [206, 241, 242, 243, 244]. We used the transwell co-culture system to mimic the BBB *in vitro*, started with cultured hCMEC/D3 cells in transwell inserts (referred to as the top well). After 10 days of culture, 0 or 7.5 nM of ES, 20 μ M CuCl₂, or a combination of ES and Cu was added to the apical side culture media of hCMEC/D3 cells. In the meantime, Cu-deficient *Cr1* knockout MEF cells (*Cr1*^{-/-}) were cultured in the bottom well. 24 hours after ES administration, *Cr1*^{-/-} cells were collected and the CCS abundance was analyzed to check

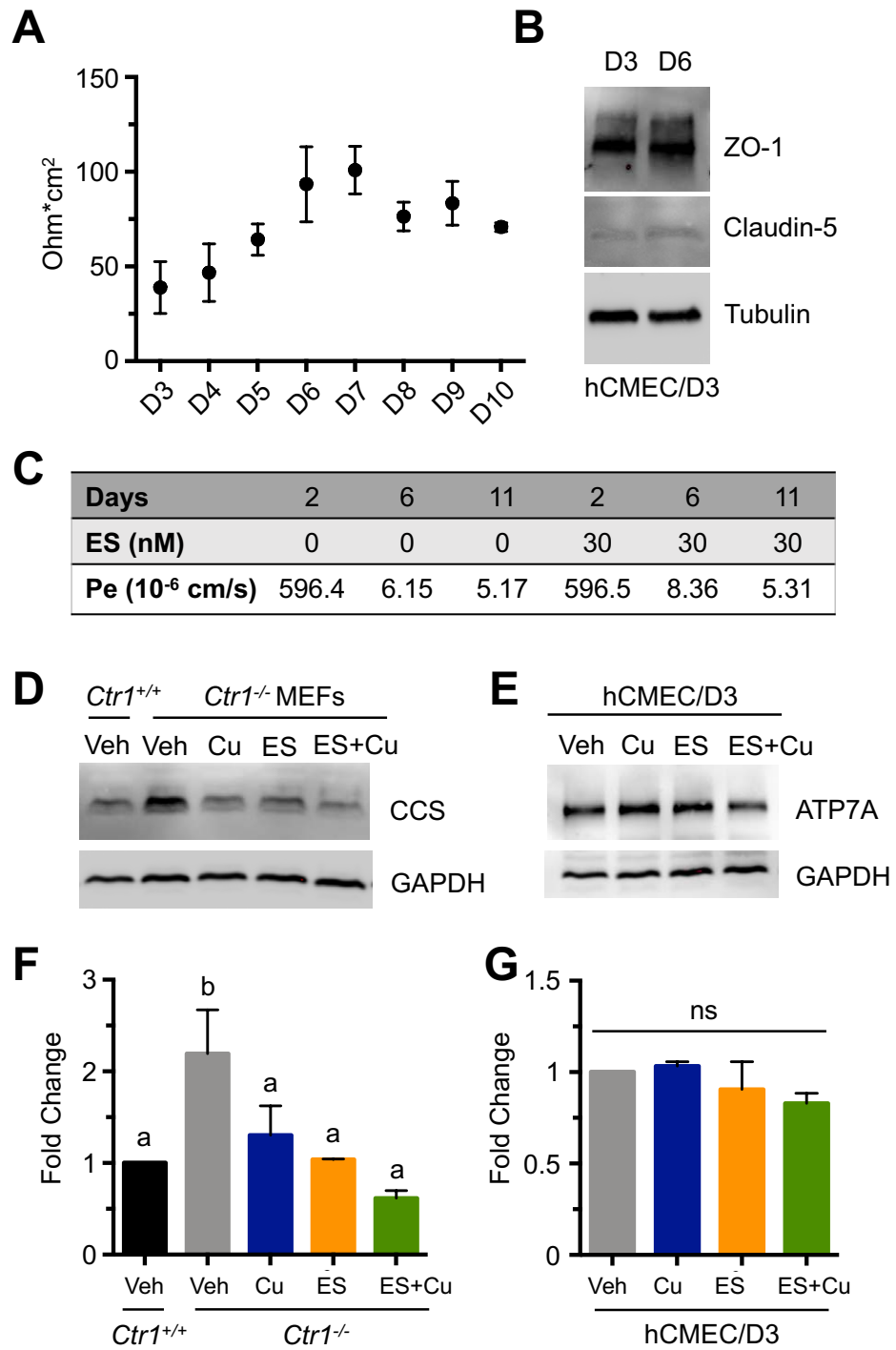
bioavailable Cu levels. Results indicated that ES administration to the apical side of BBB cells alone significantly increased the bioavailable Cu levels in the *Ctr1*^{-/-} cells cultured on the basal side of BBB cells (Figure 4.8 D and F). Neither 7.5 nM ES or 20 μ M Cu affected ATP7A protein abundance of hCMEC/D3 cells (Figure 4.8 E and G). These findings suggest ES could facilitate Cu transporting through the BBB tight junctions, which makes ES a promising treatment for Menkes-related neuronal disorders. Future *in vivo* studies will be helpful to further evaluate the permeability of ES to neuronal tissues.

4.2.7 Characterizing the effect of ES on tyrosinase activity in *ATP7A*^{-/-} cells

To assess the effect of ES on Cu delivery to cuproenzymes in the secretory pathway, tyrosinase activity was evaluated in wild-type and *ATP7A* knockout MEF cells (*ATP7A*^{-/-}) upon ES supplementation. Because a high dose of ES could inhibit cell growth and cause cytotoxicity, non-toxic concentrations of ES were first determined in MEF cells. Growth inhibition of MEF cells by ES was calculated by the total number of live cells after 1 day of treatment with various concentrations of ES. An effect on cell growth was observed upon treatment with 5 nM of ES, and the IC₅₀ of ES in MEF cells was close to 100 nM (Figure 4.9 A). Meanwhile, the LD₅₀ was not reached even with up to 7.5 μ M ES treatment (Figure 4.9 B).

Transportation of Cu to tyrosinase is dependent on ATP7A protein activity, as *ATP7A*^{-/-} MEF cells transfected with a tyrosinase-expressing vector (pTyr) showed

Figure 4.8: Apical ES treatment of BBB cells significantly increases Cu levels of cells grown on the basal side. A) Transendothelial electrical resistance (TEER) measurements of hCMEC/D3 cells grown on permeable transwell plates. Approximately 4×10^6 cells were plated on day 0 on collagen-coated 6-well inserts (surface area 4.67 cm^2) and TEER values were measured on indicated days after plating. $N=2$, error bars represent mean \pm SD. B) Expression levels of tight junction markers ZO-1 and Claudin-5 in BBB cells. C) Permeability coefficients of hCMEC/D3 to 4 kDa FITC-dextran were measured on indicated days after plating cells. Vehicle or ES was added to the apical side culture of hCMEC/D3 cells 24 hours before the assay. D) and E) 4×10^6 BBB cells were plated on collagen-coated 6-well transwell inserts. After 10 days, DMSO (Veh), 7.5 nM ES, 20 μM CuCl_2 (Cu), or ES plus Cu (ES+Cu) was added to the apical side culture media (upper well). Simultaneously, *Ctr1*^{-/-} MEFs were plated to the basal side of BBB (bottom well) for 24 hours. Protein levels of CCS in *Ctr1*^{-/-} MEFs and ATP7A in hCMEC/D3 were analyzed by immunoblottings. F) and G) Quantification of CCS and ATP7A protein abundance from two independent experiments. Groups with different letters are significantly different from each other at $p = 0.05$; ns, not significant (one-way ANOVA, Sidak post hoc test). Error bars, mean \pm SD.



no visible dopachrome formation (red color) after in-gel staining with the tyrosinase substrate L-DOPA. Tyrosinase activity was highly increased by co-transfection of *ATP7A*^{-/-} cells with both tyrosinase and ATP7A (Figure 4.10). Because this dose of ES was sufficient to rescue the mitochondrial function of *Ctr1*-depleted MEF cells in a previous study, 5 nM ES was added to wild-type and *ATP7A*^{-/-} cell culture media [175]. After 24 hours of ES treatment, *ATP7A*^{-/-} cells showed no visible tyrosinase activity (Figure 4.11 A and B). This may be due to insufficient bioavailable Cu in the tissue culture media or inside the *ATP7A*^{-/-} cells for ES to interact with. To test this possibility, a higher dose of 30 nM ES, or 30 nM ES-Cu plus 10 μ M CuCl₂ was added to the culture media. However, dopachrome formation still remained undetectable under these conditions in *ATP7A*^{-/-} cells (Figure 4.11 C and D). These results indicate a potential limitation of ES in delivering Cu into the secretory pathway. In wild-type cells, 30 nM of ES or ES-Cu significantly increased tyrosinase activity. This is likely due to increased intracellular Cu levels facilitated by ES, which are then available to be transported to tyrosinase (or other secretory pathway cuproenzymes) by ATP7A (Figure 4.11 C and D).

After treatment with 30 nM ES, total Cu levels in wild-type and *ATP7A* knockout MEF cells were assayed by ICP-MS. After 24 hours of ES treatment, the intracellular Cu levels remained unchanged in wild-type cells. Combined with previous findings, it is possible that excess Cu delivered into cells via ES was exported out of cells by ATP7A. Because cells lacking *ATP7A* are defective in Cu efflux, increased Cu levels in *ATP7A*^{-/-} cells were observed compared to wild-type cells, and ES treatment led to further Cu accumulation (Figure 4.9 C). These findings suggest

ES may inefficient to transport Cu into the trans-Golgi network in the absence of ATP7A.

4.3 Discussion

In mammals, an increased Cu requirement occurs during gestation and early postnatal periods, when compared to adulthood [245]. Cu deficiency caused by low dietary uptake, genetic polymorphisms or mutations and disease, could affect offspring from early postnatal stages, and result in dysfunction or diseased states in several organs including the brain, heart, blood and immune systems [246, 247]. In *Drosophila* and *C. elegans*, loss of Cu uptake due to Ctr1 ortholog protein dysfunction results in growth arrest at the early larvae stage, and could eventually lead to death. In mice, whole-animal Ctr1 depletion is embryonic lethal [28, 176]. Our results suggest Cu delivery via elesclomol to early larval *C. elegans* or perinatal mice could rescue the early developmental arrest and lethality in *chca-1(tm6506)* worms and *Ctr1^{hrt/hrt}* mice, respectively, supporting the critical role of Cu in embryonic and neonatal growth and development. *C. elegans* CHCA-1 is highly expressed in the intestine and hypodermis, and the growth retardation due to loss of this gene is predominantly caused by its dysfunction in the intestine [233]. Based on the finding that 50 μ M ES was sufficient to rescue *tm6506* mutant worm growth and Cu levels, it is plausible that ES could facilitate dietary Cu absorption when the intestinal Cu uptake mechanism is disrupted.

Results indicate that eight doses of ES administered from P5 to P26 at 10

Figure 4.9: **Effect of ES on Cu levels in wild-type and *ATP7A*^{-/-} MEFs.** A) Total living wild-type MEF cells treated with increasing amounts of ES. Indicated concentrations of ES were added to culture media for 24 hours before counting. Asterisk marks indicate significant difference from untreated cells as determined by one-way ANOVA (Sidak post hoc test, *** $p < 0.001$). B) Viability of cells in panel (A). (one-way ANOVA, Sidak post hoc test, * $p < 0.1$, *** $p < 0.001$). C) Cellular Cu levels of WT and *ATP7A* knockout MEF cells after 24 hours of ES treatment (30 nM). Cu levels were normalized to protein abundance as measured by BCA assay. Results present mean \pm SD from three biological replicates under each condition, and groups with different letters are statistically different from each other at $p = 0.05$ (one-way ANOVA, Sidak post hoc test).

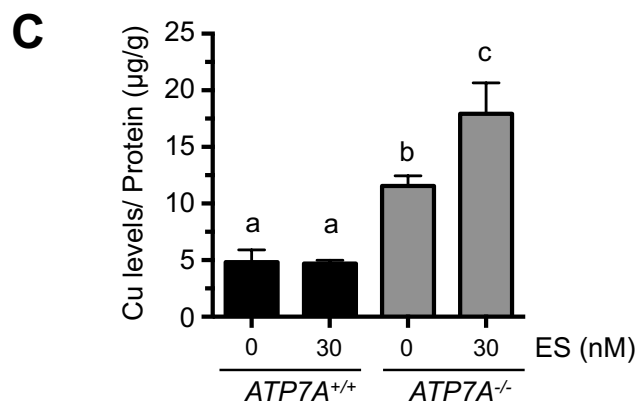
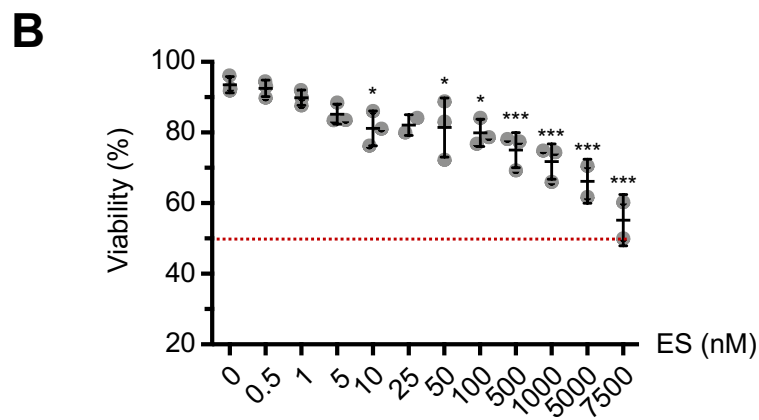
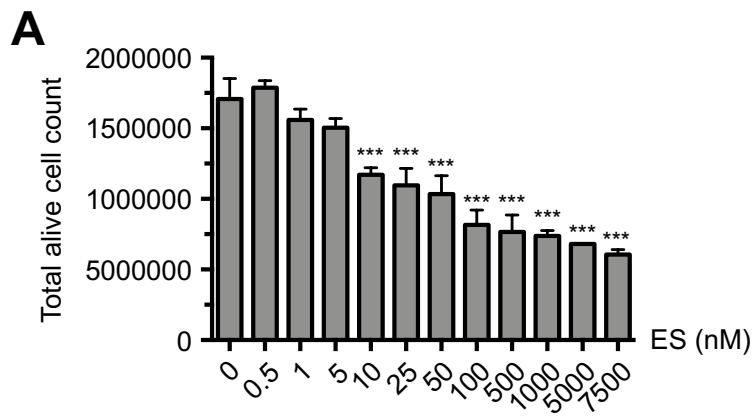


Figure 4.10: **ATP7A is required for tyrosinase activity.** A) *ATP7A*^{-/-} cells were transfected with an ATP7A-expressing vector, and ATP7A and tyrosinase protein abundance were tested by immunoblot. Tyrosinase activity was determined by the formation of dopachrome after in-gel staining with L-DOPA and 3-methyl-2-benzothiazolinone (A). B) Quantification of tyrosinase in-gel staining activity by Image J. Results from two independent experiments are presented, error bars represent mean \pm SD. Groups with different letters are significantly different from each other at $p = 0.05$ (one-way ANOVA, Sidak post hoc test).

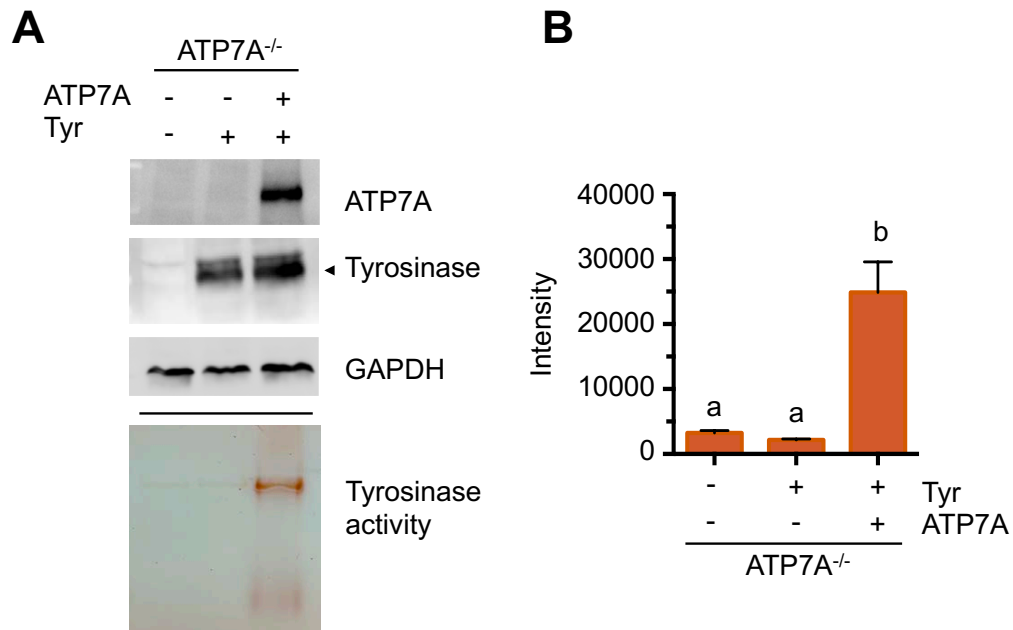
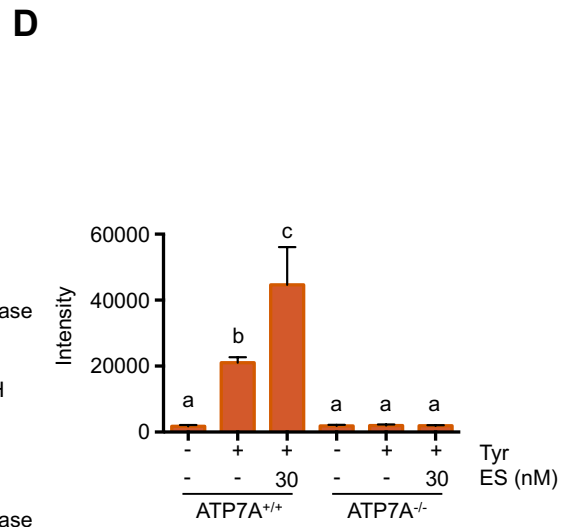
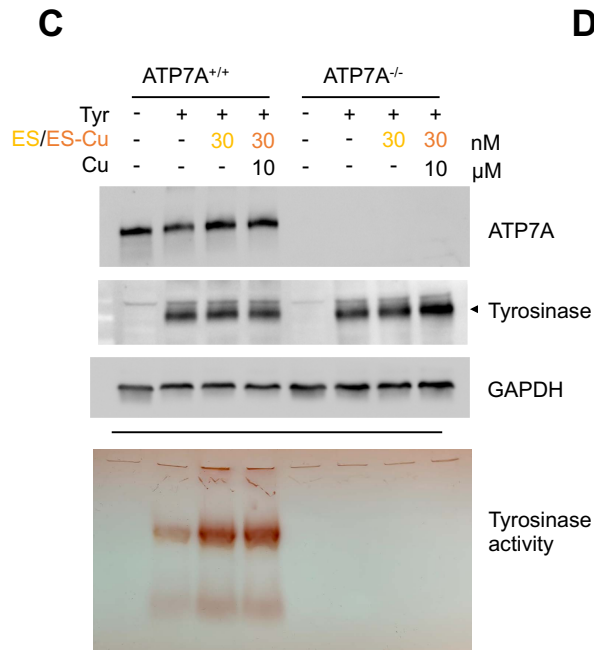
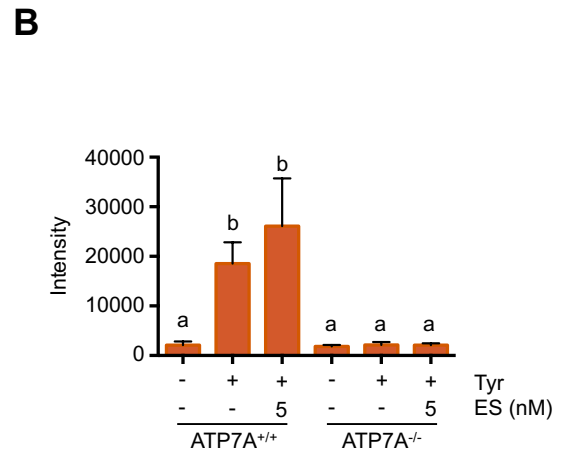
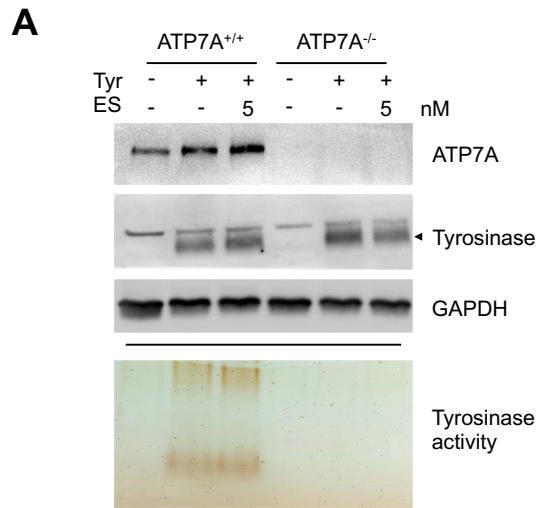


Figure 4.11: **ES is insufficient to restore tyrosinase activity in *ATP7A*^{-/-} MEF cells.** A) *ATP7A*^{+/+} and *ATP7A*^{-/-} MEF cells were transiently transfected with a tyrosinase-expressing vector pcTYR (Tyr +), or vehicle only (Tyr -), and supplemented with 0 (-) or 5 nM ES in the culture media. (Upper panels) Representative immunoblots of ATP7A and tyrosinase (~90 kDa) protein abundance from three independent experiments. GAPDH serves as loading control. (Lower panel) Tyrosinase activity on a native gel. Cells were lysed with buffer that does not contain detergents or reducing reagent and lysates were then separated on a SDS-free PAGE gel. Tyrosinase activity was colorimetrically determined by incubating gels for 30-60 minutes at 37 °C in PBS solution containing 1.5 mM L-DOPA. B) Band intensity quantification of tyrosinase activity from three independent experiments by Image J. Error bars represent mean ± SD. Groups with different letters are significantly different from each other at $p = 0.05$ (one-way ANOVA, Sidak post hoc test). C and D) Experiments were performed using *ATP7A*^{-/-} cells transfected with a *ATP7A*-expressing vector, followed by treatment with 30 nM ES, or 30 nM ES-Cu complex plus 10 μM CuCl₂. (C) Representative immunoblot and tyrosinase in-gel activity. (D) Band intensity quantification of tyrosinase activity from two independent experiments. Error bars, mean ± SD. Groups with different letters are significantly different from each other at $p = 0.05$ (one-way ANOVA, Sidak post hoc test).



mg/kg to *Ctr1^{hrt/hrt}* mice is sufficient to restore cardiac Ctr1 deficiency-related developmental defects. Heart and blood vessel abnormalities are common in Cu-deficient animals, and cardiac hypertrophy has been observed in dietary Cu-deficient mice, *Ctr1^{hrt/hrt}* mice, and *Ctr1^{int/int}* mice. ES administration is sufficient to rescue the abnormal cardiomyocyte morphology, bioavailable Cu levels and Cco abundance in the hearts of *Ctr1^{hrt/hrt}* mice, suggesting ES-mediated Cu delivery into heart, independent of Ctr1. How does subcutaneously injected ES mediate Cu transport to the heart? It has been reported that ES is able to bind Cu(II) from serum or from ceruloplasmin, one of the major Cu-binding proteins in blood [150, 154]. Thus, it is plausible that injected ES diffuses into circulation where it interacts with Cu(II) from Cu chaperone proteins such as ceruloplasmin or albumin and directs Cu transport into the heart, providing sufficient Cu to cardiac mitochondria [248].

In addition to effects on the heart, ES treatment of *Ctr1^{hrt/hrt}* mice also altered systemic ATP7A responses back to wild-type levels. As ES specifically interacts with Cu and ES treatment does not affect cardiac Ctr1 protein abundance, our results support the notion that regulation of peripheral ATP7A protein abundance is not directly due to cardiac Ctr1 ablation but a consequence of cardiac Cu deficiency. Thus, the change of systemic ATP7A levels is likely a consequence of sufficient cardiac Cu supply mediated by ES. It is possible that ES could also mediate Cu delivery to other peripheral tissues besides the Cu-deficient heart. How ES treatment affects other peripheral tissues Cu homeostasis is yet unknown. Will excess Cu delivered via ES to Cu adequate tissues yield potential oxidative stress? Answers to these questions require further investigation of ES-Cu transport mechanisms *in*

vivo.

Whole-body Cu deficiency has been suggested to correlate with defects in immune tissue development in animal models [235, 236]. However, observations of small thymus and spleens in *Ctr1^{hrt/hrt}* mice are unexpected, because unlike other findings, the *Ctr1^{hrt/hrt}* mice exhibit higher levels of Cu in the circulation. The effect of cardiac *Ctr1* depletion on thymus development may start during gestation, as perinatal mice already have a pair of thymus formed in the final position above the heart [249]. It is plausible that cardiac Cu deficiency is of higher priority in systemic Cu homeostasis regulation, so Cu-dependent spleen and thymus development are compromised under these conditions. Another explanation may be that a putative signaling molecule generated from Cu-deficient heart is released into circulation, and this signal directly or indirectly interferes with thymus and spleen development. How thymus and spleen development are affected by cardiac *Ctr1* ablation and how ES rescues these tissues needs to be elucidated in the future.

Mutations in ATP7A can lead to a rare but severe Cu-deficient Menkes disease. The rescue of lethality and embryogenesis by ES treatment in the whole body or intestinal *cua-1* depleted worms strongly suggest the capability of ES to facilitate intestinal Cu absorption and peripheral Cu distribution. Additionally, ES revealed potency to facilitate Cu delivery through polarized BBB cells. Tight junctions formed by brain endothelial cells have the highest electrical resistance and lowest permeability to drugs compared to other body parts, and access of drugs into the brain has been an important aspect in Menkes disease therapy evaluation [250, 251, 252]. Our findings in worms and BBB cells shed light on using ES in the

treatment of Cu-deficiency due to Menkes disease. It must be noted that results from the tyrosinase activity assay highlighted potential limitations of ES treatment in the delivery of Cu to cuproenzymes in the secretory pathway in the absence of ATP7A. The efficacy of ES-Cu delivery to other cuproenzymes shall be further investigated in Menkes-derived cell culture models and *mottled* mice with reduced ATP7A function, because regardless of total Cu levels in the brain or other tissues, reduced function of cuproenzymes such as PAM and DBH can still lead to movement and cognitive disorders in Menkes models. Drugs used in clinical research reveal different affinities to varying subcellular compartments, and it has been reported that ES preferentially transports Cu to the mitochondria [253]. However, the mechanism is yet unknown. ES may be able to directly release Cu to other subcellular compartments but with lower efficiency, or perhaps ES only drives Cu into mitochondria, with smaller amounts of mitochondrial Cu being transported back to the cytosol. Understanding subcellular ES-Cu transport mechanisms will benefit future therapeutics.

Chapter 5: Conclusions and future directions

5.1 Conclusions

1) Using sequence homology searches, 10 *CTR* candidate gene loci that express 15 unique proteins were identified in *C. elegans*. In general, worm CTR proteins share 30–40 % identity with hCTR1. Similar to hCTR1, all candidates contain a conserved Met–X3–Met domain close to the second TMD, and an extracellular N terminus by topology prediction.

2) Transcription of candidate genes *F58G6.3*, *F58G6.7*, and *F58G6.9* (*chca-1*) was suppressed by Cu and elevated by Cu deficiency in axenic culture medium. Expression of several other candidate genes was suppressed by high Cu but not induced by low Cu at the transcriptional level.

3) The *F58G6.9*- (*chca-1*) and *F27C1.2*-depleted worms revealed developmental and embryogenesis defects when grown under Cu deficiency conditions on NGM plates. Among candidate genes, *chca-1* RNAi worms exhibited the most significant defects in Cu accumulation under Cu-deficient conditions, suggesting *chca-1* is required for Cu acquisition under low Cu conditions. However, expressing C-terminal FLAG-tagged CHCA-1 did not rescue growth of *CTR1ΔCTR3Δ* yeast, hinting that Cu import in worms may involve other candidate genes in parallel to *chca-1*.

4) In *C. elegans* lacking *chca-1* expression, Cu-dependent CUA-1.1 intestinal localization and CUA-1.1 hypodermal expression were similar to those worms grown under Cu-deficient conditions, suggesting CHCA-1 is required for Cu acquisition and maintaining systemic Cu levels.

5) Worms lacking *chca-1* (*chca-1 (tm6506) IV*) exhibited low body Cu accumulation and defects in Cu acquisition. Similar to *chca-1* RNAi, *tm6506* animals also revealed growth and embryogenesis defects, which can be rescued specifically by Cu, but not other metals such as Fe, Mn or Zn. Taken together, these results suggest that the function of *chca-1* is Cu-specific.

6) Transgenic worms expressing GFP from the *chca-1* promoter revealed that *chca-1* is predominantly expressed in the intestine and hypodermis, and that its expression can be induced by Cu deficiency. Among the tissues in which *chca-1* is expressed, intestinal CHCA-1 played a dominant role in regulating worm growth and Cu acquisition. In addition, both intestinal and hypodermal CHCA-1 expression may contribute to regulation of Cu balance at the organismal level, as tissue-specific depletion of *chca-1* did not alter intestinal CUA-1.1 trafficking. CHCA-1 protein localizes to intracellular vesicles in the intestine, as indicated by both GFP and FLAG-tagged fusion versions of the protein, and the fusion protein abundance was not regulated by Cu availability.

7) *C. elegans* exhibit behavioral avoidance when Cu is present in toxic concentrations. Worms lacking *chca-1* expression showed reduced levels of avoidance, suggesting *chca-1* is required for sensing toxic Cu. The reduced avoidance was recapitulated in dietary Cu-deficient worms, suggesting that abnormal body Cu levels

correlate with changes in Cu sensing and avoidance behavior. It is important to note that Cu-dependent neuropeptide maturation is crucial for normal Cu-sensing behavior in *C. elegans*. This is supported by defective avoidance behavior when RNAi knockdown depletes *egl-3*, *egl-21*, and *PAMs* in worms.

8) The addition of ES rescued the growth defects of *tm6506* worms cultured under Cu-deficient conditions as well as body Cu levels in these animals. In addition, ES supplementation to whole-body or intestinal-specific *cua-1*-depleted worms significantly rescued the lethality and embryogenesis defects, suggesting that ES is able to mediate dietary Cu uptake and peripheral tissue Cu transport through the intestine when dietary Cu acquisition mechanisms are disrupted.

9) Subcutaneous injection of ES to *Ctr1^{hrt/hrt}* mice from P5 to P26 was sufficient to rescue postnatal lethality and decreased body mass of the mutant mice. The cardiac hypertrophy, abnormal thymus and spleen development were also restored to wild-type level upon ES treatment. ES itself did not affect Ctr1 or ATP7A protein expression.

10) Total and bioavailable Cu levels in *Ctr1^{hrt/hrt}* mouse hearts were significantly increased after ES administration. ES treatment until P54 fully restored cardiac mitochondrial Cox1 abundance in mutant mice. These findings suggest that ES could mediate Cu delivery to cardiac tissues of *Ctr1^{hrt/hrt}* mice and rescue the Cu deficiency and mitochondrial dysfunction observed in the hearts of these mice. In addition, the systemic Cu homeostasis responses in the cardiac Cu-deficient mice, indicated via the induction of ATP7A expression in the liver and intestine, were reduced back to normal levels after two ES treatments on P5 and P8.

11) Administration of ES to the apical side of cultured BBB cells was able to rescue the Cu deficiency in *Ctr1*^{-/-} cells grown on the basal-side of BBB, without altering BBB cells ATP7A protein abundance, suggesting that ES can mediate Cu transport through BBB tight junctions. Meanwhile, our studies in cultured *ATP7A*^{-/-} cells raised a potential limitation of ES to effectively delivery Cu to tyrosinase in the secretary pathway, as ES or ES-Cu supplementation failed to increase tyrosinase activity in *ATP7A*^{-/-} cells.

5.2 Future Directions

5.2.1 Characterizing *C. elegans* *CTR* ortholog genes

Based on *chca-1* tissue expression patterns, subcellular localization and its requirement during Cu deficiency, other Cu uptake mechanisms likely exist in parallel to *chca-1* to direct Cu to other tissues (including neurons and the pharynx), and across the apical surface of intestinal cells. Several *CTR* genes such as *F31E8.4* and *Y58A7A.1* complemented the growth of *CTR1*Δ*CTR3*Δ yeast in YPEG media, suggesting a role for these *CTR* genes in Cu transport. Further tests can be conducted in *Ctr1*^{-/-} cells expressing candidate genes to confirm and quantify their Cu transport activity with radiolabeled Cu.

Although using RNAi to individually deplete other *CTR* candidate genes does not significantly affect body Cu accumulation or intestinal CUA-1 trafficking, Ctr proteins may function together to mediate Cu uptake. To test this possibility, RNAi can be applied to multiple candidate genes simultaneously, and body Cu levels, Cu-

dependent growth, and intestinal CUA-1 localization can be analyzed. It is also worth noting that, most experimental results in this study were collected at the L4-young adult stage; it will also be necessary to characterize the stage-specific expression pattern of candidate genes, as Cu acquisition may require multiple *CTR* genes expressed under different developmental stages.

Though several *C. elegans* *CTR* candidates did not reveal Cu-dependent regulation at the transcriptional level, such regulation may occur at the translational or post-translational levels, or perhaps Cu availability might affect the protein localization. Generating translational fusion worms that express GFP-tagged versions of the candidate genes driven by their endogenous promoters will help in the characterization of their Cu-dependent responses. Moreover, organisms may maintain a constant rate of Cu uptake regardless of Cu availability. Thus, Cu-dependent regulation may not occur for every *C. elegans* *CTR* gene. This would be similar to *Drosophila* Ctr1A, a Ctr ortholog ubiquitously expressed through development and into adulthood, the expression of which is not affected by Cu availability.

5.2.2 Identifying the neuronal components required for Cu sensing in *C. elegans*

Our results suggest that body Cu status and Cu-dependent maturation of neuropeptides both play a role in Cu sensation and avoidance behavior in *C. elegans*. *C. elegans* has been used for many such studies as neuronal signaling pathways are well conserved between humans and worms [254, 255]. Several sensory neurons such

as ADL and ASH and the interneuron RIC have been reported to be involved in the sensation of hazardous stimuli (including Cu) in worms [212, 213, 256]. Thus, *C. elegans* would serve as an excellent tool to decipher the role of neuropeptides in Cu avoidance behavior, and to identify conserved neuronal components required for Cu sensation.

C. elegans contains 119 genes that encode more than 250 neuropeptides. An RNAi-based Cu avoidance screening can be performed on the neuropeptide coding genes to identify candidates involved in Cu-induced avoidance behavior. The Cu specificity of candidate peptides would be further tested with gradient plates generated by other heavy metals such as iron, cobalt and cadmium. The functions of candidates could be confirmed with the loss of function mutant strains already available or generated by CRISPR-Cas9.

In order to determine the sensory/inter-/afferent neurons where the candidate neuropeptides express and affect neuronal activities, transcriptional and translational fusion reporters can be generated for candidate peptides to identify the sites of expression and regulation by Cu. Next, calcium flow experiments can be performed under Cu stimuli to determine the neuronal activities in these candidate peptides-expressed neurons, and the requirement of these neurons in Cu-sensing behavior could be further confirmed using photo-inducible cell ablation [257].

Neuropeptides commonly rely on G-protein coupled receptors or neuropeptide receptors to trigger downstream signaling pathways, and many neuropeptide receptors have been identified. If candidate peptides have known or putative receptors, the requirement of these candidate peptides in Cu sensation can be directly

determined using RNAi knockdown and the avoidance assay.

5.2.3 Elucidating elesclomol-mediated Cu transport in mouse

Our results show that ES-mediated Cu transport into the hearts of *Ctr1^{hrt/hrt}* mice restores Cu levels and suppresses cardiac hypertrophy. Aberrant ATP7A expression in peripheral tissues in response to cardiac Cu deficiency was also returned to wild-type levels by ES treatment. Precisely how ES affects regulation of systemic Cu homeostasis remains an important question to answer. According to previous studies, ES can bind Cu in the serum and then enter cells by diffusion in the form of an ES-Cu complex. How effective ES-mediated Cu transport to tissues other than the heart can be determined by measuring the presence of ES in these tissues shortly after ES administration, as ES is rapidly eliminated from the plasma with a half-life of ~ 1 hour *in vitro* [139, 140]. Do different tissues exhibit distinct affinities for ES-Cu uptake? Is the ES-Cu membrane diffusion rate affected by ES or Cu concentration gradients? If a Cu concentration gradient drives ES-Cu diffusion, then Cu transport may be prioritized to Cu-deficient tissues such as the heart and liver in *Ctr1^{hrt/hrt}* mice, and less so to other tissues not affected by cardiac Cu deficiency (for example, the muscle and brain). It is also possible that multiple peripheral tissues may obtain ES-Cu simultaneously, as long as cells of these tissues are permeable to the ES-Cu complex. To address these questions, time-dependent tissue Cu accumulation in varying tissues during ES treatment can be analyzed in both wild-type and Cu-deficient mice models (such as *Ctr1^{hrt/hrt}* mice and *mottled* mice). Positron

emission tomography (PET imaging) can be used to trace ES-⁶⁴Cu trafficking and time-dependent tissue accumulation in mice [258, 259]. Cu overloaded *ATP7A*^{-/-} cells that lack Cu efflux may also be useful to monitor ES-mediated radio-labeled Cu import/export.

In addition, though abnormal development of the thymus and spleen in *Ctr1*^{hrt/hrt} mice may involve systemic Cu sequestration regulation and unknown signaling pathways, analyzing the Cu levels and cuproenzymes activities in these tissues before and after ES administration would provide valuable information to establish the correlation between underdeveloped tissue and Cu deficiency.

5.2.4 Evaluation of elesclomol treatment using Menkes disease models

Mottled mice provide a useful *in vivo* model for pre-clinical drug testing for Menkes disease. The *macular*, *mosaic*, and *brindled* mutation strains are postnatal lethal within three weeks and would be beneficial to determine the efficacy of ES treatment during early postnatal stages. ES can be introduced through subcutaneous or intravenous injection to new-born mice until Cu-dependent development has been completed. Body mass, survival rates and disease-related phenotypes such as kinky whiskers and pigmentation may be monitored.

If ES can rescue Menkes mice body mass and lethality, further analysis shall be performed to examine Cu distribution among tissues and Cu-related neuronal functions after ES treatment. Circulating Cu levels and Cu distribution in periph-

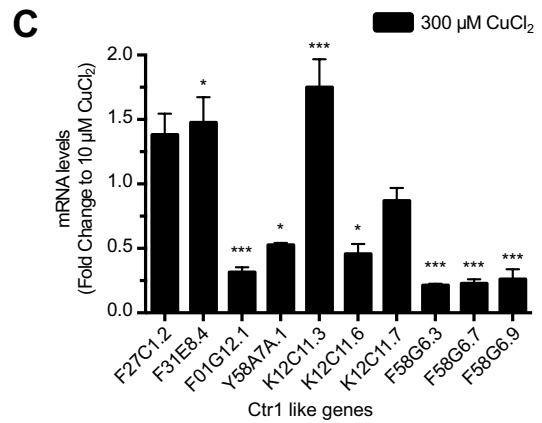
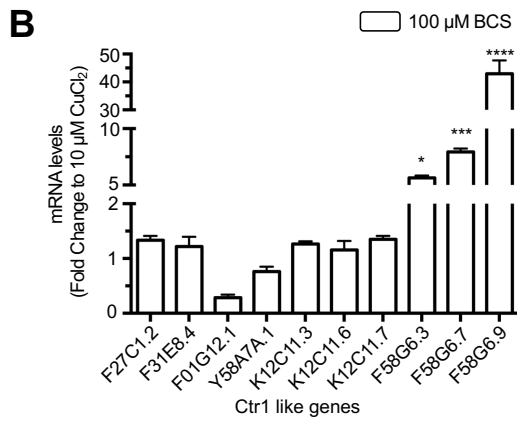
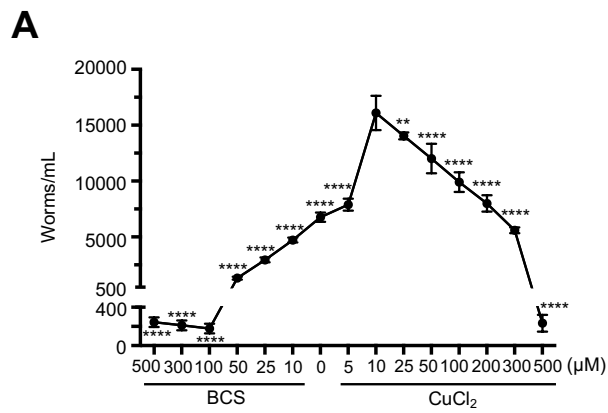
eral tissues such as the heart, brain and liver can be assayed by ICP-MS, and the cuproenzymes activities such as Cco, DBH can be tested simultaneously. Assessments of motor balance, coordination, muscle strength and locomotive activity can also be performed on ES-treated *mottled* mice [260, 261].

Though our studies revealed limitations to the ability of ES to effectively assist incorporation of Cu into tyrosinase in *ATP7A*^{-/-} MEF cells, further experiments using Menkes patient-derived cells and *mottled* mice could provide more thorough and clinically-relevant information regarding the efficacy of ES-mediated Cu transport into the secretory pathway. Because neuronal Cu abundance and Cu-dependent enzyme activity has been the main focus in evaluating Menkes therapies, it would also be necessary to characterized other cuproenzymes such as Cco, DBH and PAM activities in these future studies.

Appendix

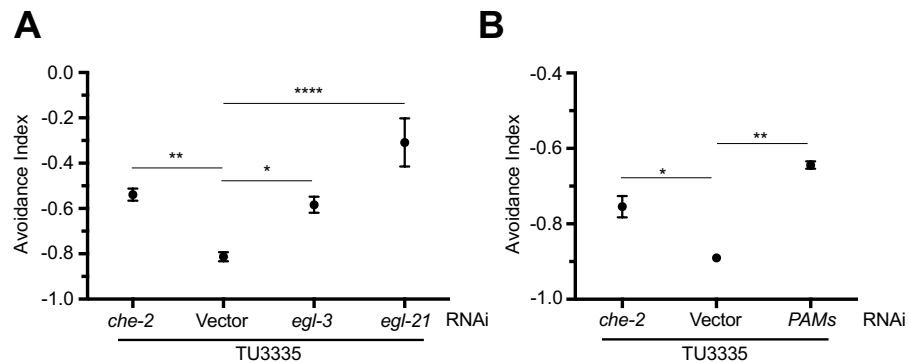
I Transcriptional regulation of *C. elegans* CTR1 candidate genes by Cu

Figure I: A) Cu-dependent *C. elegans* growth in axenic media. Total worm numbers were calculated for three independent experiments. Asterisks indicate significant difference from optimal 10 μM CuCl₂ condition (One-way ANOVA, Dunnett post hoc test, ** $p < 0.01$, **** $p < 0.0001$). B) and C) qRT-PCR analysis of *C. elegans* CTR candidate genes under Cu-limited (B) and high Cu (C) conditions. Worms were synchronized and supplemented with 100 μM BCS, 10 μM CuCl₂ or 300 μM CuCl₂ from L1 to L4 stage in axenic media. Individual gene expression was normalized first to *pmp-3*, then to its own expression under Cu-optimal conditions. Two independent experiments were conducted under each condition. Asterisks indicate significant difference from indicated gene expression levels under optimal conditions. (Two-way ANOVA, Sidak post hoc test, * $p < 0.05$, ** $p < 0.001$, **** $p < 0.0001$). Error bars, mean \pm SEM. This figure is contributed by previous lab member Alexandria Richart.



II Cu-dependent neuropeptide maturation is associated with Cu avoidance behavior

Figure II: A) Avoidance index of RNAi-hypersensitive worms (TU3335) lacking the *egl-3* or *egl-21* gene on 10 mM Cu gradient plates. Error bars indicate mean \pm SEM of eight independent experiments under each condition. Values with asterisks are significantly different from each other (One-way ANOVA, Dunnett post hoc test, $*p < 0.05$, $**p < 0.01$, $****p < 0.0001$). B) PAM genes (*pgal-1*, *pghm-1* and *pamn-1*) were co-depleted by RNAi for two consecutive generations in TU3335 strain, followed by the avoidance assay on 10 mM Cu-gradient plates. Error bars indicate mean \pm SEM of two independent experiments. Values with asterisk are significantly different (One-way ANOVA, Dunnett post hoc test, $*p < 0.05$, $**p < 0.01$). This figure is contributed by the previous lab member Anuj Sharma.



III Cox1 abundance in P10 Veh/ES administered *Ctr1^{hrt/hrt}* mice.

Figure III: Left: Cco component Cox1 abundance of P10 cardiac tissues from three independent experiments. ATP5A was used as loading control. One-way ANOVA, Sidak post hoc test. Error bars represent mean \pm SD. This figure is contributed by Shivatheja Soma, Texas A&M University.

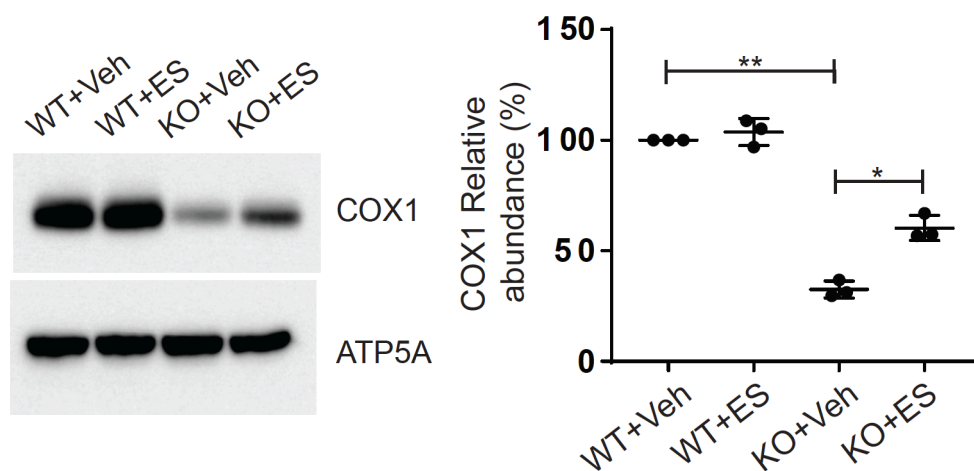
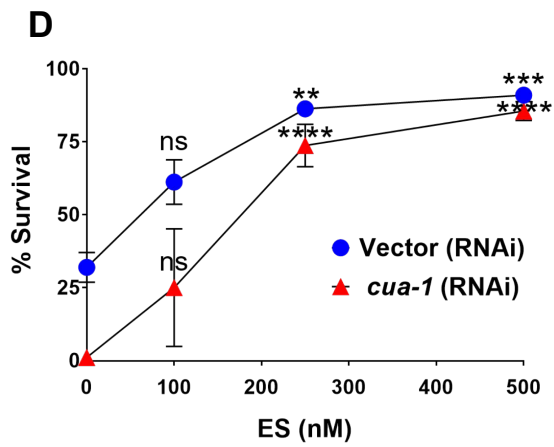
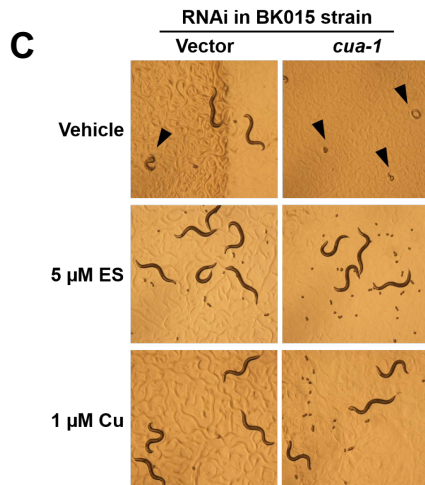
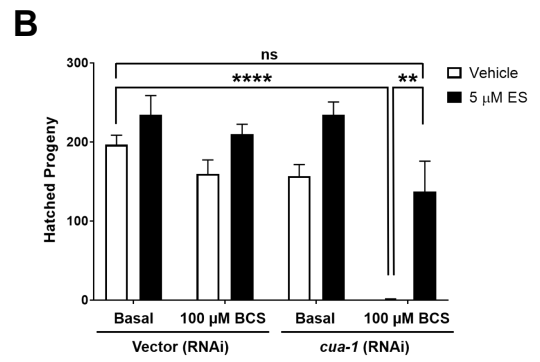
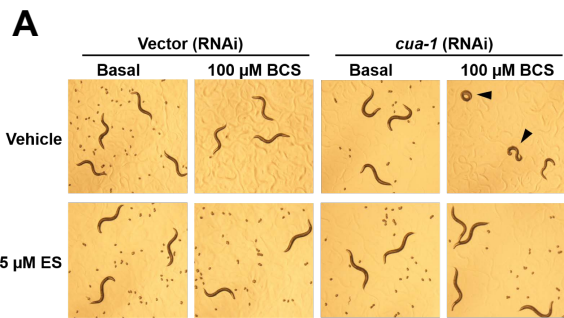


Figure IV: A) (top row) Wild-type worms (N2 strain) were exposed to RNAi from the L1 stage for 4 days with or without 100 μ M BCS treatment in the presence of vehicle (DMSO); (bottom row) worms grown under identical conditions as above supplemented with 5 μ M ES. Representative microscope images from three independent replicates are shown; arrowheads indicate dead worms. B) Wild-type worms (N2 strain) grown under varying RNAi and BCS conditions supplemented with vehicle (DMSO) or 5 μ M ES were picked to individual plates at the L4 stage in triplicate, allowed to lay eggs, and transferred to fresh plates every 24 h for 3 days. Eggs were incubated overnight to allow hatching and progeny number was determined as the total hatched larvae, $n = 3$ biological replicates (**** $p < 0.0001$, ** $p < 0.01$; two-way ANOVA, Tukey's post hoc test). Error bars represent mean \pm SEM. C) Transgenic worms [BK015 strain, $P_{vha-6}::CUA-1.1::GFP::unc-54$ 3'UTR; $cua-1(ok904)$] were cultured on RNAi plates supplemented with either vehicle (DMSO), 1 μ M Cu, or 5 μ M ES from the L1 stage for 4 days. Representative microscope images from three independent replicates are shown; arrowheads indicate dead worms. D) BK015 strain worms were cultured on RNAi plates supplemented with either vehicle (DMSO) or 5 μ M ES from the L1 stage for 4 days and then scored for survival. Animals were considered dead when no signs of viability (movement, pharyngeal pumping, or response to prodding) were detected, $n = 3$ biological replicates (**** $p < 0.0001$, *** $p < 0.001$, ** $p < 0.01$ when compared with vehicle control condition; two-way ANOVA, Bonferonni's post hoc test). Error bars represent mean \pm SEM. This figure is contributed by Tamara Korolnek.



IV Primers used for qRT-PCR assays

Table I: Primers labeled with * were redesigned outside of the RNAi construct targeting region, in order to test the RNAi effectiveness.

Gene	FW 5'-3'	REV 5'-3'
<i>pmp-3</i>	TGGCCGGATGATGGTGTCCG	ACGAACAATGCCAAAGGCCAGC
<i>gpd-2</i>	TGCTCACGAGGGAGACTAC	CGGTGGACTCAACGACATAG
<i>F27C1.2</i>	GGCTGTGGCTTTGGTGGTTGC	CATCGGGCACAGGAACCGCT
<i>F31E8.4</i>	CACATCGCACCACCTTGTTC	GCCTGAAGTCCGTAGAGAGC
	AGGCTCTCCTTGCTTACA*	GGTACCAGTAACAACAGAATACA*
<i>Y58A7A.1</i>	ACCGTCTTAAGAGATCCCCTC	CGGTGAAGAAACAGAGATAGGCA
<i>F01G12.1</i>	CCCCAGAAGTTAGACATCCCG	TCCGAGAATTACCGCGAGC
	GATCAACTGGATGTGCATACT*	AGCACAACTTCATCGAACC*
<i>K12C11.3</i>	CGGTGACGTAGATCGGAGAA	CCGAGGCATAGAGAGAGGCA
	CACGTTGTTCAAGCAATGTATC*	AAGCCGAGATCCGAAGAA*
<i>K12C11.6</i>	CCATGGTTTGGGTTTGCTGT	GGGAAATGTAGCTCCGGCTTA
<i>K12C11.7</i>	GTTGGAGACATTTTGCGTCTTCT	GGCGTGGCCTGCTAAAAG
<i>F58G6.3</i>	GGAAAAATGGTTTGGGCGTGT	GAGAGCAGGCGGGAATGT
<i>F58G6.7</i>	GAAACCACTGAACACCACTGC	AGCAGCAATCTACTTTCTTTTCCA
<i>F58G6.9</i> (<i>chca-1</i>)	ACCGGGGAAGAGTGAGAAATA	AGCAAATGTAGACCGAGAAAACC
<i>egl-3</i>	GTCTCCATCGGATCCACTTTAT	ATCCACTCCGTCATCCATAATC
<i>egl-21</i>	GCCGCTGAAGGATACGATATT	GCGATTTGCTCTTGCTCATTC
<i>che-2</i>	CGAGATCGTGCCGACAATAA	CTGATTCACAGTCAGCTCTACAA
<i>pghm-1</i>	GTGATGAGCTTGTGGGATTG	GTGACGGATGTTGCTGTCT
<i>pamn-1</i>	GCTGCTAGTCACGAGGATTATG	CTGTGGTCCCATTGTTCTCT
<i>pgal-1</i>	TCGTCGTTCCACACTCTTTG	GTCGGTGGCCGAAGTTATT

V List of transgenic animals used in Chapter 3

Table II: List of transgenic animals used in Chapter 3.

Strain Name	Background	Transgene
BK058	<i>unc-119 (ed3) III</i>	$P_{F58G6.9}::GFP::unc-54$ 3'UTR; <i>unc-119 rescue</i>
BK059	N2	$P_{vha-6}::CHCA-1::GFP::unc-54$ 3' UTR
BK060	<i>CHCA-1 (tm6506) IV</i>	$P_{vha-6}::CHCA-1::GFP::unc-54$ 3' UTR
BK061	N2	$P_{vha-6}::CHCA-1::SL2::GFP::unc-54$ 3' UTR
BK062	<i>CHCA-1 (tm6506) IV</i>	$P_{vha-6}::CHCA-1::SL2::GFP::unc-54$ 3' UTR
BK063	N2	$P_{vha-6}::CHCA-1-2xflag::SL2::GFP::unc-54$ 3' UTR
BK014	N2	$P_{vha-6}::CUA-1.1::GFP::unc-54$ 3' UTR
BK015	<i>cua-1 (ok904) III</i>	$P_{vha-6}::CUA-1.1::GFP::unc-54$ 3' UTR
BK017	<i>cua-1 (ok904) III</i>	$P_{cua-1}::CUA-1.1::GFP::unc-54$ 3' UTR
WM27	<i>rde-1(ne219) V</i>	-
VP303	<i>rde-1(ne219) V</i>	$P_{nhx-2}::RDE-1$; <i>rol-6 marker</i>
NR222	<i>rde-1(ne219) V</i>	$P_{lin-26}::nls-gfp$; $P_{lin-26}::RDE-1$; <i>rol-6 marker</i>
WM118	<i>rde-1(ne300) V</i>	$P_{myo-3}::HA::RDE-1$; <i>rol-6 marker</i>
BK027	<i>rde-1(ne219) V</i>	$P_{vha-6}::CUA-1.1::GFP::unc-54$ 3' UTR
BK033	<i>rde-1(ne219) V</i>	$P_{vha-6}::CUA-1.1::GFP::unc-54$ 3' UTR; $P_{nhx-2}::RDE-1$; <i>rol-6 marker</i>
BK022	<i>rde-1(ne219) V</i>	$P_{vha-6}::CUA-1.1::GFP::unc-54$ 3' UTR; $P_{lin-26}::RDE-1$; <i>rol-6 marker</i>
TU3335	<i>lin-15B (n744) X</i>	$P_{unc-119}::SID-1$; $P_{unc-119}::YFP$; $P_{mec-6}::MEC-6$

References

- [1] Byung-Eun Kim, Tracy Nevitt, and Dennis J Thiele. Mechanisms for Copper Acquisition, Distribution and Regulation. *Nature Chemical Biology*, 4(3):176, 2008. ISSN 1552-4469. doi:10.1038/nchembio.72.
- [2] Maria C Linder. *Biochemistry of Copper*, volume 10. Springer Science & Business Media, 2013. ISBN 1475794320.
- [3] Ricardo Uauy, Manuel Olivares, and Mauricio Gonzalez. Essentiality of Copper in Humans. *He American Journal of Clinical Nutrition*, 67(5):952S–959S, 1998. ISSN 0002-9165. doi:10.1093/ajcn/67.5.952S.
- [4] Tracy Nevitt, Helena ÅŰhrvik, and Dennis J Thiele. Charting the Travels of Copper in Eukaryotes From Yeast to Mammals. *Biochimica Et Biophysica Acta (BBA)-Molecular Cell Research*, 1823(9):1580–1593, 2012. ISSN 0167-4889. doi:10.1016/j.bbamcr.2012.02.011.
- [5] Erik Madsen and Jonathan D Gitlin. Copper and Iron Disorders of the Brain. *Annu. Rev. Neurosci*, 30:317–337, 2007. ISSN 0147-006X. doi:10.1146/annurev.neuro.30.051606.094232.
- [6] Stephen G Kaler. ATP7A-Related Copper Transport Diseases—Emerging Concepts and Future Trends. *Nature Reviews Neurology*, 7(1):15, 2011. ISSN 1759-4766. doi:10.1038/nrneurol.2010.180.
- [7] Keith A Koch, Ma Marjorette O PeÁsa, and Dennis J Thiele. Copper-Binding Motifs in Catalysis, Transport, Detoxification and Signaling. *Chemistry & Biology*, 4(8):549–560, 1997. ISSN 1074-5521.
- [8] Janet Y Uriu-Adams and Carl L Keen. Copper, Oxidative Stress, and Human Health. *Molecular Aspects of Medicine*, 26(4-5):268–298, 2005. ISSN 0098-2997. doi:10.1016/j.mam.2005.07.015.
- [9] Barry Halliwell and JMe Gutteridge. Oxygen Toxicity, Oxygen Radicals, Transition Metals and Disease. *Biochemical Journal*, 219(1):1, 1984.

- [10] Elena Georgatsou, Lampros A Mavrogiannis, George S Fragiadakis, and Despina Alexandraki. The Yeast Fre1p/Fre2p Cupric Reductases Facilitate Copper Uptake and Are Regulated by the Copper-Modulated Mac1p Activator. *Journal of Biological Chemistry*, 272(21):13786–13792, 1997. ISSN 0021-9258.
- [11] Robert S Ohgami, Dean R Campagna, Alice McDonald, and Mark D Fleming. The Steap Proteins Are Metalloreductases. *Blood*, 108(4):1388–1394, 2006. ISSN 0006-4971. doi:10.1182/blood.
- [12] Steven Wyman, Robert J Simpson, Andrew T McKie, and Paul A Sharp. Dcytb (Cybrd1) Functions As Both a Ferric and a Cupric Reductase in Vitro. *FEBS Letters*, 582(13):1901–1906, 2008. ISSN 0014-5793. doi:10.1016/j.febslet.2008.05.010.
- [13] Helena Öhrvik and Dennis J Thiele. How copper traverses cellular membranes through the mammalian copper transporter 1, ctr1. *Annals of the New York Academy of Sciences*, 1314(1):32–41, 2014.
- [14] Jaekwon Lee, Maria Marjorette O Peña, Yasuhiro Nose, and Dennis J Thiele. Biochemical characterization of the human copper transporter ctr1. *Journal of Biological Chemistry*, 277(6):4380–4387, 2002.
- [15] Stephen G Aller and Vinzenz M Unger. Projection structure of the human copper transporter ctr1 at 6-Å resolution reveals a compact trimer with a novel channel-like architecture. *Proceedings of the National Academy of Sciences*, 103(10):3627–3632, 2006.
- [16] Christopher J De Feo, Stephen G Aller, Gnana S Siluvai, Ninian J Blackburn, and Vinzenz M Unger. Three-dimensional structure of the human copper transporter hctr1. *Proceedings of the National Academy of Sciences*, 106(11):4237–4242, 2009.
- [17] Xiaobin Wu, Devis Sinani, Heejeong Kim, and Jaekwon Lee. Copper transport activity of yeast ctr1 is down-regulated via its c terminus in response to excess copper. *Journal of Biological Chemistry*, 284(7):4112–4122, 2009.
- [18] Sergi Puig, Jaekwon Lee, Miranda Lau, and Dennis Thiele. Biochemical and Genetic Analyses of Yeast and Human High Affinity Copper Transporters Suggest a Conserved Mechanism for Copper Uptake. *Journal of Biological Chemistry*, 277(29):26021–26030, 2002. ISSN 0021-9258. doi:10.1074/jbc.M202547200.
- [19] John F Eisses and Jack H Kaplan. The mechanism of copper uptake mediated by human ctr1 a mutational analysis. *Journal of Biological Chemistry*, 280(44):37159–37168, 2005.
- [20] Adriana EM Klomp, BJ Bastiaan, ET Inge, Ruud Berger, and Leo WJ Klomp. Biochemical Characterization and Subcellular Localization of Human Copper

- Transporter 1 (hCTR1). *Biochemical Journal*, 364(2):497–505, 2002. ISSN 0264-6021. doi:10.1042/BJ20011803.
- [21] Edward B Maryon, Shannon A Molloy, and Jack H Kaplan. O-Linked Glycosylation at Threonine 27 Protects the Copper Transporter HCTR1 From Proteolytic Cleavage in Mammalian Cells. *Journal of Biological Chemistry*, 282(28):20376–20387, 2007. ISSN 0021-9258. doi:10.1074/jbc.M701806200.
- [22] Cheng-Yu Tsai, Christopher A Larson, Roohangiz Safaei, and Stephen B Howell. Molecular Modulation of the Copper and Cisplatin Transport Function of CTR1 and Its Interaction With IRS-4. *Biochemical Pharmacology*, 90(4):379–387, 2014. ISSN 0006-2952. doi:10.1016/j.bcp.2014.06.019.
- [23] Lothar Kussmaul and Judy Hirst. The Mechanism of Superoxide Production by NADH: Ubiquinone Oxidoreductase (complex I) From Bovine Heart Mitochondria. *Proceedings of the National Academy of Sciences*, 103(20):7607–7612, 2006. doi:10.1161/circresaha.114.300559.
- [24] Sagar Antala. *Molecular Insights of the Human Zinc Transporter HZIP4*. PhD thesis, Worcester Polytechnic Institute, 2016.
- [25] Edward B Maryon, Shannon A Molloy, and Jack H Kaplan. Cellular Glutathione Plays a Key Role in Copper Uptake Mediated by Human Copper Transporter 1 (hCTR1). *American Journal of Physiology-Cell Physiology*, 2013. doi:10.1152/ajpcell.00417.2012.
- [26] Edward B Maryon, Shannon A Molloy, Kristin Ivy, Huijun Yu, and Jack H Kaplan. Rate and regulation of copper transport by human copper transporter 1 (hctr1). *Journal of Biological Chemistry*, 288(25):18035–18046, 2013.
- [27] Dominik Steiger, Michael Fetchko, Alla Vardanyan, Lilit Atanesyan, Kurt Steiner, Michelle L Turski, Dennis J Thiele, Oleg Georgiev, and Walter Schaffner. The Drosophila Copper Transporter Ctr1C Functions in Male Fertility. *Journal of Biological Chemistry*, 285(22):17089–17097, 2010. ISSN 0021-9258. doi:10.1074/jbc.M109.090282.
- [28] Michelle L Turski and Dennis J Thiele. Drosophila Ctr1A Functions As a Copper Transporter Essential for Development. *Journal of Biological Chemistry*, 282(33):24017–24026, 2007. ISSN 0021-9258.
- [29] Anand Selvaraj, Kuppusamy Balamurugan, Hasmik Yepiskoposyan, Hao Zhou, Dieter Egli, Oleg Georgiev, Dennis J Thiele, and Walter Schaffner. Metal-Responsive Transcription Factor (MTF-1) Handles Both Extremes, Copper Load and Copper Starvation, by Activating Different Genes. *Genes & Development*, 19(8):891–896, 2005. ISSN 0890-9369. doi:10.1101/gad.1301805.
- [30] M Portnoy, P Schmidt, R Rogers, and V Culotta. Metal Transporters That Contribute Copper to Metallochaperones in *Saccharomyces Cerevisiae*. *Molecular Genetics and Genomics*, 265(5):873–882, 2001. ISSN 1617-4615.

- [31] Joern Jungmann, Hans-Albert Reins, Jinhwa Lee, Annette Romeo, Richard Hassett, Daniel Kosman, and S Jentsch. Mac1, a nuclear regulatory protein related to cu-dependent transcription factors is involved in cu/fe utilization and stress resistance in yeast. *The EMBO Journal*, 12(13):5051–5056, 1993.
- [32] Hao Zhou, Ken M Cadigan, and Dennis J Thiele. A Copper-Regulated Transporter Required for Copper Acquisition, Pigmentation, and Specific Stages of Development in Drosophila Melanogaster. *Journal of Biological Chemistry*, 278(48):48210–48218, 2003. doi:10.1074/jbc.M309820200.
- [33] Helena Öhrvik, Yasuhiro Nose, L Kent Wood, Byung-Eun Kim, Sophie-Charlotte Gleber, Martina Ralle, and Dennis J Thiele. Ctr2 Regulates Biogenesis of a Cleaved Form of Mammalian Ctr1 Metal Transporter Lacking the Copper-And Cisplatin-Binding Ecto-Domain. *Proceedings of the National Academy of Sciences*, 110(46):E4279–E4288, 2013. doi:10.1073/pnas.1311749110.
- [34] Helena Öhrvik, Brandon Logeman, Boris Turk, Thomas Reinheckel, and Dennis J Thiele. Cathepsin Protease Controls Copper and Cisplatin Accumulation Via Cleavage of the Ctr1 Metal-Binding Ectodomain. *Journal of Biological Chemistry*, 291(27):13905–13916, 2016. doi:10.1074/jbc.M116.731281.
- [35] Cheng-Yu Tsai, Janika K Liebig, Igor F Tsigelny, and Stephen B Howell. The Copper Transporter 1 (CTR1) Is Required to Maintain the Stability of Copper Transporter 2 (CTR2). *Metallomics*, 7(11):1477–1487, 2015. doi:10.1039/c5mt00131e.
- [36] Yasuhiro Nose, L Kent Wood, Byung-Eun Kim, Joseph R Prohaska, Robert S Fry, Jerry W Spears, and Dennis J Thiele. Ctr1 Is an Apical Copper Transporter in Mammalian Intestinal Epithelial Cells in Vivo That Is Controlled at the Level of Protein Stability. *Journal of Biological Chemistry*, 285(42):32385–32392, 2010. ISSN 0021-9258. doi:10.1074/jbc.M110.143826.
- [37] Zakery N Baker, Kimberly Jett, Aren Boulet, Amzad Hossain, Paul A Cobine, Byung-Eun Kim, Amr M El Zawily, Ling Lee, Glen F Tibbits, Michael J Petris, et al. The Mitochondrial Metallochaperone SCO1 Maintains CTR1 at the Plasma Membrane to Preserve Copper Homeostasis in the Murine Heart. *Human Molecular Genetics*, 26(23):4617–4628, 2017. doi:10.1093/hmg/ddx344.
- [38] Christopher J Hlynialuk, Binbing Ling, Zakery N Baker, Paul A Cobine, D Yu Lisa, Aren Boulet, Timothy Wai, Amzad Hossain, Amr M El Zawily, and Pamela J McFie. The Mitochondrial Metallochaperone SCO1 Is Required to Sustain Expression of the High-Affinity Copper Transporter CTR1 and Preserve Copper Homeostasis. *Cell Reports*, 10(6):933–943, 2015. ISSN 2211-1247. doi:10.1016/j.celrep.2015.01.019.
- [39] Natalia C Mackenzie, Mónica Brito, Ariel E Reyes, and Miguel L Allende. Cloning, Expression Pattern and Essentiality of the High-Affinity

- Copper Transporter 1 (ctr1) Gene in Zebrafish. *Gene*, 328:113–120, 2004. doi:10.1016/j.gene.2003.11.019.
- [40] Yien-Ming Kuo, Bing Zhou, Dominique Cosco, and Jane Gitschier. The Copper Transporter CTR1 Provides an Essential Function in Mammalian Embryonic Development. *Proceedings of the National Academy of Sciences*, 98(12):6836–6841, 2001. doi:10.1073/pnas.111057298.
- [41] Yasuhiro Nose, Byung-Eun Kim, and Dennis J Thiele. Ctr1 Drives Intestinal Copper Absorption and Is Essential for Growth, Iron Metabolism, and Neonatal Cardiac Function. *Cell Metabolism*, 4(3):235–244, 2006. doi:10.1258/ebm.2010.010256.
- [42] James Camakaris, Michael J Petris, Leanne Bailey, Peiyan Shen, Paul Lockhart, Thomas W Glover, Christine L Barcroft, Janet Patton, and Julian FB Mercer. Gene Amplification of the Menkes (MNK; ATP7A) P-Type ATPase Gene of CHO Cells Is Associated With Copper Resistance and Enhanced Copper Efflux. *Human Molecular Genetics*, 4(11):2117–2123, 1995. ISSN 1460-2083. doi:10.1177/002215549904701207.
- [43] Aimee S Payne and Jonathan D Gitlin. Functional Expression of the Menkes Disease Protein Reveals Common Biochemical Mechanisms Among the Copper-Transporting P-Type ATPases. *Journal of Biological Chemistry*, 273(6):3765–3770, 1998. ISSN 0021-9258.
- [44] Lucia Banci, Ivano Bertini, Simone Ciofi-Baffoni, Christos T Chasapis, Nick Hadjiladis, and Antonio Rosato. An NMR Study of the Interaction Between the Human Copper (I) Chaperone and the Second and Fifth Metal-binding Domains of the Menkes Protein. *The FEBS Journal*, 272(3):865–871, 2005. ISSN 1742-464X. doi:10.1111/j.1742.
- [45] Werner KÄijhlbrandt. Biology, Structure and Mechanism of P-Type ATPases. *Nature Reviews Molecular Cell Biology*, 5(4):282, 2004. ISSN 1471-0080. doi:10.1038/nrm1354.
- [46] Atin K Mandal, Ying Yang, Tzipporah M Kertesz, and JosÄI M ArgÄijello. Identification of the Transmembrane Metal Binding Site in Cu+-Transporting PIB-Type ATPases. *Journal of Biological Chemistry*, 279(52):54802–54807, 2004. ISSN 0021-9258. doi:10.15252/embr.201439927.
- [47] Lelita T Braiterman, Lydia Nyasae, Yan Guo, Rodrigo Bustos, Svetlana Lutsenko, and Ann Hubbard. Apical Targeting and Golgi Retention Signals Reside Within a 9 Amino Acid Sequence in the Copper-ATPase, ATP7B. *American Journal of Physiology-Gastrointestinal and Liver Physiology*, 2009. doi:10.1152/ajpgi.90489.2008.
- [48] Michael J Petris, James Camakaris, Mark Greenough, Sharon LaFontaine, and Julian FB Mercer. A C-Terminal Di-Leucine Is Required for Localization of

- the Menkes Protein in the Trans-Golgi Network. *Human Molecular Genetics*, 7(13):2063–2071, 1998. ISSN 1460-2083.
- [49] Sharon La Fontaine and Julian FB Mercer. Trafficking of the Copper-ATPases, ATP7A and ATP7B: Role in Copper Homeostasis. *Archives of Biochemistry and Biophysics*, 463(2):149–167, 2007. ISSN 0003-9861. doi:10.1016/j.abb.2007.04.021.
- [50] Mee Y Bartee, Martina Ralle, and Svetlana Lutsenko. The Loop Connecting Metal-Binding Domains 3 and 4 of ATP7B Is a Target of a Kinase-Mediated Phosphorylation. *Biochemistry*, 48(24):5573–5581, 2009. ISSN 0006-2960. doi:10.1021/bi900325k.
- [51] Mark Schaefer, Robin G Hopkins, Mark L Failla, and Jonathan D Gitlin. Hepatocyte-Specific Localization and Copper-Dependent Trafficking of the Wilson’s Disease Protein in the Liver. *American Journal of Physiology-Gastrointestinal and Liver Physiology*, 276(3):G639–G646, 1999. ISSN 1522-1547. doi:10.1152/ajpgi.1999.276.3.G639.
- [52] Kunihiro Terada, Tatsushi Nakako, Xiao-Li Yang, Masatake Iida, Namiko Aiba, Yoshihiro Minamiya, Michio Nakai, Toshiyuki Sakaki, Naoyuki Miura, and Toshihiro Sugiyama. Restoration of Holoceruloplasmin Synthesis in LEC Rat After Infusion of Recombinant Adenovirus Bearing WND CDNA. *Journal of Biological Chemistry*, 273(3):1815–1820, 1998. ISSN 0021-9258.
- [53] Giacomo Carlo Sturniolo, Cinzia Mestriner, Paola Irato, Vincenzo Albergoni, Giuseppe Longo, and Renata D’incÃ. Zinc Therapy Increases Duodenal Concentrations of Metallothionein and Iron in Wilson’s Disease Patients. *The American Journal of Gastroenterology*, 94(2):334, 1999. ISSN 1572-0241. doi:10.1111/j.1572.
- [54] Barry Halliwell and John MC Gutteridge. *Free Radicals in Biology and Medicine*. Oxford University Press, USA, 2015. ISBN 0198717482.
- [55] John A Tainer, Elizabeth D Getzoff, Jane S Richardson, and David C Richardson. Structure and Mechanism of Copper, Zinc Superoxide Dismutase. *Nature*, 306(5940):284, 1983. ISSN 1476-4687. doi:10.1021/bi982284u.
- [56] Valeria Cizewski Culotta, Leo WJ Klomp, Jeffrey Strain, Ruby Leah B Casareno, Bernhard Krebs, and Jonathan D Gitlin. The Copper Chaperone for Superoxide Dismutase. *Journal of Biological Chemistry*, 272(38):23469–23472, 1997. ISSN 0021-9258.
- [57] Amy L Caruano-Yzermans, Thomas B Bartnikas, and Jonathan D Gitlin. Mechanisms of the Copper-Dependent Turnover of the Copper Chaperone for Superoxide Dismutase. *Journal of Biological Chemistry*, 281(19):13581–13587, 2006. ISSN 0021-9258. doi:10.1074/jbc.M601580200.

- [58] Nina M Brown, Andrew S Torres, Peter E Doan, and Thomas V O'Halloran. Oxygen and the Copper Chaperone CCS Regulate Posttranslational Activation of Cu, Zn Superoxide Dismutase. *Proceedings of the National Academy of Sciences*, 101(15):5518–5523, 2004. ISSN 0027-8424. doi:10.1021/bi201353y.
- [59] Iqbal Hamza, Anja Faisst, Joseph Prohaska, Joseph Chen, Peter Gruss, and Jonathan D Gitlin. The Metallochaperone Atox1 Plays a Critical Role in Perinatal Copper Homeostasis. *Proceedings of the National Academy of Sciences*, 98(12):6848–6852, 2001. ISSN 0027-8424. doi:10.1073/pnas.111058498.
- [60] Iqbal Hamza, Joseph Prohaska, and Jonathan D Gitlin. Essential Role for Atox1 in the Copper-Mediated Intracellular Trafficking of the Menkes ATPase. *Proceedings of the National Academy of Sciences*, 100(3):1215–1220, 2003. ISSN 0027-8424. doi:10.1073/pnas.0336230100.
- [61] Shinichi Itoh, Ha Won Kim, Osamu Nakagawa, Kiyoshi Ozumi, Susan M Lessner, Hiroki Aoki, Kamran Akram, Ronald D McKinney, Masuko Ushio-Fukai, and Tohru Fukai. Novel Role of Antioxidant-1 (Atox1) As a Copper-Dependent Transcription Factor Involved in Cell Proliferation. *Journal of Biological Chemistry*, 283(14):9157–9167, 2008. ISSN 0021-9258. doi:10.1074/jbc.M709463200.
- [62] Steven R Davis and Robert J Cousins. Metallothionein Expression in Animals: a Physiological Perspective on Function. *The Journal of Nutrition*, 130(5):1085–1088, 2000. ISSN 0022-3166. doi:10.1093/jn/130.5.1085.
- [63] Jung D Park, Yaping Liu, and Curtis D Klaassen. Protective Effect of Metallothionein Against the Toxicity of Cadmium and Other Metals. *Toxicology*, 163(2-3):93–100, 2001. ISSN 0300-483X.
- [64] Kazuo T Suzuki, Akiyoshi Someya, Yoshiko Komada, and Yasumitsu Ogra. Roles of Metallothionein in Copper Homeostasis: Responses to Cu-Deficient Diets in Mice. *Journal of Inorganic Biochemistry*, 88(2):173–182, 2002. ISSN 0162-0134.
- [65] Lucia Tapia, Mauricio González-Agüero, Mónica F Cisternas, Miriam Suazo, Verónica Cambiazo, UAI Ricardo, and Mauricio Gonzalez. Metallothionein Is Crucial for Safe Intracellular Copper Storage and Cell Survival at Normal and Supra-Physiological Exposure Levels. *Biochemical Journal*, 378(2):617–624, 2004. ISSN 0264-6021. doi:10.1042/BJ20031174.
- [66] Rainer Heuchel, Freddy Radtke, O Georgiev, G Stark, M Aguet, and W Schaffner. The Transcription Factor MTF-1 Is Essential for Basal and Heavy Metal-induced Metallothionein Gene Expression. *The EMBO Journal*, 13(12):2870–2875, 1994. ISSN 0261-4189. doi:10.1002/j.1460-2075.1994.tb06581.x.

- [67] Jonathan H Freedman, Maria Rosa Ciriolo, and Jack Peisach. The Role of Glutathione in Copper Metabolism and Toxicity. *Journal of Biological Chemistry*, 264(10):5598–5605, 1989. ISSN 0021-9258. doi:10.1034/j.1399-3054.1999.106302.x.
- [68] C Oswald, U Krause-Buchholz, and G RÄüdel. Knockdown of Human COX17 Affects Assembly and Supramolecular Organization of Cytochrome C Oxidase. *Journal of Molecular Biology*, 389(3):470–479, 2009. ISSN 0022-2836. doi:10.1016/j.jmb.2009.04.034.
- [69] D Moira Glerum, Andrey Shtanko, and Alexander Tzagoloff. Characterization of COX17, a Yeast Gene Involved in Copper Metabolism and Assembly of Cytochrome Oxidase. *Journal of Biological Chemistry*, 271(24):14504–14509, 1996. ISSN 0021-9258.
- [70] Paul A Cobine, Luis D Ojeda, Kevin M Rigby, and Dennis R Winge. Yeast Contain a Non-Proteinaceous Pool of Copper in the Mitochondrial Matrix. *Journal of Biological Chemistry*, 279(14):14447–14455, 2004. doi:10.1074/jbc.M312693200.
- [71] Yih-Chern Horng, Paul A Cobine, Andrew B Maxfield, Heather S Carr, and Dennis R Winge. Specific Copper Transfer From the Cox17 Metallochaperone to Both Sco1 and Cox11 in the Assembly of Yeast Cytochrome C Oxidase. *Journal of Biological Chemistry*, 279(34):35334–35340, 2004. ISSN 0021-9258. doi:10.1074/jbc.M404747200.
- [72] Laree Hiser, Marilena Di Valentin, Alicia G Hamer, and Jonathan P Hosler. Cox11p Is Required for Stable Formation of the CuBand Magnesium Centers of Cytochrome C Oxidase. *Journal of Biological Chemistry*, 275(1):619–623, 2000. ISSN 0021-9258.
- [73] Scot C Leary, Brett A Kaufman, Giovanna Pellecchia, Guy-Hellen Guercin, Andre Mattman, Michaela Jaksch, and Eric A Shoubridge. Human SCO1 and SCO2 Have Independent, Cooperative Functions in Copper Delivery to Cytochrome C Oxidase. *Human Molecular Genetics*, 13(17):1839–1848, 2004. ISSN 1460-2083. doi:10.1093/hmg/ddh197.
- [74] David Pacheu-Grau, Bettina Bareth, Jan Dudek, Lisa Juris, F-Nora VÄügtle, Mirjam Wissel, Scot C Leary, Sven Dennerlein, Peter Rehling, and Markus Deckers. Cooperation Between COA6 and SCO2 in COX2 Maturation During Cytochrome C Oxidase Assembly Links Two Mitochondrial Cardiomyopathies. *Cell Metabolism*, 21(6):823–833, 2015. ISSN 1550-4131. doi:10.1016/j.cmet.2015.04.012.
- [75] David A Stroud, Megan J Maher, Caroline Lindau, F-Nora VÄügtle, Ann E Frazier, Elliot Surgenor, Hayley Mountford, Abeer P Singh, Matteo Bonas, and Silke Oeljeklaus. COA6 Is a Mitochondrial Complex IV Assembly Factor

- Critical for Biogenesis of MtDNA-Encoded COX2. *Human Molecular Genetics*, 24(19):5404–5415, 2015. ISSN 1460-2083. doi:10.1093/hmg/ddv265.
- [76] Manuela Bode, Michael W Woellhaf, Maria Bohnert, Martin van der Laan, Frederik Sommer, Martin Jung, Richard Zimmermann, Michael Schroda, and Johannes M Herrmann. Redox-Regulated Dynamic Interplay Between Cox19 and the Copper-Binding Protein Cox11 in the Intermembrane Space of Mitochondria Facilitates Biogenesis of Cytochrome C Oxidase. *Molecular Biology of the Cell*, 26(13):2385–2401, 2015. ISSN 1059-1524. doi:10.1091/mbc.E14-11-1526.
- [77] Katherine E Vest, Scot C Leary, Dennis R Winge, and Paul A Cobine. Copper Import Into the Mitochondrial Matrix in *Saccharomyces Cerevisiae* Is Mediated by Pic2, a Mitochondrial Carrier Family Protein. *Journal of Biological Chemistry*, pages jbc–M113, 2013. doi:10.1098/rsob.150223.
- [78] Zakery N Baker, Paul A Cobine, and Scot C Leary. The mitochondrion: a central architect of copper homeostasis. *Metallomics*, 9(11):1501–1512, 2017.
- [79] Isabelle Valnot, Sandrine Osmond, Nadine Gigarel, Blandine Mehaye, Jeanne Amiel, Valérie Cormier-Daire, Arnold Munnich, Jean-Paul Bonnefont, Pierre Rustin, and Agnès Rüting. Mutations of the SCO1 Gene in Mitochondrial Cytochrome C Oxidase Deficiency With Neonatal-Onset Hepatic Failure and Encephalopathy. *The American Journal of Human Genetics*, 67(5):1104–1109, 2000. ISSN 0002-9297. doi:10.1016/S0002.
- [80] Juliana Gurgel-Giannetti, Guilherme Oliveira, Geraldo Brasileiro Filho, Poliana Martins, Mariz Vainzof, and Michio Hirano. Mitochondrial Cardioencephalomyopathy Due to a Novel SCO2 Mutation in a Brazilian Patient: Case Report and Literature Review. *JAMA Neurology*, 70(2):258–261, 2013. ISSN 2168-6149. doi:10.1001/jamaneurol.2013.595.
- [81] Zakery N Baker. *Sco1 Mouse Models of Human Disease: a Tool to Investigate the Role of Mitochondria in the Regulation of Copper Homeostasis*. PhD thesis, University of Saskatchewan, 2018.
- [82] Fabian Baertling, Mariel AM van den Brand, Jozef L Hertecant, Aisha Al-Shamsi, Lambert P van den Heuvel, Felix Distelmaier, Ertan Mayatepek, Jan A Smeitink, Leo GJ Nijtmans, and Richard JT Rodenburg. Mutations in COA 6 Cause Cytochrome C Oxidase Deficiency and Neonatal Hypertrophic Cardiomyopathy. *Human Mutation*, 36(1):34–38, 2015. ISSN 1059-7794. doi:10.1002/humu.22715.
- [83] P Freisinger, R Horvath, C Macmillan, J Peters, and M Jaksch. Reversion of Hypertrophic Cardiomyopathy in a Patient With Deficiency of the Mitochondrial Copper Binding Protein Sco2: Is There a Potential Effect of Copper? *Journal of Inherited Metabolic Disease*, 27(1):67–79, 2004. ISSN 0141-8955. doi:10.1177/1535370218813988.

- [84] KI Tishchenko, EK Beloglazkina, AG Mazhuga, and NV Zyk. Copper-Containing Enzymes: Site Types and Low-Molecular-Weight Model Compounds. *Review Journal of Chemistry*, 6(1):49–82, 2016. ISSN 2079-9780. doi:10.1021/bi0521893.
- [85] Ken Iozumi, George E Hoganson, Raffaele Pennella, Mark A Everett, and Bryan B Fuller. Role of Tyrosinase As the Determinant of Pigmentation in Cultured Human Melanocytes. *Journal of Investigative Dermatology*, 100(6):806–811, 1993. ISSN 0022-202X.
- [86] Vincent J Hearing Jr, Thomas M Ekel, Paul M Montague, and Jesse M Nicholson. Mammalin Tyrosinase. Stoichiometry and Measurement of Reaction Products. *Biochimica Et Biophysica Acta (BBA)-Enzymology*, 611(2):251–268, 1980. ISSN 0005-2744.
- [87] Vishal Desai and Stephen G Kaler. Role of Copper in Human Neurological Disorders. *American Journal of Clinical Nutrition*, 88(3):855S–858S, 2008. ISSN 0002-9165. doi:6.
- [88] Betty A Eipper, Doris A Stoffers, and Richard E Mains. The Biosynthesis of Neuropeptides: Peptide Alpha-Amidation. *Annual Review of Neuroscience*, 15(1):57–85, 1992. ISSN 0147-006X. doi:10.1146/annurev.ne.15.030192.000421.
- [89] Alicja Woronowicz, Niamh X Cawley, Su-Youne Chang, Hisatsugu Koshimizu, Andr   W Phillips, Zhi-Gang Xiong, and Y Peng Loh. Carboxypeptidase E Knockout Mice Exhibit Abnormal Dendritic Arborization and Spine Morphology in Central Nervous System Neurons. *Journal of Neuroscience Research*, 88(1):64–72, 2010. ISSN 0360-4012. doi:10.1002/jnr.22174.
- [90] Danielle Bousquet-Moore, Richard E Mains, and Betty A Eipper. Peptidyl-glycine Î-amidating Monooxygenase and Copper: a Gene–nutrient Interaction Critical to Nervous System Function. *Journal of Neuroscience Research*, 88(12):2535–2545, 2010. ISSN 0360-4012. doi:10.1002/jnr.22404.
- [91] Earl Frieden and H Steve Hsieh. Ceruloplasmin: the Copper Transport Protein With Essential Oxidase Activity. *Adv Enzymol Relat Areas Mol Biol*, 44:187–236, 1976. ISSN 0065-258X. doi:10.1007/978-1-4613-0537-8.
- [92] Huijun Chen, Gang Huang, Trent Su, Hua Gao, Zouhair K Attieh, Andrew T McKie, Gregory J Anderson, and Chris D Vulpe. Decreased Hephaestin Activity in the Intestine of Copper-Deficient Mice Causes Systemic Iron Deficiency. *The Journal of Nutrition*, 136(5):1236–1241, 2006. ISSN 0022-3166. doi:10.1093/jn/136.5.1236.
- [93] Lynda I Smith-Mungo and Herbert M Kagan. Lysyl Oxidase: Properties, Regulation and Multiple Functions in Biology. *Matrix Biology*, 16(7):387–398, 1998. ISSN 0945-053X. doi:10.1007/978-3-0348-8397-15.

- [94] Robert B Rucker, Taru Kosonen, Michael S Clegg, Alyson E Mitchell, Brian R Rucker, Janet Y Uriu-Hare, and Carl L Keen. Copper, Lysyl Oxidase, and Extracellular Matrix Protein Cross-Linking. *The American Journal of Clinical Nutrition*, 67(5):996S–1002S, 1998. ISSN 0002-9165. doi:10.1093/ajcn/67.5.996S.
- [95] Adriana M Zimnicka, Kristin Ivy, and Jack H Kaplan. Acquisition of Dietary Copper: a Role for Anion Transporters in Intestinal Apical Copper Uptake. *American Journal of Physiology-Cell Physiology*, 300(3):C588–C599, 2010. ISSN 0363-6143. doi:10.1152/ajpcell.00054.2010.
- [96] Yien-Ming Kuo, Anna A Gybina, Joshua W Pyatskowitz, Jane Gitschier, and Joseph R Prohaska. Copper Transport Protein (Ctr1) Levels in Mice Are Tissue Specific and Dependent on Copper Status. *The Journal of Nutrition*, 136(1):21–26, 2006. ISSN 0022-3166. doi:10.1093/jn/136.1.21.
- [97] Jennifer J Ravia, Renu M Stephen, Fayez K Ghishan, and James F Collins. Menkes Copper ATPase (Atp7a) Is a Novel Metal-Responsive Gene in Rat Duodenum, and Immunoreactive Protein Is Present on Brush-Border and Basolateral Membrane Domains. *Journal of Biological Chemistry*, 280(43):36221–36227, 2005. ISSN 0021-9258. doi:10.1074/jbc.M506727200.
- [98] Laura A Meyer, Alison P Durley, Joseph R Prohaska, and Z Leah Harris. Copper Transport and Metabolism Are Normal in Aceruloplasminemic Mice. *Journal of Biological Chemistry*, 276(39):36857–36861, 2001. ISSN 0021-9258. doi:6.
- [99] Mizue Moriya, Yi-Hsuan Ho, Anne Grana, Linh Nguyen, Arrissa Alvarez, Rita Jamil, M Leigh Ackland, Agnes Michalczyk, Pia Hamer, and Danny Ramos. Copper Is Taken Up Efficiently From Albumin and Alpha-2-Macroglobulin by Cultured Human Cells by More Than One Mechanism. *American Journal of Physiology-Cell Physiology*, 2008. doi:10.1096/fasebj.22..supplement.443.3.
- [100] EDWARD J Vargas, ANGELA R Shoho, and MARIA C Linder. Copper Transport in the Nagase Analbuminemic Rat. *American Journal of Physiology-Gastrointestinal and Liver Physiology*, 267(2):G259–G269, 1994. ISSN 0193-1857. doi:10.1007/978-1-4615-4723-8.
- [101] Haarin Chun, Tracy Catterton, Heejeong Kim, Jaekwon Lee, and Byung-Eun Kim. Organ-Specific Regulation of ATP7A Abundance Is Coordinated With Systemic Copper Homeostasis. *Scientific Reports*, 7(1):12001, 2017. ISSN 2045-2322.
- [102] Byung-Eun Kim, Michelle L Turski, Yasuhiro Nose, Michelle Casad, Howard A Rockman, and Dennis J Thiele. Cardiac Copper Deficiency Activates a Systemic Signaling Mechanism That Communicates With the Copper Acquisition and Storage Organs. *Cell Metabolism*, 11(5):353–363, 2010. doi:10.1177/1535370218813988.

- [103] Małgorzata Lenartowicz, Krzysztof Wieczerzak, Wojciech Krzeptowski, Paulina Dobosz, Paweł Grzmil, Rafał Starzyński, and Paweł Lipiński. Developmental Changes in the Expression of the *Atp7a* Gene in the Liver of Mice During the Postnatal Period. *Ecological Genetics and Physiology*, 313(4):209–217, 2010. ISSN 1932-5223. doi:10.1002/jez.586.
- [104] Katrina J Allen, Nicole E Buck, Daphne MY Cheah, Sophie Gazeas, Prithi Bhathal, and Julian FB Mercer. Chronological Changes in Tissue Copper, Zinc and Iron in the Toxic Milk Mouse and Effects of Copper Loading. *Biometals*, 19(5):555–564, 2006. ISSN 0966-0844. doi:10.1007/s10534.
- [105] Mee Y Bartee and Svetlana Lutsenko. Hepatic Copper-Transporting ATPase ATP7B: Function and Inactivation at the Molecular and Cellular Level. *Biometals*, 20(3-4):627, 2007. ISSN 0966-0844. doi:10.1007/s10534.
- [106] Abigael Muchenditsi, Haojun Yang, James P Hamilton, Lahari Koganti, Franck Housseau, Lisa Aronov, Hongni Fan, Hannah Pierson, Ashima Bhattacharjee, Robert C Murphy, Sears C, Potter J, Wooton-Kee CR, and Lutsenko S. Targeted Inactivation of Copper-Transporter *Atp7b* in Hepatocytes Causes Liver Steatosis and Obesity in Mice. *American Journal of Physiology-Heart and Circulatory Physiology*, 2017. doi:10.1152/ajpgi.00312.2016.
- [107] Svetlana Lutsenko, Natalie L Barnes, Mee Y Bartee, and Oleg Y Dmitriev. Function and Regulation of Human Copper-Transporting ATPases. *Physiological Reviews*, 87(3):1011–1046, 2007. doi:10.1152/physrev.00004.2006.
- [108] Prim de Bie, Bart van de Sluis, Ezra Burstein, Peter VE van de Berghe, Patricia Muller, Ruud Berger, Jonathan D Gitlin, Cisca Wijmenga, and Leo WJ Klomp. Distinct Wilson’s Disease Mutations in ATP7B Are Associated With Enhanced Binding to COMMD1 and Reduced Stability of ATP7B. *Gastroenterology*, 133(4):1316–1326, 2007. ISSN 0016-5085. doi:10.1053/j.gastro.2007.07.020.
- [109] Lawrence W Gray, Fangyu Peng, Shannon A Molloy, Venkata S Pendyala, Abigael Muchenditsi, Otto Muzik, Jaekwon Lee, Jack H Kaplan, and Svetlana Lutsenko. Urinary Copper Elevation in a Mouse Model of Wilson’s Disease Is a Regulated Process to Specifically Decrease the Hepatic Copper Load. *PLoS One*, 7(6):e38327, 2012. ISSN 1932-6203. doi:10.1371/journal.pone.0038327.
- [110] Heejeong Kim, Hwa-Young Son, Sarah M Bailey, and Jaekwon Lee. Deletion of Hepatic *Ctr1* Reveals Its Function in Copper Acquisition and Compensatory Mechanisms for Copper Homeostasis. *American Journal of Physiology-Gastrointestinal and Liver Physiology*, 2009. doi:10.1152/ajpgi.90632.2008.
- [111] Natalie Barnes, Mee Y Bartee, Lita Braiterman, Arnab Gupta, Vladimir Ustiyani, Vesna Zuzel, Jack H Kaplan, Ann L Hubbard, and Svetlana Lutsenko. Cell-Specific Trafficking Suggests a New Role for Renal ATP7B in the

- Intracellular Copper Storage. *Traffic*, 10(6):767–779, 2009. ISSN 1398-9219. doi:10.1111/j.1600-0854.2009.00901.x.
- [112] Joseph R Prohaska and Lois J Heller. Mechanical Properties of the Copper-Deficient Rat Heart. *The Journal of Nutrition*, 112(11):2142–2150, 1982. ISSN 1541-6100. doi:10.1093/jn/112.11.2142.
- [113] Denis M Medeiros, Jeanette Davidson, and James E Jenkins. A Unified Perspective on Copper Deficiency and Cardiomyopathy. *Proceedings of the Society for Experimental Biology and Medicine*, 203(3):262–273, 1993. ISSN 0037-9727. doi:10.3181/00379727-203-43599.
- [114] Youchun Jiang, Corey Reynolds, Chang Xiao, Wenke Feng, Zhanxiang Zhou, Walter Rodriguez, Suresh C Tyagi, John W Eaton, Jack T Saari, and Y James Kang. Dietary Copper Supplementation Reverses Hypertrophic Cardiomyopathy Induced by Chronic Pressure Overload in Mice. *Journal of Experimental Medicine*, 204(3):657–666, 2007. ISSN 0022-1007. doi:10.1177/1535370218813988.
- [115] Blase A Carabello. Concentric Versus Eccentric Remodeling. *Journal of Cardiac Failure*, 8(6):S258–S263, 2002. ISSN 1071-9164. doi:10.1007/978-1-4614-5203-8x22.
- [116] Christiana M Schannwell, Tobias Zimmermann, Markus Schneppenheim, Gunnar Plehn, Roger Marx, and Bodo E Strauer. Left Ventricular Hypertrophy and Diastolic Dysfunction in Healthy Pregnant Women. *Cardiology*, 97(2):73–78, 2002. ISSN 0008-6312. doi:10.1159/000057675.
- [117] Anna A Gybina and Joseph R Prohaska. Variable Response of Selected Cuproproteins in Rat Choroid Plexus and Cerebellum Following Perinatal Copper Deficiency. *Genes & Nutrition*, 1(1):51–59, 2006. ISSN 1555-8932. doi:10.1021/pr0501012.
- [118] MJ Niciu, X-M Ma, R El Meskini, GV Ronnett, RE Mains, and BA Eipper. Developmental Changes in the Expression of ATP7A During a Critical Period in Postnatal Neurodevelopment. *Neuroscience*, 139(3):947–964, 2006. ISSN 0306-4522. doi:10.1016/j.neuroscience.2006.01.044.
- [119] Anita U Rao, Lynn K Carta, Emmanuel Lesuisse, and Iqbal Hamza. Lack of Heme Synthesis in a Free-Living Eukaryote. *Proceedings of the National Academy of Sciences*, 102(12):4270–4275, 2005. ISSN 0027-8424. doi:10.1073/pnas.0500877102.
- [120] Tamara Korolnek, Jianbing Zhang, Simon Beardsley, George L Scheffer, and Iqbal Hamza. Control of Metazoan Heme Homeostasis by a Conserved Multidrug Resistance Protein. *Cell Metabolism*, 19(6):1008–1019, 2014. doi:10.1016/j.cmet.2014.03.030.

- [121] Diana E Davis, Hyun Cheol Roh, Krupa Deshmukh, Janelle J Bruinsma, Daniel L Schneider, James Guthrie, J David Robertson, and Kerry Kornfeld. The Cation Diffusion Facilitator Gene *Cdf-2* Mediates Zinc Metabolism in *Caenorhabditis Elegans*. *Genetics*, 182(4):1015–1033, 2009. doi:10.1534/genetics.109.103614.
- [122] Cole P Anderson and Elizabeth A Leibold. Mechanisms of Iron Metabolism in *Caenorhabditis Elegans*. *Frontiers in Pharmacology*, 5:113, 2014. doi:10.3389/fphar.2014.00113.
- [123] Laran T Jensen and Valeria Cizewski Culotta. Activation of CuZn Superoxide Dismutases From *Caenorhabditis Elegans* Does Not Require the Copper Chaperone CCS. *Journal of Biological Chemistry*, 280(50):41373–41379, 2005. ISSN 0021-9258. doi:10.1074/jbc.M509142200.
- [124] Tokumitsu Wakabayashi, Norihiro Nakamura, Yoshihiro Sambongi, Yoh Wada, Toshihiko Oka, and Masamitsu Futai. Identification of the Copper Chaperone, CUC-1, in *Caenorhabditis Elegans*: Tissue Specific Co-Expression With the Copper Transporting ATPase, CUA-1. *FEBS Letters*, 440(1-2):141–146, 1998. ISSN 0014-5793.
- [125] M Imagawa, T Onozawa, K Okumura, S Osada, T Nishihara, and M Kondo. Characterization of Metallothionein cDNAs Induced by Cadmium in the Nematode *Caenorhabditis Elegans*. *Biochemical Journal*, 268(1):237–240, 1990.
- [126] Haarin Chun, Anuj Kumar Sharma, Jaekwon Lee, Jefferson Chan, Shang Jia, and Byung-Eun Kim. The Intestinal Copper Exporter CUA-1 Is Required for Systemic Copper Homeostasis in *Caenorhabditis Elegans*. *Journal of Biological Chemistry*, 292(1):1–14, 2017. ISSN 0021-9258.
- [127] Yoshihiro Sambongi, Tokumitsu Wakabayashi, Takao Yoshimizu, Hiroshi Omote, Toshihiko Oka, and Masamitsu Futai. *Caenorhabditis Elegans* cDNA for a Menkes/Wilson Disease Gene Homologue and Its Function in a Yeast CCC2 Gene Deletion Mutant. *The Journal of Biochemistry*, 121(6):1169–1175, 1997. ISSN 0021-924X.
- [128] C. elegans Deletion Mutant Consortium. Large-Scale Screening for Targeted Knockouts in the *Caenorhabditis Elegans* Genome. *G3: Genes, Genomes, Genetics*, 2(11):1415–1425, 2012. ISSN 2160-1836. doi:10.1534/g3.
- [129] Jonathan H Freedman, Lee W Slice, Dennis Dixon, Andrew Fire, and Charles S Rubin. The Novel Metallothionein Genes of *Caenorhabditis Elegans*. Structural Organization and Inducible, Cell-Specific Expression. *Journal of Biological Chemistry*, 268(4):2554–2564, 1993. ISSN 0021-9258.
- [130] Sukaina Zeitoun-Ghandour, John M Charnock, Mark E Hodson, Oksana I Leszczyszyn, Claudia A Blindauer, and Stephen R St.Åijrzenbaum. The Two

- Caenorhabditis Elegans Metallothioneins (CeMT-1 and CeMT-2) Discriminate Between Essential Zinc and Toxic Cadmium. *The FEBS Journal*, 277(11):2531–2542, 2010. ISSN 1742-464X. doi:10.1021/ic048871n.
- [131] SC Swain, K Keusekotten, R Baumeister, and SR StÄijrzenbaum. C. Elegans Metallothioneins: New Insights Into the Phenotypic Effects of Cadmium Toxicosis. *Journal of Molecular Biology*, 341(4):951–959, 2004. ISSN 0022-2836. doi:10.1016/j.jmb.2004.06.050.
- [132] Lori H Moilanen, Tetsunari Fukushige, and Jonathan Freedman. Regulation of Metallothionein Gene Transcription Identification of Upstream Regulatory Elements and Transcription Factors Responsible for Cell-Specific Expression of the Metallothionein Genes From Caenorhabditis Elegans. *Journal of Biological Chemistry*, 274(42):29655–29665, 1999. ISSN 0021-9258.
- [133] Hyun Cheol Roh, Ivan Dimitrov, Krupa Deshmukh, Guoyan Zhao, Kurt Warnhoff, Daniel Cabrera, Wendy Tsai, and Kerry Kornfeld. A Modular System of DNA Enhancer Elements Mediates Tissue-Specific Activation of Transcription by High Dietary Zinc in C. Elegans. *Nucleic Acids Research*, 43(2):803–816, 2014. ISSN 1362-4962. doi:10.1093/nar/gku1360.
- [134] Kurt Warnhoff, Hyun C Roh, Zuzana Kocsisova, Chieh-Hsiang Tan, Andrew Morrison, Damari Crosswell, Daniel L Schneider, and Kerry Kornfeld. The Nuclear Receptor HIZR-1 Uses Zinc As a Ligand to Mediate Homeostasis in Response to High Zinc. *PLoS Biology*, 15(1):e2000094, 2017. ISSN 1545-7885. doi:10.1371/journal.pbio.2000094.
- [135] Ronald K Blackman and Vojo Vukovic. Preselection of Subjects for Therapeutic Treatment With Elesclomol Based on Hypoxic Status, 2014. US Patent App. 14/141,883.
- [136] Nha Huu Vo, Zhiqiang Xia, Jason Hanko, Tong Yun, Steve Bloom, Jianhua Shen, Keizo Koya, Lijun Sun, and Shoujun Chen. Synthesis, Crystallographic Characterization and Electrochemical Property of a Copper (II) Complex of the Anticancer Agent Elesclomol. *Journal of Inorganic Biochemistry*, 130:69–73, 2014. doi:10.1016/j.jinorgbio.2013.10.005.
- [137] Shoujun Chen, Lijun Sun, Keizo Koya, Noriaki Tatsuta, Zhiqiang Xia, Timothy Korbut, Zhenjian Du, Jim Wu, Guiqing Liang, Jun Jiang, et al. Syntheses and Antitumor Activities of N' 1, N' 3-Dialkyl-N' 1, N' 3-Di-(alkylcarbonothioyl) Malonohydrazide: the Discovery of Elesclomol. *Bioorganic & Medicinal Chemistry Letters*, 23(18):5070–5076, 2013. doi:10.1021/jm049556d.
- [138] Steven O'Day, Rene Gonzalez, David Lawson, Robert Weber, Laura Hutchins, Clay Anderson, Jonathan Haddad, Steven Kong, Anthony Williams, and Eric Jacobson. Phase II, Randomized, Controlled, Double-Blinded Trial

- of Weekly Elesclomol Plus Paclitaxel Versus Paclitaxel Alone for Stage IV Metastatic Melanoma. *Journal of Clinical Oncology*, 27(32):5452–5458, 2009. doi:10.1200/JCO.2008.17.1579.
- [139] David Hedley, Aisha Shamas-Din, Sue Chow, Deborah Sanfelice, Andre C Schuh, Joseph M Brandwein, Matthew D Seftel, Vikas Gupta, Karen WL Yee, and Aaron D Schimmer. A Phase I Study of Elesclomol Sodium in Patients With Acute Myeloid Leukemia. *Leukemia & Lymphoma*, 57(10):2437–2440, 2016. doi:10.3109/10428194.2016.1138293.
- [140] Anna Berkenblit, Joseph P Eder, David P Ryan, Michael V Seiden, Noriaki Tatsuta, Matthew L Sherman, Thomas A Dahl, Bruce J Dezube, and Jeffrey G Supko. Phase I Clinical Trial of STA-4783 in Combination With Paclitaxel in Patients With Refractory Solid Tumors. *Clinical Cancer Research*, 13(2): 584–590, 2007. doi:10.1200/jco.2005.23.1_suppl.9069.
- [141] Giancarlo Solaini, Gianluca Sgarbi, and Alessandra Baracca. Oxidative Phosphorylation in Cancer Cells. *Biochimica Et Biophysica Acta (BBA)-Bioenergetics*, 1807(6):534–542, 2011. doi:10.1158/1078.
- [142] Maik Hüttemann, Petr Pecina, Matthew Rainbolt, Thomas H Sanderson, Valerian E Kagan, Lobelia Samavati, Jeffrey W Doan, and Icksoo Lee. The Multiple Functions of Cytochrome C and Their Regulation in Life and Death Decisions of the Mammalian Cell: From Respiration to Apoptosis. *Mitochondrion*, 11(3):369–381, 2011. doi:10.1016/j.mito.2011.01.010.
- [143] Dunyaporn Trachootham, Jerome Alexandre, and Peng Huang. Targeting Cancer Cells by ROS-Mediated Mechanisms: a Radical Therapeutic Approach? *Nature Reviews Drug Discovery*, 8(7):579, 2009. doi:10.1038/nrd2803.
- [144] Andrea Glasauer and Navdeep S Chandel. Targeting Antioxidants for Cancer Therapy. *Biochemical Pharmacology*, 92(1):90–101, 2014. doi:10.1016/j.bcp.2014.07.017.
- [145] Peng Huang, Li Feng, Elizabeth A Oldham, Michael J Keating, and William Plunkett. Superoxide Dismutase As a Target for the Selective Killing of Cancer Cells. *Nature*, 407(6802):390, 2000. doi:10.1038/35030140.
- [146] Hélène Pelicano, Li Feng, Yan Zhou, Jennifer S Carew, Elizabeth O Hileman, William Plunkett, Michael J Keating, and Peng Huang. Inhibition of Mitochondrial Respiration a Novel Strategy to Enhance Drug-Induced Apoptosis in Human Leukemia Cells by a Reactive Oxygen Species-Mediated Mechanism. *Journal of Biological Chemistry*, 278(39):37832–37839, 2003. doi:10.1074/jbc.M301546200.
- [147] Peter L Toogood. Mitochondrial Drugs. *Current Opinion in Chemical Biology*, 12(4):457–463, 2008. doi:10.1016/j.cbpa.2008.06.002.

- [148] Jessica R Kirshner, Suqin He, Vishwasenani Balasubramanyam, Jane Kepros, Chin-Yu Yang, Mei Zhang, Zhenjian Du, James Barsoum, and John Bertin. Elesclomol Induces Cancer Cell Apoptosis Through Oxidative Stress. *Molecular Cancer Therapeutics*, 7(8):2319–2327, 2008. doi:10.1158/1535.
- [149] Mathias Gehrman. Drug Evaluation: STA-4783-Enhancing Taxane Efficacy by Induction of Hsp70. *Current Opinion in Investigational Drugs (London, England: 2000)*, 7(6):574–580, 2006.
- [150] Masazumi Nagai, Nha Vho, Elena Kostik, Suqin He, Jane Kepros, Luisa S Ogawa, Takayo Inoue, Ronald K Blackman, Yumiko Wada, and James Barsoum. The Oxidative Stress Inducer Elesclomol Requires Copper Chelation for Its Anticancer Activity. *Molecular Cancer Therapeutics*, 2009. doi:10.1016/j.freeradbiomed.2012.03.017.
- [151] Brian B Hasinoff, Xing Wu, Arun A Yadav, Daywin Patel, Hui Zhang, De-Shen Wang, Zhe-Sheng Chen, and Jack C Yalowich. Cellular Mechanisms of the Cytotoxicity of the Anticancer Drug Elesclomol and Its Complex With Cu (II). *Biochemical Pharmacology*, 93(3):266–276, 2015. doi:10.1016/j.bcp.2014.12.008.
- [152] Lianming Wu, Leon Zhou, David Q Liu, Frederick G Vogt, and Alireza S Kord. LC-MS/MS and Density Functional Theory Study of Copper (II) and Nickel (II) Chelating Complexes of Elesclomol (a Novel Anticancer Agent). *Journal of Pharmaceutical and Biomedical Analysis*, 54(2):331–336, 2011. doi:10.1021/ja000127o.
- [153] Stuart H Laurie and Bibudhendra Sarkar. Potentiometric and Spectroscopic Study of the Equilibria in the Aqueous Copper (II)-3, 6-Diazaoctane-1, 8-Diamine System and an Equilibrium-Di-Alysis Examination of the Ternary System of Human Serum Albumin-Copper (II)-3, 6-Diazaoctane-1, 8-Diamine. *Journal of the Chemical Society, Dalton Transactions*, 1(19):1822–1827, 1977. doi:10.1039/DT9770001822.
- [154] Arun A Yadav, Daywin Patel, Xing Wu, and Brian B Hasinoff. Molecular Mechanisms of the Biological Activity of the Anticancer Drug Elesclomol and Its Complexes With Cu (II), Ni (II) and Pt (II). *Journal of Inorganic Biochemistry*, 126:1–6, 2013. doi:10.1021/ja012668z.
- [155] Brian B Hasinoff, Arun A Yadav, Daywin Patel, and Xing Wu. The Cytotoxicity of the Anticancer Drug Elesclomol Is Due to Oxidative Stress Indirectly Mediated Through Its Complex With Cu (II). *Journal of Inorganic Biochemistry*, 137:22–30, 2014. doi:10.1016/j.jinorgbio.2014.04.004.
- [156] Masazumi Nagai, Nha H Vo, Luisa Shin Ogawa, Dinesh Chimmanamada, Takayo Inoue, John Chu, Britte C Beaudette-Zlatanova, Rongzhen Lu, Ronald K Blackman, James Barsoum, et al. The Oncology Drug Elesclomol Selectively Transports Copper to the Mitochondria to Induce Oxidative

- Stress in Cancer Cells. *Free Radical Biology and Medicine*, 52(10):2142–2150, 2012. doi:10.1016/j.freeradbiomed.2012.03.017.
- [157] Cristina Marzano, Maura Pellei, Francesco Tisato, and Carlo Santini. Copper Complexes As Anticancer Agents. *Anti-Cancer Agents in Medicinal Chemistry (Formerly Current Medicinal Chemistry-Anti-Cancer Agents)*, 9(2):185–211, 2009. doi:10.1021/cr400135x.
- [158] Brian W Morrison, Nicole A Doudican, Kirtesh R Patel, and Seth J Orlow. Disulfiram Induces Copper-Dependent Stimulation of Reactive Oxygen Species and Activation of the Extrinsic Apoptotic Pathway in Melanoma. *Melanoma Research*, 20(1):11–20, 2010. doi:10.1021/jm049568z.
- [159] Marian Elizabeth Helsel. *Evaluation and Development of Metal-Binding Agents That Alter Copper Bioavailability*. PhD thesis, Duke University, 2014.
- [160] Ronald K Blackman, Kahlin Cheung-Ong, Marinella Gebbia, David A Proia, Suqin He, Jane Kepros, Aurelie Jonneaux, Philippe Marchetti, Jerome Kluza, Patricia E Rao, et al. Mitochondrial Electron Transport Is the Cellular Target of the Oncology Drug Elesclomol. *PloS One*, 7(1):e29798, 2012. doi:10.1371/journal.pone.0029798.
- [161] Pek Yee Lum, Christopher D Armour, Sergey B Stepaniants, Guy Cavet, Maria K Wolf, J Scott Butler, Jerald C Hinshaw, Philippe Garnier, Glenn D Prestwich, Amy Leonardson, et al. Discovering Modes of Action for Therapeutic Compounds Using a Genome-Wide Screen of Yeast Heterozygotes. *Cell*, 116(1):121–137, 2004.
- [162] Bradley J Monk, James T Kauderer, Katherine M Moxley, Albert J Bonebrake, Summer B Dewdney, Angeles Alvarez Secord, Frederick R Ueland, Carolyn M Johnston, and Carol Aghajanian. A Phase II Evaluation of Elesclomol Sodium and Weekly Paclitaxel in the Treatment of Recurrent or Persistent Platinum-Resistant Ovarian, Fallopian Tube or Primary Peritoneal Cancer: an NRG Oncology/gynecologic Oncology Group Study. *Gynecologic Oncology*, 151(3):422–427, 2018. doi:10.1200/jco.2008.19.2963.
- [163] R Gonzalez, DH Lawson, RW Weber, LF Hutchins, CM Anderson, KN Williams, S Kong, E Jacobson, and SJ O’Day. Phase II Trial of Elesclomol (formerly STA-4783) and Paclitaxel in Stage IV Metastatic Melanoma (MM): Subgroup Analysis by Prior Chemotherapy. *Journal of Clinical Oncology*, 26(15):9036–9036, 2008. doi:10.1200/jco.2008.26.1_suppl.9036.
- [164] DH Lawson, R Gonzalez, RW Weber, LF Hutchins, CM Anderson, KN Williams, S Kong, E Jacobson, and SJ O’Day. 2-Year Overall Survival (OS) Results of a Phase II Trial of Elesclomol (formerly STA-4783) and Paclitaxel in Stage IV Metastatic Melanoma (MM). *Journal of Clinical Oncology*, 26(15):20023–20023, 2008. ISSN 0732-183X. doi:10.1200/jco.2008.26.1_suppl.20023.

- [165] Balakrishnan Ramanathan, Kun-Yan Jan, Chien-Hung Chen, Tzyh-Chyuan Hour, Hong-Jen Yu, and Yeong-Shiau Pu. Resistance to Paclitaxel Is Proportional to Cellular Total Antioxidant Capacity. *Cancer Research*, 65(18): 8455–8460, 2005. doi:10.1158/0008.
- [166] VM Vukovic, A Hauschild, AM Eggermont, and S O’Day. Phase III, Randomized, Double-Blind Study of Elesclomol and Paclitaxel Versus Paclitaxel Alone in Stage IV Metastatic Melanoma (MM): 1-Year OS Update. *Journal of Clinical Oncology*, 28(15):8550–8550, 2010. doi:10.1200/jco.2010.28.1_suppl.8550.
- [167] Steven J O’Day, Alexander MM Eggermont, Vanna Chiarion-Sileni, Richard Kefford, Jean Jacques Grob, Laurent Mortier, Caroline Robert, Jacob Schachter, Alessandro Testori, Jacek Mackiewicz, et al. Final Results of Phase III SYMMETRY Study: Randomized, Double-Blind Trial of Elesclomol Plus Paclitaxel Versus Paclitaxel Alone As Treatment for Chemotherapy-Naive Patients With Advanced Melanoma. *Journal of Clinical Oncology*, 31(9):1211–1218, 2013. doi:10.1200/JCO.2012.44.5585.
- [168] Jérôme Kluza, Paola Corazao-Rozas, Yasmine Touil, Manel Jendoubi, Cyril Maire, Pierre Guerreschi, Aurélie Jonneaux, Caroline Ballot, Stéphane Balayssac, Samuel Valable, et al. Inactivation of the HIF-1 α /PDK3 Signaling Axis Drives Melanoma Toward Mitochondrial Oxidative Metabolism and Potentiates the Therapeutic Activity of Pro-Oxidants. *Cancer Research*, 72(19): 5035–5047, 2012. doi:10.1158/0008.
- [169] Andile H Ngwane, Ray-Dean Petersen, Bienyameen Baker, Ian Wiid, Ho Ning Wong, and Richard K Haynes. The Evaluation of the Anti-Cancer Drug Elesclomol That Forms a Redox-Active Copper Chelate As a Potential Anti-Tubercular Drug. *IUBMB Life*, 2019. doi:10.1002/iub.2002.
- [170] Yi-Jie Ren, Xiao-Hui Wang, Cheng Ji, Yi-Di Guan, Xian-Jiu Lu, Xian-Rong Liu, Hong-Han Zhang, Ling-Chuan Guo, Qiong-Hua Xu, Wei-Dong Zhu, et al. Silencing of NAC1 Expression Induces Cancer Cells Oxidative Stress in Hypoxia and Potentiates the Therapeutic Activity of Elesclomol. *Frontiers in Pharmacology*, 8:804, 2017. doi:10.3389/fphar.2017.00804.
- [171] Gulsah Albayrak, Funda Demirtas Korkmaz, Duygu Tozcu, and Irem Dogan Turacli. The Outcomes of an Impaired Powerhouse in KRAS Mutant Lung Adenocarcinoma Cells by Elesclomol. *Journal of Cellular Biochemistry*, 2019. doi:10.1002/jcb.28342.
- [172] Alba Timón-Gómez, Eva Nyíltová, Luciano A Abriata, Alejandro J Vila, Jonathan Hosler, and Antoni Barrientos. Mitochondrial Cytochrome C Oxidase Biogenesis: Recent Developments. In *Seminars in Cell & Developmental Biology*, volume 76, pages 163–178. Elsevier, Elsevier, 2018. doi:10.1016/j.semcdb.2017.08.055.

- [173] M Fátima Lucas, Denis L Rousseau, and Victor Guallar. Electron Transfer Pathways in Cytochrome C Oxidase. *Biochimica Et Biophysica Acta (BBA)-Bioenergetics*, 1807(10):1305–1313, 2011. doi:10.1016/j.bbabo.2011.03.003.
- [174] Paul A Cobine, Fabien Pierrel, Megan L Bestwick, and Dennis R Winge. Mitochondrial Matrix Copper Complex Used in Metallation of Cytochrome Oxidase and Superoxide Dismutase. *Journal of Biological Chemistry*, 281(48):36552–36559, 2006. doi:10.1074/jbc.M606839200.
- [175] Shivatheja Soma, Andrew J Latimer, Haarin Chun, Alison C Vicary, Shrishiv A Timbalia, Aren Boulet, Jennifer J Rahn, Sherine SL Chan, Scot C Leary, Byung-Eun Kim, et al. Elesclomol Restores Mitochondrial Function in Genetic Models of Copper Deficiency. *Proceedings of the National Academy of Sciences*, 115(32):8161–8166, 2018. doi:10.1073/pnas.1806296115.
- [176] Jaekwon Lee, Joseph R Prohaska, and Dennis J Thiele. Essential Role for Mammalian Copper Transporter Ctr1 in Copper Homeostasis and Embryonic Development. *Proceedings of the National Academy of Sciences*, 98(12):6842–6847, 2001. doi:10.1073/pnas.111058698.
- [177] Yanfang Wang, Sha Zhu, Gary A Weisman, Jonathan D Gitlin, and Michael J Petris. Conditional Knockout of the Menkes Disease Copper Transporter Demonstrates Its Critical Role in Embryogenesis. *PloS One*, 7(8):e43039, 2012. doi:10.1371/journal.pone.0043039.
- [178] Michelle L Turski, Donita C Brady, Hyung J Kim, Byung-Eun Kim, Yasuhiro Nose, Christopher M Counter, Dennis R Winge, and Dennis J Thiele. A Novel Role for Copper in Ras/mitogen-Activated Protein Kinase Signaling. *Molecular and Cellular Biology*, 32(7):1284–1295, 2012. doi:10.1128/MCB.05722.
- [179] Hiroko Kodama, Yoshiko Murata, and Masaaki Kobayashi. Clinical Manifestations and Treatment of Menkes Disease and Its Variants. *Pediatrics International*, 41(4):423–429, 1999. doi:10.1046/j.1442-200x.1999.01095.x.
- [180] Stephen G Kaler. ATP7A-Related Copper Transport Disorders. In *GeneReviews*®[Internet]. University of Washington, Seattle, 2016.
- [181] John H Menkes, Milton Alter, Gerd K Steigleder, David R Weakley, and Joo Ho Sung. A Sex-Linked Recessive Disorder With Retardation of Growth, Peculiar Hair, and Focal Cerebral and Cerebellar Degeneration. *Pediatrics*, 29(5):764–779, 1962.
- [182] MJ Petris, JF Mercer, JG Culvenor, P Lockhart, PA Gleeson, and J Camakaris. Ligand-regulated Transport of the Menkes Copper P-type ATPase Efflux Pump From the Golgi Apparatus to the Plasma Membrane: a Novel Mechanism of Regulated Trafficking. *The EMBO Journal*, 15(22):6084–6095, 1996. ISSN 0261-4189. doi:10.1002/j.1460-2075.1996.tb00997.x.

- [183] Zeynep TÃijmer. An Overview and Update of ATP7A Mutations Leading to Menkes Disease and Occipital Horn Syndrome. *Human Mutation*, 34(3): 417–429, 2013. ISSN 1059-7794. doi:10.1002/humu.22266.
- [184] Małgorzata Lenartowicz, Wojciech Krzeptowski, Paweł Lipiński, Paweł Grzmil, Rafał Starzyński, Olga Pierzchała, and Lisbeth Birk Møller. Mottled Mice and Non-Mammalian Models of Menkes Disease. *Frontiers in Molecular Neuroscience*, 8:72, 2015. ISSN 1662-5099. doi:10.3389/fnmol.2015.00072.
- [185] Chiara Cecchi, Michel Biasotto, Mario Tosi, and Philip Avner. The Mottled Mouse As a Model for Human Menkes Disease: Identification of Mutations in the *Atp7a* Gene. *Human Molecular Genetics*, 6(3):425–433, 1997. ISSN 1460-2083.
- [186] Stephen G Kaler, Courtney S Holmes, David S Goldstein, Jingrong Tang, Sarah C Godwin, Anthony Donsante, Clarissa J Liew, Susumu Sato, and Nicholas Patronas. Neonatal Diagnosis and Treatment of Menkes Disease. *New England Journal of Medicine*, 358(6):605–614, 2008. ISSN 0028-4793. doi:10.1046/j.1442-200x.1999.01095.x.
- [187] Stephen G Kaler, Soma Das, Barbara Levinson, David S Goldstein, Courtney S Holmes, Nicholas J Patronas, Seymour Packman, and William A Gahl. Successful Early Copper Therapy in Menkes Disease Associated With a Mutant Transcript Containing a Small In-Frame Deletion. *Biochemical and Molecular Medicine*, 57(1):37–46, 1996. ISSN 1077-3150.
- [188] Stephen G Kaler. Menkes Disease Mutations and Response to Early Copper Histidine Treatment. *Nature Genetics*, 13(1):21, 1996. ISSN 1546-1718. doi:10.1002/ana.410380613.
- [189] Marie Reine Haddad, Charles J Macri, Courtney S Holmes, David S Goldstein, Beryl E Jacobson, Jose A Centeno, Edwina J Popek, Willam A Gahl, and Stephen G Kaler. In Utero Copper Treatment for Menkes Disease Associated With a Severe ATP7A Mutation. *Molecular Genetics and Metabolism*, 107(1-2):222–228, 2012. ISSN 1096-7192. doi:10.1016/j.ymgme.2012.05.008.
- [190] Anthony Donsante, Ling Yi, Patricia M Zerfas, Lauren R Brinster, Patricia Sullivan, David S Goldstein, Joseph Prohaska, Jose A Centeno, Elisabeth Rushing, and Stephen G Kaler. ATP7A Gene Addition to the Choroid Plexus Results in Long-Term Rescue of the Lethal Copper Transport Defect in a Menkes Disease Mouse Model. *Molecular Therapy*, 19(12):2114–2123, 2011. ISSN 1525-0016. doi:10.1038/mt.2011.143.
- [191] Marie Reine Haddad, Eun-Young Choi, Patricia M Zerfas, Ling Yi, Diego Martinelli, Patricia Sullivan, David S Goldstein, Jose A Centeno, Lauren R Brinster, Martina Development. Cerebrospinal Fluid-Directed RAAV9-RsATP7A Plus Subcutaneous Copper Histidinate Advance Survival and Outcomes in a

- Menkes Disease Mouse Model. *Molecular Therapy - Methods & Clinical Development*, 10:165–178, 2018. ISSN 2329-0501. doi:10.1016/j.omtm.2018.07.002.
- [192] Wattanaporn Bhadhprasit, Hiroko Kodama, Chie Fujisawa, Tomoko Hiroki, Eishin Ogawa, and Biology. Effect of Copper and Disulfiram Combination Therapy on the Macular Mouse, a Model of Menkes Disease. *Journal of Trace Elements in Medicine and Biology*, 26(2-3):105–108, 2012. ISSN 0946-672X. doi:10.1016/j.jtemb.2012.05.002.
- [193] Shiho Nomura, Satoshi Nozaki, Takashi Hamazaki, Taisuke Takeda, Eiichi Ninomiya, Satoshi Kudo, Emi Hayashinaka, Yasuhiro Wada, Tomoko Hiroki, and Chie Fujisawa. PET Imaging Analysis With ^{64}Cu in Disulfiram Treatment for Aberrant Copper Biodistribution in Menkes Disease Mouse Model. *Journal of Nuclear Medicine*, 55(5):845–851, 2014. ISSN 0161-5505. doi:10.2967/jnumed.113.131797.
- [194] Takao Hoshina, Satoshi Nozaki, Takashi Hamazaki, Satoshi Kudo, Yuka Nakatani, Hiroko Kodama, Haruo Shintaku, and Yasuyoshi Watanabe. Disulfiram Enhanced Delivery of Orally Administered Copper Into the Central Nervous System in Menkes Disease Mouse Model. *Journal of Inherited Metabolic Disease*, 41(6):1285–1291, 2018. ISSN 0141-8955. doi:10.1007/s10545.
- [195] Eishin Ogawa and Hiroko Kodama. Effects of Disulfiram Treatment in Patients With Menkes Disease and Occipital Horn Syndrome. *Journal of Trace Elements in Medicine and Biology*, 26(2-3):102–104, 2012. ISSN 0946-672X. doi:10.1002/1096-8628.
- [196] Sydney Brenner. The Genetics of *Caenorhabditis Elegans*. *Genetics*, 77(1):71–94, 1974. ISSN 0016-6731.
- [197] Shohei Mitani. Nematode, an Experimental Animal in the National BioResource Project. *Experimental Animals*, 58(4):351–356, 2009. ISSN 1341-1357.
- [198] Ravi S Kamath, Andrew G Fraser, Yan Dong, Gino Poulin, Richard Durbin, Monica Gotta, Alexander Kanapin, Nathalie Le Bot, Sergio Moreno, and Marc Sohrmann. Systematic Functional Analysis of the *Caenorhabditis Elegans* Genome Using RNAi. *Nature*, 421(6920):231, 2003. ISSN 1476-4687. doi:10.1038/nature01278.
- [199] Jean-François Rual, Julian Ceron, John Koreth, Tong Hao, Anne-Sophie Nicot, Tomoko Hirozane-Kishikawa, Jean Vandenhaute, Stuart H Orkin, David E Hill, and Sander van den Heuvel. Toward Improving *Caenorhabditis Elegans* Phenome Mapping With an ORFeome-Based RNAi Library. *Genome Research*, 14(10b):2162–2168, 2004. ISSN 1088-9051. doi:10.1101/gr.2505604.
- [200] Jennifer L Anderson, Levi T Morran, and Patrick C Phillips. Outcrossing and the Maintenance of Males Within *C. Elegans* Populations. *Journal of Heredity*, 101(1):S62–S74, 2010. ISSN 1465-7333. doi:10.1093/jhered/esq003.

- [201] Michael Finney and Gary Ruvkun. The Unc-86 Gene Product Couples Cell Lineage and Cell Identity in *C. Elegans*. *Cell*, 63(5):895–905, 1990. ISSN 0092-8674.
- [202] Xiaojing Yuan, Olga Protchenko, Caroline C Philpott, and Iqbal Hamza. Topologically Conserved Residues Direct Heme Transport in HRG-1-Related Proteins. *Journal of Biological Chemistry*, 287(7):4914–4924, 2012. ISSN 0021-9258. doi:10.1074/jbc.M111.326785.
- [203] Huijun Chen, Trent Su, Zouhair K Attieh, Tama C Fox, Andrew T McKie, Gregory J Anderson, and Chris D Vulpe. Systemic Regulation of Hephaestin and Ireg1 Revealed in Studies of Genetic and Nutritional Iron Deficiency. *Blood*, 102(5):1893–1899, 2003. ISSN 0006-4971. doi:10.1182/blood.
- [204] BE Kim, K Smith, and MJ Petris. A Copper Treatable Menkes Disease Mutation Associated With Defective Trafficking of a Functional Menkes Copper ATPase. *Journal of Medical Genetics*, 40(4):290–295, 2003. ISSN 0022-2593. doi:10.1007/978-1-60327-161-122.
- [205] Roméo Cecchelli, Bénédicte Dehouck, Laurence Descamps, Laurence Fenart, Valérie Buée-Scherrer, C Duhem, Stefan Lundquist, M Rentfel, Gérard Torpier, and Marie-Pierre Dehouck. In vitro model for evaluating drug transport across the blood–brain barrier. *Advanced drug delivery reviews*, 36(2-3):165–178, 1999.
- [206] Hans C Helms, N Joan Abbott, Malgorzata Burek, Romeo Cecchelli, Pierre-Olivier Couraud, Maria A Deli, Carola Förster, Hans J Galla, Ignacio A Romero, Eric V Shusta, et al. In vitro models of the blood–brain barrier: an overview of commonly used brain endothelial cell culture models and guidelines for their use. *Journal of Cerebral Blood Flow & Metabolism*, 36(5):862–890, 2016.
- [207] Jaekwon Lee, Joseph R Prohaska, Susan L Dagenais, Thomas W Glover, and Dennis J Thiele. Isolation of a Murine Copper Transporter Gene, Tissue Specific Expression and Functional Complementation of a Yeast Copper Transport Mutant. *Gene*, 254(1-2):87–96, 2000. doi:10.1369/jhc.6A6970.2006.
- [208] Michael J Petris, Kathryn Smith, Jaekwon Lee, and Dennis J Thiele. Copper-Stimulated Endocytosis and Degradation of the Human Copper Transporter, HCtr1. *Journal of Biological Chemistry*, 278(11):9639–9646, 2003. doi:10.1074/jbc.M209455200.
- [209] C Eng Ooi, E Rabinovich, A Dancis, JS Bonifacino, and RD Klausner. Copper-Dependent Degradation of the *Saccharomyces Cerevisiae* Plasma Membrane Copper Transporter Ctr1p in the Apparent Absence of Endocytosis. *The EMBO Journal*, 15(14):3515–3523, 1996. doi:10.1002/j.1460-2075.1996.tb00720.x.

- [210] Toshihiko Oka, Takao Toyomura, Kenta Honjo, Yoh Wada, and Masamitsu Futai. Four Subunit a Isoforms OfCaenorhabditis Elegans Vacuolar H⁺-ATPase CELL-SPECIFIC EXPRESSION DURING DEVELOPMENT. *Journal of Biological Chemistry*, 276(35):33079–33085, 2001.
- [211] Hiroshi Qadota, Makiko Inoue, Takao Hikita, Mathias Köppen, Jeffrey D Hardin, Mutsuki Amano, Donald G Moerman, and Kozo Kaibuchi. Establishment of a Tissue-Specific RNAi System in C. Elegans. *Gene*, 400(1-2): 166–173, 2007. doi:10.1016/j.gene.2007.06.020.
- [212] Yoshihiro Sambongi, Takashi Nagae, Yanna Liu, Takao Yoshimizu, Kenji Takeda, Yoh Wada, and Masamitsu Futai. Sensing of Cadmium and Copper Ions by Externally Exposed ADL, ASE, and ASH Neurons Elicits Avoidance Response in Caenorhabditis Elegans. *Neuroreport*, 10(4):753–757, 1999. ISSN 0959-4965.
- [213] Min Guo, Tai-Hong Wu, Yan-Xue Song, Ming-Hai Ge, Chun-Ming Su, Wei-Pin Niu, Lan-Lan Li, Zi-Jing Xu, Chang-Li Ge, and Maha TH Al-Mhanawi. Reciprocal Inhibition Between Sensory ASH and ASI Neurons Modulates Nociception and Avoidance in Caenorhabditis Elegans. *Nature Communications*, 6:5655, 2015. ISSN 2041-1723. doi:10.1038/ncomms6655.
- [214] Limin Hao, Evgeni Efimenko, Peter Swoboda, and Jonathan M Scholey. The Retrograde IFT Machinery of C. Elegans Cilia: Two IFT Dynein Complexes? *PLoS One*, 6(6):e20995, 2011. doi:10.1371/journal.pone.0020995.
- [215] Andrea Calixto, Dattananda Chelur, Irini Topalidou, Xiaoyin Chen, and Martin Chalfie. Enhanced Neuronal RNAi in C. Elegans Using SID-1. *Nature Methods*, 7(7):554, 2010. doi:10.1038/nmeth.1463.
- [216] Steven J Husson, Tom Janssen, Geert Baggerman, Brigitte Bogert, Amanda H Kahn-Kirby, Kaveh Ashrafi, and Liliane Schoofs. Impaired Processing of FLP and NLP Peptides in Carboxypeptidase E (EGL-21)-Deficient Caenorhabditis Elegans As Analyzed by Mass Spectrometry. *Journal of Neurochemistry*, 102(1):246–260, 2007. doi:10.1111/j.1471-4159.2007.04474.x.
- [217] Jamie Kass, Tija C Jacob, Peter Kim, and Joshua M Kaplan. The EGL-3 Proprotein Convertase Regulates Mechanosensory Responses of Caenorhabditis Elegans. *Journal of Neuroscience*, 21(23):9265–9272, 2001.
- [218] Jude Beaudoin, Dennis J Thiele, Simon Labbe, and Sergi Puig. Dissection of the Relative Contribution of the Schizosaccharomyces Pombe Ctr4 and Ctr5 Proteins to the Copper Transport and Cell Surface Delivery Functions. *Microbiology*, 157(Pt 4):1021, 2011. doi:10.1099/mic.0.046854.
- [219] Hyun Cheol Roh, Sara Collier, James Guthrie, J David Robertson, and Kerry Kornfeld. Lysosome-Related Organelles in Intestinal Cells Are a

- Zinc Storage Site in *C. Elegans*. *Cell Metabolism*, 15(1):88–99, 2012. doi:10.1016/j.cmet.2011.12.003.
- [220] Brett L Gourley, Samuel B Parker, Barbara J Jones, Kimberly B Zumbrennen, and Elizabeth A Leibold. Cytosolic Aconitase and Ferritin Are Regulated by Iron In *Caenorhabditis Elegans*. *Journal of Biological Chemistry*, 278(5):3227–3234, 2003. doi:10.1074/jbc.M210333200.
- [221] Caiyong Chen, Tamika K Samuel, Michael Krause, Harry A Dailey, and Iqbal Hamza. Heme Utilization in the *Caenorhabditis Elegans* Hypodermal Cells Is Facilitated by Heme-Responsive Gene-2. *Journal of Biological Chemistry*, 287(12):9601–9612, 2012. doi:10.1074/jbc.M111.307694.
- [222] Ho Yi Mak. Lipid Droplets As Fat Storage Organelles in *Caenorhabditis Elegans* Thematic Review Series: Lipid Droplet Synthesis and Metabolism: From Yeast to Man. *Journal of Lipid Research*, 53(1):28–33, 2012. doi:10.1194/jlr.R021006.
- [223] Ichiro Aoki and Ikue Mori. Molecular biology of thermosensory transduction in *c. elegans*. *Current opinion in neurobiology*, 34:117–124, 2015.
- [224] Andrew Jonathan Bretscher, Karl Emanuel Busch, and Mario de Bono. A carbon dioxide avoidance behavior is integrated with responses to ambient oxygen and food in *caenorhabditis elegans*. *Proceedings of the National Academy of Sciences*, 105(23):8044–8049, 2008.
- [225] Andrew Jonathan Bretscher, Eiji Kodama-Namba, Karl Emanuel Busch, Robin Joseph Murphy, Zoltan Soltesz, Patrick Laurent, and Mario de Bono. Temperature, oxygen, and salt-sensing neurons in *c. elegans* are carbon dioxide sensors that control avoidance behavior. *Neuron*, 69(6):1099–1113, 2011.
- [226] Cornelia I Bargmann, Erika Hartweg, and H Robert Horvitz. Odorant-selective genes and neurons mediate olfaction in *c. elegans*. *Cell*, 74(3):515–527, 1993.
- [227] Yun Zhang, Hang Lu, and Cornelia I Bargmann. Pathogenic bacteria induce aversive olfactory learning in *caenorhabditis elegans*. *Nature*, 438(7065):179, 2005.
- [228] Massimo A Hilliard, Alfonso J Apicella, Rex Kerr, Hiroshi Suzuki, Paolo Bazzicalupo, and William R Schafer. In Vivo Imaging of *C. Elegans* ASH Neurons: Cellular Response and Adaptation to Chemical Repellents. *The EMBO Journal*, 24(1):63–72, 2005. doi:10.1038/sj.emboj.7600493.
- [229] Min Du and Dayong Wang. The Neurotoxic Effects of Heavy Metal Exposure on GABAergic Nervous System in Nematode *Caenorhabditis Elegans*. *Environmental Toxicology and Pharmacology*, 27(3):314–320, 2009. doi:10.1016/j.etap.2008.11.011.

- [230] Eric Block, Victor S Batista, Hiroaki Matsunami, Hanyi Zhuang, and Lucky Ahmed. The Role of Metals in Mammalian Olfaction of Low Molecular Weight Organosulfur Compounds. *Natural Product Reports*, 34(5):529–557, 2017. doi:10.1021/acs.jpcc.7b00486.
- [231] Lotte Frooninckx, Liesbeth Van Rompay, Liesbet Temmerman, Elien Van Sinay, Isabel Beets, Tom Janssen, Steven J Husson, and Liliane Schoofs. Neuropeptide GPCRs in *C. Elegans*. *Frontiers in Endocrinology*, 3:167, 2012. doi:10.3389/fendo.2012.00167.
- [232] C Li and K Kim. Neuropeptides, WormBook, Ed. the *C. Elegans* Research Community, WormBook, Doi/10.1895/wormbook. 1.142. 1, 2008.
- [233] Sai Yuan, Anuj Kumar Sharma, Alexandria Richart, Jaekwon Lee, and Byung-Eun Kim. CHCA-1 Is a Copper-Regulated CTR1 Homolog Required for Normal Development, Copper Accumulation, and Copper-Sensing Behavior in *Caenorhabditis Elegans*. *Journal of Biological Chemistry*, 293(28):10911–10925, 2018. ISSN 0021-9258. doi:10.1074/jbc.RA118.003503.
- [234] David M Klurfeld. *Nutrition and Immunology*. Springer Science & Business Media, 2013. ISBN 146152900X.
- [235] Joseph R Prohaska, Stephen W Downing, and Omelan A Lukasewycz. Chronic Dietary Copper Deficiency Alters Biochemical and Morphological Properties of Mouse Lymphoid Tissues. *The Journal of Nutrition*, 113(8):1583–1590, 1983. ISSN 0022-3166. doi:10.1007/978-1-4613-0553-11.
- [236] Joseph J Korte and Joseph R Prohaska. Dietary Copper Deficiency Alters Protein and Lipid Composition of Murine Lymphocyte Plasma Membranes. *The Journal of Nutrition*, 117(6):1076–1084, 1987. ISSN 0022-3166. doi:10.1093/jn/117.6.1076.
- [237] Anthony Donsante, Paul Johnson, Laura A Jansen, and Stephen G Kaler. Somatic Mosaicism in Menkes Disease Suggests Choroid Plexus-mediated Copper Transport to the Developing Brain. *American Journal of Medical Genetics Part A*, 152(10):2529–2534, 2010. ISSN 1552-4825. doi:10.1002/ajmg.a.34065.
- [238] Babette Weksler, Ignacio A Romero, and Pierre-Olivier Couraud. The HCMEC/D3 Cell Line As a Model of the Human Blood Brain Barrier. *Fluids and Barriers of the CNS*, 10(1):16, 2013. ISSN 2045-8118. doi:10.1186/2045.
- [239] Antje Appelt-Menzel, Alevtina Cubukova, and Marco Metzger. Establishment of a Human Blood-Brain Barrier Co-Culture Model Mimicking the Neurovascular Unit Using Induced Pluripotent Stem Cells. *Current Protocols in Stem Cell Biology*, 47(1):e62, 2018. ISSN 1941-7322. doi:10.1016/j.stemcr.2017.02.021.

- [240] Kiem Vu, Babette Weksler, Ignacio Romero, Pierre-Olivier Couraud, and Angie Gelli. Immortalized Human Brain Endothelial Cell Line HCMEC/D3 As a Model of the Blood-Brain Barrier Facilitates in Vitro Studies of Central Nervous System Infection by *Cryptococcus Neoformans*. *Eukaryotic Cell*, 8 (11):1803–1807, 2009. ISSN 1535-9778. doi:10.1096/fj.04-3458fje.
- [241] Carola Förster, Malgorzata Burek, Ignacio A Romero, Babette Weksler, Pierre-Olivier Couraud, and Detlev Drenckhahn. Differential effects of hydrocortisone and $\text{tnf}\alpha$ on tight junction proteins in an in vitro model of the human blood–brain barrier. *The Journal of physiology*, 586(7):1937–1949, 2008.
- [242] András Harazin, Alexandra Bocsik, Lilla Barna, András Kincses, Judit Váradi, Ferenc Fenyvesi, Vilmos Tubak, Maria A Deli, and Miklós Vecsernyés. Protection of cultured brain endothelial cells from cytokine-induced damage by α -melanocyte stimulating hormone. *PeerJ*, 6:e4774, 2018.
- [243] Pieter Jaap Gaillard and Albertus Gerrit de Boer. Relationship between permeability status of the blood–brain barrier and in vitro permeability coefficient of a drug. *European journal of pharmaceutical sciences*, 12(2):95–102, 2000.
- [244] P Marc D Watson, Judy C Paterson, George Thom, Ulrika Ginman, Stefan Lundquist, and Carl I Webster. Modelling the endothelial blood-cns barriers: a method for the production of robust in vitro models of the rat blood-brain barrier and blood-spinal cord barrier. *BMC neuroscience*, 14(1):59, 2013.
- [245] Janet Y Uriu-Adams, Rachel E Scherr, Louise Lanoue, and Carl L Keen. Influence of Copper on Early Development: Prenatal and Postnatal Considerations. *Biofactors*, 36(2):136–152, 2010. ISSN 1872-8081. doi:10.1002/biof.85.
- [246] Carl L Keen, Janet Y Uriu-Hare, Susan N Hawk, Margaret A Jankowski, George P Daston, Catherine L Kwik-Urbe, and Robert B Rucker. Effect of Copper Deficiency on Prenatal Development and Pregnancy Outcome. *The American Journal of Clinical Nutrition*, 67(5):1003S–1011S, 1998. ISSN 0002-9165. doi:10.1093/ajcn/67.5.1003S.
- [247] Bonnie Ransom Stern, Marc Solioz, Daniel Krewski, Peter Aggett, Tar-Ching Aw, Scott Baker, Kenny Crump, Michael Dourson, Lynne Haber, and Rick Hertzberg. Copper and Human Health: Biochemistry, Genetics, and Strategies for Modeling Dose-Response Relationships. *Journal of Toxicology and Environmental Health, Part B*, 10(3):157–222, 2007. ISSN 1093-7404. doi:10.1080/10937400600755911.
- [248] Danny Ramos, David Mar, Michael Ishida, Rebecca Vargas, Michaella Gaité, Aaron Montgomery, and Maria C Linder. Mechanism of Copper Uptake From Blood Plasma Ceruloplasmin by Mammalian Cells. *PLoS One*, 11(3): e0149516, 2016. ISSN 1932-6203. doi:10.1096/fasebj.30._supplement.1026.1.

- [249] Julie Gordon and Nancy R Manley. Mechanisms of Thymus Organogenesis and Morphogenesis. *Development*, 138(18):3865–3878, 2011. ISSN 0950-1991. doi:10.1242/dev.059998.
- [250] Anny-Claude Luissint, CÃaldric Artus, Fabienne Glacial, Kayathiri Ganeshamoorthy, and Pierre-Olivier Couraud. Tight Junctions at the Blood Brain Barrier: Physiological Architecture and Disease-Associated Dysregulation. *Fluids and Barriers of the CNS*, 9(1):23, 2012. ISSN 2045-8118. doi:10.1177/0271678X15616978.
- [251] Balaji Srinivasan, Aditya Reddy Kolli, Mandy Brigitte Esch, Hasan Erbil Abaci, Michael L Shuler, and James J Hickman. TEER Measurement Techniques for in Vitro Barrier Model Systems. *Journal of Laboratory Automation*, 20(2):107–126, 2015. ISSN 2211-0682. doi:10.1177/2211068214561025.
- [252] Dulantha Ulluwishewa, Rachel C Anderson, Warren C McNabb, Paul J Moughan, Jerry M Wells, and Nicole C Roy. Regulation of Tight Junction Permeability by Intestinal Bacteria and Dietary Components. *The Journal of Nutrition*, 141(5):769–776, 2011. ISSN 0022-3166. doi:10.3945/jn.110.135657.
- [253] Obinna C Ubah and Heather M Wallace. Cancer Therapy: Targeting Mitochondria and Other Sub-Cellular Organelles. *Current Pharmaceutical Design*, 20(2):201–222, 2014. ISSN 1381-6128.
- [254] Fernando Calahorro and Manuel Ruiz-Rubio. Caenorhabditis Elegans As an Experimental Tool for the Study of Complex Neurological Diseases: Parkinson’s Disease, Alzheimer’s Disease and Autism Spectrum Disorder. *Invertebrate Neuroscience*, 11(2):73–83, 2011. doi:10.1177/1179069518798628.
- [255] Jia Li and Weidong Le. Modeling Neurodegenerative Diseases in Caenorhabditis Elegans. *Experimental Neurology*, 250:94–103, 2013. doi:10.1016/j.expneurol.2013.09.024.
- [256] Gareth Harris, Holly Mills, Rachel Wragg, Vera Hapiak, Michelle Castelletto, Amanda Korchnak, and Richard Komuniecki. The Monoaminergic Modulation of Sensory-Mediated Aversive Responses in Caenorhabditis Elegans Requires Glutamatergic/peptidergic Cotransmission. *Journal of Neuroscience*, 30(23):7889–7899, 2010. ISSN 0270-6474. doi:10.1523/JNEUROSCI.0497.
- [257] Yingchuan B Qi, Emma J Garren, Xiaokun Shu, Roger Y Tsien, and Yishi Jin. Photo-Inducible Cell Ablation in Caenorhabditis Elegans Using the Genetically Encoded Singlet Oxygen Generating Protein MiniSOG. *Proceedings of the National Academy of Sciences*, 109(19):7499–7504, 2012. ISSN 0027-8424. doi:10.1073/pnas.1204096109.
- [258] Erica M Andreozzi, Julia BaguÃasa Torres, Kavitha Sunassee, Joel Dunn, Simon Walker-Samuel, Istvan Szanda, and Philip J Blower. Studies of Copper Trafficking in a Mouse Model of Alzheimer’s Disease by Positron Emission

Tomography: Comparison of ^{64}Cu Acetate and ^{64}Cu GTSM. *Metallomics*, 9(11):1622–1633, 2017. doi:10.1021/ja035737d.

- [259] Lei Jiang, Yingfeng Tu, Xiang Hu, Ande Bao, Hao Chen, Xiaowei Ma, Tim Doyle, Hongcheng Shi, and Zhen Cheng. Pilot Study of ^{64}Cu (I) for PET Imaging of Melanoma. *Scientific Reports*, 7(1):2574, 2017. ISSN 2045-2322. doi:10.1038/s41598.
- [260] Douglas Wahlsten. *Mouse Behavioral Testing: How to Use Mice in Behavioral Neuroscience*. Academic Press, 2010. ISBN 0123756758.
- [261] S Teegarden. Behavioral Phenotyping in Rats and Mice. *Mater Methods*, 2: 122, 2012.